University of California
Santa Barbara

Urban tree drought resilience and outdoor water conservation in a Mediterranean climate: insights from an ecohydrologic model

A dissertation submitted in partial satisfaction
of the requirements for the degree

Doctor of Philosophy
in
Environmental Science and Management

by

Rachel Torres

Committee in charge:

Professor Naomi Tague, Chair
Professor Joe McFadden
Professor Sam Stevenson

March 2024

The Dissertation of Rachel Torres is approved.

Professor Joe McFadden

Professor Sam Stevenson

Professor Naomi Tague, Committee Chair

December 2023

Urban tree drought resilience and outdoor water conservation in a Mediterranean climate: insights from an ecohydrologic model

by

Rachel Torres

Acknowledgements

This dissertation would not be possible without the unwavering support of my community, both within and beyond academia.

First and foremost, heartfelt gratitude to my advisor, Naomi Tague, whose persistent support and boundless patience made her an exceptional mentor. Naomi not only introduced me to the field of ecohydrology and research in environmental modeling, but also supported me when research was not my first priority in academia. Your guidance has transformed me into a better coder, writer, scientist, and individual.

I extend my sincere thanks to my committee members. Sam Stevenson, your expertise and research on climate and drought have been invaluable. Joe McFadden, your extensive knowledge on all things vegetation, along with your endless support, is deeply appreciated. I am grateful for the support, stimulating discussions, and your editing skills, which have enriched my work.

A special acknowledgment goes to the Ph.D. students who preceded me—Mike Alonzo, David Miller, Will Burke, and Catherine Shields. Your methods and data collection have had a direct influence on this dissertation.

I express my gratitude to my Bren School cohort, a group that has not only been a pleasure to learn and grow with but has also made the journey enjoyable. Elliot, Ignacia, Phoebe, Nicol, Jacob, Vincent, Albert, Erin, Casey, Juan Carlos, Yang, Jiajia, Qian, Mary, Rahul, Julia, and Sean, thank you for the camaraderie.

Acknowledgment is also due to the Bren School for their support over the years, especially to Satie, Kristine, Aleah, and Sage. Special thanks to the compute team, Kat and Garett, for always being available to address wifi and VPN issues. Thank you to Steve Miley for setting up the remote R server, facilitating my work from home.

To the Tague lab, thank you for your constant support and time spent discussing trees

over happy hours. Special thanks to Janet Choate for teaching me how to use RHESSys and for being a great companion during AGU conferences. Thoughtful conversations and valuable feedback from Chris Heckman, Will Burke, Ty Brandt, Zion Klos, Erin Hanan, Louis Graup, Ojas Sarup, Kate Voss, and Sloane Stephenson have greatly enhanced my time here.

A heartfelt thanks to those who inspired my study of urban environments—Joe McFadden, David Miller, Erin Wetherley, and Timnit Kefela. Your willingness to engage in discussions when I was new to the field was invaluable.

I am grateful to my peer support system for their professional support in proofreading and practicing talks. Special thanks to Jessica Couture, Elizabeth Hiroyasu, Timnit Kefela, and Molly Schwarz for the encouragement and solidarity over texts and dinners.

Entering the sixth year of my Ph.D., I received funding that introduced me to a network of professional support across Hispanic Serving Institutions. I am immensely thankful for this opportunity and the assistance from Carlos, Angela, Yvette, Sean, Blake, and Emily.

Finally, I want to acknowledge the funding sources that made this journey possible. Funding from the Bren School for my first year, the Coastal Fund and Groundwater Resources Association in my first summer, the UCSB Crossroads Fellowship for one quarter, the NSF AGEP program for two quarters, and Grad Div and Academic Senate for conference travel have been instrumental. The majority of my Ph.D. journey was funded through my work as a teaching assistant, allowing me to evolve as a teacher and find a distinct niche within academia. Special thanks to instructors Sam Stevenson, Naomi Tague, Kelly Caylor, Emily Fairfax, and Stephanie Moret, as well as from instructional development, Lisa Berry, and from the Summer Research Academies, Lina Kim, for their support.

Curriculum Vitæ

Rachel Torres

Education

2023	Ph.D. in Environmental Science and Management, University of California, Santa Barbara.
2016	B.S. in Physics, North Park University

Teaching Experience

Summer Research Academies

INT 93LS Our Dynamic Earth, Instructor

Environmental Studies Program

ENV S 2 Introduction to Environmental Science, Lead TA

Bren School, Master's of Environmental Science and Management

ESM 203 Earth Systems Science, TA

EDS230 / ESM232 Environmental Modeling, TA

Research Experience

Graduate Student Research, Bren School of Environmental Science and Management

SERI-Fire Environmental Model Visualization Development

Visualizing Environmental Models, Crossroads Fellow

Awards and Honors

2023 Bren Environmental Leaders Program, Friends of Michael Mantell, Mentor

2023 Bren School of Environmental Science and Management, Teaching Assistant Award

2022 NSF Alliance for Graduate Education and the Professoriate, California HSI Alliance, Fellow

2022 UCSB Graduate Student Association, Excellence in Teaching Award

Publications

Torres, R.D., Tague, C. L., McFadden, J.P. "Exploring potential trade-offs in outdoor water use reductions and urban tree health during an extreme drought in Southern California." *under revision for Frontiers in Climate: Climate, Ecology and People.*

Abstract

Urban tree drought resilience and outdoor water conservation in a Mediterranean climate: insights from an ecohydrologic model

by

Rachel Torres

Trees in cities can make communities more resilient to climate change and provide sustainable infrastructure for heat mitigation and stormwater regulation. Urban areas around the world are growing, and there is potential to plan for urban forestry to be equitable and sustainable. In the Southwestern United States, growing populations along with a higher frequency of drought and heat waves poses a need for urban forestry management in conjunction with efficient water use.

This dissertation used a mechanistic model, the Regional Eco-Hydrologic Simulation System (RHESSys), to simulate urban tree carbon and water fluxes during a multi-year drought in Southern California. Tree leaf area index (LAI), net primary productivity (NPP), and water use were estimated under different scenarios of temperature, irrigation, and neighboring land cover. In the first chapter, I used high spatial resolution remote sensing data from Santa Barbara, California of tree species, LAI, and changes to the Normalized Differential Vegetation Index during the 2012-2016 drought to create tree species parameter sets for five common urban tree species. With these urban tree parameter sets, I estimated tree drought resistance and resilience for LAI and NPP and showed how they differ in the case of a drought with similar precipitation patterns and different temperatures. I demonstrated how temperature plays an important role for tree productivity post-drought and can increase resilience. Warmer temperatures increased resilience, but only to a certain extent: 1.8° C of warming increased post-drought pro-

ductivity leading to higher resilience compared to the cooler temperature scenarios, but extreme warming of 4° C hindered growth. In the second chapter, I used the same tree species parameters to simulate how irrigation inputs to the system would affect drought resilience and water use efficiency (WUE). The response of the average tree NPP to irrigation input during drought was non-linear, with a break-point analysis displaying a steeper decline in NPP beyond irrigation reductions of 25% to 50% depending on tree species. Transpiration was linearly related to irrigation input, and this caused WUE to increase with less irrigation. In the third chapter, I went a step further to explore irrigation effects by incorporating neighboring irrigation on turfgrass. In some city locations, mature trees on their own may not be directly receiving irrigation. However, in this study I found that trees may be receiving excess irrigation water from turfgrass area. This study also highlighted an example of hydrologic modeling with sub-grid water routing, and showed how impervious surfaces disconnected from the stormwater drainage system can increase tree productivity.

Contents

Introduction

Urban trees provide a wealth of ecosystem services including cooling and shade provision, air filtering, stormwater management, and cultural and psychological benefits (1; 2). To maximize these benefits, trees need to be able to withstand various stressors from climate and the built environment (3), and managing this requires a deeper understanding of how urban trees affect carbon and water cycling. In Southern California and other arid to semi-arid regions that experience heat waves, the ability for the urban forest to cool the surface with shade from canopy coverage and contribute to microclimate cooling with evapotranspiration (ET) is especially important for communities (4; 5). At the same time, a vital water source for vegetation in semi-arid regions is typically irrigation (6), which is often the first municipal water use to be restricted during drought, making urban trees more vulnerable to drought.

California experienced an extreme drought from 2012-2016 that included a concurrent heat wave in 2014 (7; 8), which caused widespread mortality across natural forests (9; 10). However, the effects of drought and heat on urban forests received less attention despite the potential for managing urban forests for drought resilience and climate change adaptation (11). Finding a balance between efficient water use and maintaining tree health will be crucial for long-term urban forestry and water resources management, as climate change will increase drought and extreme heat events. This dissertation consisted of three studies on the interactions between drought and heat, water use, and tree carbon

and water fluxes in Santa Barbara, California, a coastal semi-arid urban location.

To further understand the complex eco-hydrologic processes within an urban forest that contribute to drought resilience, this dissertation used a mechanistic numerical modeling approach and leveraged fine spatial resolution remote sensing data. The Regional Hydro-Ecological Simulation System (RHESSys) is a coupled eco-hydrologic model that simulates physical mechanisms of carbon and water cycling (12). It was applied at a $10m^2$ patch level, the smallest spatial unit in the model, to capture the dynamic changes to tree carbon and water fluxes in response to changes in the environment. Using a process-based model allowed me to vary forcings and simulate drought scenarios to examine their effects on tree carbon and water fluxes. With the 2012-2016 California drought as context, I assessed tree productivity in the year leading up to the drought, during the drought, and post drought using model estimations of tree carbon fluxes, leaf area index (LAI), and water use. To inform future urban forestry and water resources management decisions for a warmer and drier climate, I simulated different scenarios of temperature, outdoor water use, and land cover for five commonly found urban tree species. Along with finding practical results on water conservation and tree drought resilience, I developed novel methods to integrate remote sensing data with RHESSys that have potential for future applications in urban land surface models.

In the first chapter, I explored how different ecophysiological traits contributed to tree drought resilience, and tested how warmer temperatures during drought affected resilience. I used data derived from high-spatial resolution ($3.7m^2$) hyperspectral imagery and lidar data at the tree species level (13) that included: pre-drought LAI (14) and changes to the Normalized Difference Vegetation Index (NDVI) during the drought (15). Because these data sets were at the tree species level with a short time series, I used them to validate model outcomes of LAI and reduce parameter uncertainty for five common tree species in the study region. Climate data from 2011–2017 was used to generate baseline

model estimates of LAI and net primary production (NPP). I then ran a Sobol sensitivity analysis to identify the sensitivity of tree LAI, net primary productivity (NPP), and drought resilience to key vegetation parameters and account for parameter uncertainty. To compare the baseline with possible future events, I simulated cooler and warmer temperature droughts. I found that drought with increased temperatures of 1.8°C would likely cause greater declines in LAI, but faster recovery post-drought relative to the baseline. With more extreme warming of 4.6°C, simulated LAI did not fully recover post-drought. While most trees were sensitive to the different temperatures, the deciduous tree, California Sycamore, was highly resilient due to its high leaf turnover rate, as shown by the vegetation parameter sensitivity analysis. The findings suggested that future extremes in warmer temperatures during drought could lead to a decline in urban tree drought resilience, which should be considered in urban tree species selection.

The first study was unique in the use of tree species level data for vegetation parameterization. Typically, coupled land surface models have a general 'type' for representing vegetation. The type could be differentiated between tree, grass, or shrub, that could further be specified by plant functional type or phenology. This study went a step further to quantify tree species differences, taking advantage of species level tree data in Santa Barbara, California (13). I created parameter sets that differentiate tree species while maintaining parameter uncertainty due to spatial variation in the data and equifinality within the model. This method of vegetation parameterization laid the groundwork for the following chapters in the dissertation where I used the same tree species, and provided an example for reducing vegetation parameter uncertainty with remote sensing data.

The second chapter aimed to quantify trade-offs in urban tree ecosystem services and outdoor water use. Ecosystem services were represented by tree water and carbon fluxes, with a focus on urban heat island mitigation. Specifically, during drought the direct loss of productivity and LAI leads to a reduction in shade, while the decrease in tree

transpiration results in less evaporative cooling (5). I simulated a range of irrigation input scenarios during drought based on average monthly outdoor water use data from 2010-2020 from the Santa Barbara Water Resources department. Irrigation scenarios were compared across tree species and warmer temperatures. I analyzed the response of model outcomes of tree carbon fluxes, LAI, and tree transpiration. Results showed that reducing irrigation up to 25%, a comparable amount as the California statewide mandate in 2015, has minimal effects on tree primary productivity and water use efficiency. Transpiration was linearly related to irrigation input, causing a short-term loss of evaporative cooling with irrigation reductions during drought. However, primary productivity and LAI had a nonlinear response to irrigation, indicating shade provision could be maintained throughout drought with partial irrigation reductions. These results varied with tree species, with some species showing greater sensitivity of primary productivity to water input and temperature.

The findings in the second study had implications for the effects of water conservation on urban trees in semi-arid regions. Results showed that for most of the tree species used, outdoor water use could be reduced by 25% while maintaining tree productivity during a multi-year drought. However, this study assumed trees have access to the additional irrigation water when in reality there is some uncertainty in urban tree water sources (16; 17). One common vegetation in cities that does receive direct irrigation is turfgrass, which is often found in mixed land use areas and interspersed with trees. During the drought in California, a statewide mandate targeted turfgrass irrigation for water conservation (18), which may have had indirect effects on neighboring trees. To explore the small-scale hydrologic interactions between turfgrass and trees, and between different land covers, I used a novel modeling approach called multiscale routing (19), which accounts for sub-grid water routing. I developed a version of multiscale routing to be used for surface routing in places with land covers that have differences in infiltration

rates, such as urban areas with impervious surfaces.

The third chapter explored whether water management for turfgrass during drought affects urban trees. I simulated scenarios of tree growth with neighboring irrigated turfgrass and subsequent reductions in irrigation, and compared this for small-scale areas with and without nearby impervious surface area. Impervious surfaces are known to increase runoff, and if connected to neighboring vegetated spaces may lead to increased infiltration (20; 21). This study compared tree level evapotranspiration (ET), productivity (NPP), and drought resilience across irrigation and land cover scenarios. I found that maintaining turfgrass irrigation during drought increased neighboring tree ET and NPP. With irrigation turned off for water conservation, tree ET and NPP declined during the drought. LAI drought resilience responses to irrigation reduction was dependent on tree species. In some cases with connected impervious areas routing surface water, the additional water input offset irrigation shut-off and caused a greater tree ET and NPP during the drought compared to the landscape without impervious areas. By quantifying small-scale hydrologic interactions, this study may inform landscaping management strategies that save water while maintaining ecosystem services from urban trees during drought.

Introduction References

[1] S. J. Livesley, G. M. McPherson, and C. Calfapietra, *The Urban Forest and Ecosystem Services: Impacts on Urban Water, Heat, and Pollution Cycles at the Tree, Street, and City Scale*, *Journal of Environment Quality* **45** (2016), no. 1 119.

[2] K. L. Wolf, S. T. Lam, J. K. McKeen, G. R. A. Richardson, M. van den Bosch, and A. C. Bardekjian, *Urban Trees and Human Health: A Scoping Review*, *International Journal of Environmental Research and Public Health* **17** (2020), no. 12 4371. Number: 12 Publisher: Multidisciplinary Digital Publishing Institute.

[3] E. McPherson, A. M. Berry, and N. S. van Doorn, *Performance testing to identify climate-ready trees*, *Urban Forestry & Urban Greening* **29** (2018) 28–39.

[4] R. I. McDonald, T. Kroeger, P. Zhang, and P. Hamel, *The Value of US Urban Tree Cover for Reducing Heat-Related Health Impacts and Electricity Consumption*, *Ecosystems* (2019).

[5] M. A. Rahman, L. M. F. Stratopoulos, A. Moser-Reischl, T. Zölch, K.-H. Häberle, T. Rötzer, H. Pretzsch, and S. Pauleit, *Traits of trees for cooling urban heat islands: A meta-analysis*, *Building and Environment* **170** (2020) 106606.

[6] C. Mini, T. S. Hogue, and S. Pincetl, *Estimation of residential outdoor water use in Los Angeles, California*, *Landscape and Urban Planning* **127** (2014) 124–135.

[7] N. S. Diffenbaugh, D. L. Swain, and D. Touma, *Anthropogenic warming has increased drought risk in California*, *Proceedings of the National Academy of Sciences* **112** (2015), no. 13 3931–3936.

[8] D. Griffin and K. J. Anchukaitis, *How unusual is the 2012–2014 California drought?*, *Geophysical Research Letters* **41** (2014), no. 24 9017–9023.

[9] C. J. Fettig, L. A. Mortenson, B. M. Bulaon, and P. B. Foulk, *Tree mortality following drought in the central and southern Sierra Nevada, California, U.S.*, *Forest Ecology and Management* **432** (2019) 164–178.

[10] Lund Jay, Medellin-Azuara Josue, Durand John, and Stone Kathleen, *Lessons from California's 2012–2016 Drought*, *Journal of Water Resources Planning and Management* **144** (2018), no. 10 04018067.

[11] E. G. McPherson, Q. Xiao, N. S. van Doorn, J. de Goede, J. Bjorkman, A. Hollander, R. M. Boynton, J. F. Quinn, and J. H. Thorne, *The structure, function and value of urban forests in California communities*, *Urban Forestry & Urban Greening* **28** (2017) 43–53.

[12] C. L. Tague and L. E. Band, *RHESSys: Regional Hydro-Ecologic Simulation System—An Object-Oriented Approach to Spatially Distributed Modeling of Carbon, Water, and Nutrient Cycling*, *Earth Interactions* **8** (2004), no. 19 1–42.

[13] M. Alonzo, B. Bookhagen, and D. A. Roberts, *Urban tree species mapping using hyperspectral and lidar data fusion*, *Remote Sensing of Environment* **148** (2014) 70–83.

[14] M. Alonzo, J. P. McFadden, D. J. Nowak, and D. A. Roberts, *Mapping urban forest structure and function using hyperspectral imagery and lidar data*, *Urban Forestry & Urban Greening* **17** (2016) 135–147.

[15] D. L. Miller, M. Alonzo, D. A. Roberts, C. L. Tague, and J. P. McFadden, *Drought response of urban trees and turfgrass using airborne imaging spectroscopy*, *Remote Sensing of Environment* **240** (2020) 111646.

[16] N. S. Bijoor, H. R. McCarthy, D. Zhang, and D. E. Pataki, *Water sources of urban trees in the Los Angeles metropolitan area*, *Urban Ecosystems* **15** (2012), no. 1 195–214.

[17] D. E. Pataki, H. R. McCarthy, E. Litvak, and S. Pincetl, *Transpiration of urban forests in the Los Angeles metropolitan area*, *Ecological Applications* **21** (2011), no. 3 661–677.

[18] E. G. Brown, *Executive order b-29-15*, 2015.

[19] W. Burke and C. N. Tague, *Multiscale Routing – Integrating the Tree-scale Effects of Disturbance into a Watershed Ecohydrologic Model*, AGU, 2019.

[20] C. Shields and C. Tague, *Ecohydrology in semiarid urban ecosystems: Modeling the relationship between connected impervious area and ecosystem productivity*, *Water Resources Research* **51** (2015), no. 1 302–319.

[21] C. B. Voter and S. P. Loheide, *Urban Residential Surface and Subsurface Hydrology: Synergistic Effects of Low-Impact Features at the Parcel Scale*, *Water Resources Research* **54** (2018), no. 10 8216–8233.

Chapter 1

Urban tree resilience to drought and extreme heat: modeling differences in tree species parameterized with remote sensing data

1.1 Introduction

Trees are essential for climate change adaptation in cities because of their ability to provide stormwater management and filtering, air pollution reduction, habitat for biodiversity, and cultural and social significance (1; 2; 3). They also provide shade for human thermal comfort, and evapotranspiration that mitigates urban heat islands (4; 5). However, the benefits of tree ecosystem services depend on tree health and resilience to extreme events like drought. From 2012-2016, California experienced a drought that was especially detrimental to forests due to historically low precipitation occurring simultaneously with one of the warmest periods on record in California (6; 7; 8), a pattern that is expected to increase in frequency with climate change (9; 10). While the effects on natural forests were devastating, the effects on urban forests remain understudied, and likely more varied due to the assortment of nonnative tree species and access to additional inputs of water in cities (11; 12; 13; 14; 15).

Urban forestry management has the potential to contribute to climate change adaptation in cities through tree species selection, where tree species should be considered not only for their benefits but for their ability to survive climate related impacts such as drought (16; 17; 18; 19). Compared to their natural forest counterparts, urban trees are highly managed and often planted based on specific aesthetic attributes and socioeconomic preferences (20). In California and other semi-arid climates especially, long-term climate adaptation requires understanding which tree species and ecophysiological traits contribute to drought resilience (21). Resilience is the ability of a system to return to pre-disturbance conditions following the disturbance (22). In the case of a long-term dis-

turbance, such as a multi-year drought, resilience is connected to the ability to maintain functioning during the disturbance, or the resistance of a system. Resilience and resistance have been used to quantify and describe how trees respond to drought using data from tree rings (23; 24) and remote sensing (25; 26), but has been less used to describe urban trees.

To quantify resilience and resistance, temporal observations of vegetation characteristics over the course of a disturbance are needed, which can be captured using remote sensing methods. In Southern California, various characteristics of urban vegetated areas have been studied including land surface temperature (27; 28), tree species (29), and leaf area index (LAI) and carbon storage (25). More recent studies used short-term time series of airphotos and hyperspectral imagery to quantify changes in vegetation greenness indices and fractional cover (30; 31). These methods are valuable for observing vegetation conditions before and after drought, but are temporally limited to the times of data acquisition. Limited time series may not capture changes happening throughout the course of a multi-year drought, and may not always include the data needed to explain patterns in observations or estimate tree responses to future conditions. In this study, we (1) calibrate an ecohydrologic model's tree parameters with remote sensing data of the historic drought and identify which ecophysiological traits are important for drought resilience and (2) consider how drought responses of selected urban trees may be different under altered temperature scenarios.

Building on a short-term remote sensing time series and taking advantage of high spatial resolution urban tree data, this study used data from (29; 32), and (30) to parameterize an ecohydrologic model, the Regional Hydro Ecologic Simulation System or RHESSys, to investigate urban forest drought resilience in Santa Barbara, California for a historic drought and in the case of potential future droughts. In the years leading up to the 2012 drought, Alonzo used high-resolution lidar data and hyperspectral imagery to identify individual tree species and estimate canopy LAI and carbon storage. Miller quantified changes to species-level vegetation indices using airborne imaging spectroscopy from 2011, 2014, and 2017. The information on urban tree characteristics and changes in vegetation greenness provided by these studies is uniquely useful when paired with the model in order to inform which ecophysiological traits contribute to changes to vegetation. With this parameterized model, we can then generalize and extend results from the 2012-2016 drought to explore how trees may respond to future droughts. While the 2012-2016 drought is a historic example of an extreme event, with climate change we can expect future droughts to become warmer (33), and we use the model to test the effects of temperature differences on drought resistance and resilience.

1.2 Methods

We used an ecohydrologic model, RHESSys, paired with high spatial resolution remote sensing data to derive tree species level vegetation parameters. First, we performed a sensitivity analysis to identify key vegetation and soil parameters that influence model

estimates of drought resilience and to select parameter sets that correspond with observed behaviors for the urban tree species of interest. Vegetation parameter sets were calibrated to the historic drought using changes in Normalized Difference Vegetation Index (NDVI) (34) and model output of LAI. These parameter sets were then used to estimate the resistance and resilience of LAI and plant net primary productivity (NPP) for the historic drought and to compare across tree species. The results from the historic drought were then compared to model estimates for future droughts with different temperatures.

1.2.1 RHESSys model

The Regional Hydro-Ecologic Simulation System (RHESSys) is a spatially distributed, mechanistic model which simulates energy, carbon, water, and nutrient cycling (35); this study used version 7.2 (36). RHESSys has been used for the Santa Barbara region in previous studies to evaluate vegetation water and carbon flux responses to stormwater distribution (37) and for studying post-fire vegetation regrowth (38). It has also been used in urban settings for simulating stormwater management systems on the east coast (39; 40). Parameter uncertainty specific to RHESSys has previously been explored for vegetation parameters in a mountainous region of the Western U.S. (41), and soil parameters in the headwaters of the urban watershed used in this study (42).

For this study we used the smallest spatial unit within the model, a 'patch'. In this study, a single patch represents an area of $10m^2$ with a single tree species and no lateral hydrologic flow. The main source of water is precipitation which goes towards interception by the canopy and infiltration into the soil. Evapotranspiration is estimated using the Penman-Monteith equation, which depends on temperature, vapor pressure deficit, and radiation. Soil is vertically stratified into a rooting zone, unsaturated zone, and deeper saturated store. The soil is a shallow, sandy-loam type based on parameters previously used in Santa Barbara modeling studies (38; 37). This study does not include the effects of the spatial distribution of trees on the urban landscape, and it is assumed that no additional water is added to the precipitation input. While street trees may receive direct or indirect irrigation, many of the selected species exist in parks and coastal bluff areas that may not have direct irrigation systems.

Carbon cycling within RHESSys is coupled to water fluxes through stomatal conductance and leaf area, both of which regulate gross primary productivity (GPP). GPP is estimated using the Farquhar model (43), which depends on light, temperature, and stomatal conductance. Stomatal conductance is a function of vapor pressure deficit, root accessible soil moisture, temperature, light, and CO_2 (44). Plant respiration consists of growth and maintenance respiration, which is a function of temperature, leaf nitrogen, and plant properties. Plant carbon stores accumulate daily assimilated carbon partitioned into stem and leaf biomass, and fine and coarse roots. The amount partitioned into each plant organ is dependent on the carbon allocation strategy and the accompanying parameters. Turnover of these stores depends on species ecophysiologic parameters. This study used a semi-mechanistic carbon allocation strategy dependent on resource

limitation (45), where leaf carbon allocation is prioritized until there is limited water or nitrogen and then it shifts to prioritizing root carbon. Leaf carbon allocation depends on allometric scaling of carbon to LAI, the potential photosynthetic capacity, and the proportion of newly assimilated carbon allocated to leaves. This approach prioritizes leaf growth in developing forests and resource limitation in mature trees (41). Leaf phenology is simulated with parameters for day-of-year timing on new leaf growth and senescence. For a detailed description of RHESSys hydrologic and ecophysiological submodules, see Tague and Band 2004 (35), and for a comprehensive description of plant carbon allocation strategies, see Garcia et al. 2016 (41).

1.2.2 Study Site and Data

Santa Barbara, California (34.42° N, 119.69° W) is representative of a coastal Southern California city with an extensive and diverse urban forest. Santa Barbara has a Mediterranean climate with hot, dry summers and wet winters and is projected to experience an increasing likelihood of warming and drought (9). The average annual rainfall at the Santa Barbara Downtown precipitation gauge (SB County station 234) is 479.5mm averaged over 1990-2020.

While the area is highly developed, the urban forest is made up of a mix of public parks, natural areas, and street trees composed of native and non-native species. The most common tree species include various palms (*Archontophoenix cunninghamiana*, *Phoenix canariensis*, *Syagrus romanzoffiana*), native coastal live oak (*Quercus agrifolia*), non-native eucalyptus trees (*Eucalyptus ficifolia*, *Eucalyptus globulus*), and various conifers (*Pinus canariensis*, *Pinus pinea*) (29).

There were five tree species common in the area selected to use for this study. These include Coast Live Oak (*Quercus agrifolia*), a native broadleaf evergreen, California Sycamore (*Platanus racemosa*), a native broadleaf deciduous, Blue Gum Eucalyptus (*Eucalyptus globulus*) and Victorian Box (*Pittosporum undulatum*), nonnative broadleaf evergreens, and Canary Island Pine (*Pinus canariensis*), a nonnative conifer.

We used species level LAI estimates from Alonzo et al. 2016 (32) and a time-series of the normalized differential vegetation index (NDVI) from Miller et al. 2020 (30) to calibrate vegetation parameters. The LAI estimates were derived from airborne hyperspectral imagery and lidar data in 2010, with a spatial resolution of $10m^2$. The NDVI data was derived from airborne imaging spectroscopy captured in a sequence of years during the drought, in 2011, 2014, and 2017 at $7.5m^2$ spatial resolution.

The climate data used as daily input to the model comes from two sources: daily maximum and minimum temperatures were taken from NOAA (station USC00047902) , and daily precipitation was from a rain gauge located in downtown Santa Barbara (station ID 234) at 39.6m elevation, from Santa Barbara County Public Works Water Resources. Scenarios of future drought were developed based on data from statistically downscaled climate projections (46). Downscaled climate projection data from Cal-Adapt was downloaded for the city of Santa Barbara, including four global climate models

(HadGEM2-ES, CNRM-CM5, CanESM2, MIROC5) for two representative concentration pathways (RCP) run for the Coupled Model Intercomparison Project Phase 5: medium emissions (RCP4.5), and high emissions (RCP8.5). The time ranges are from 2006-2099 and 2006-2100. Trends of annual precipitation and temperature anomalies were analyzed for possible temperature differences during a future drought-like period, as described in section 1.2.4 below.

1.2.3 Sobol Sensitivity Analysis and Parameters Selection

Sensitivity analysis

Sobol sensitivity analysis is based on variance decomposition and has been applied to complex environmental models to quantify uncertainty in interactions across large parameter spaces (47; 48; 49).

This method of sensitivity analysis considers the interaction between different parameters and their total effect on the outcome as well as the individual effect on the outcome (50). First order indices are a measure of the direct contribution to the output by an individual parameter. Total order indices measure the overall contribution of a parameter to the output while considering both its direct effect and its interaction with other parameters. Sobol is used here to identify which selected RHESSys vegetation and soil parameters have the largest effect on LAI, NPP, and LAI and NPP drought resilience.

Parameters used in the sensitivity analysis were selected based on previous studies (41; 42) and whether the parameter is used in a key process for tree carbon cycling. These include two soil parameters that influence field capacity storage potential and 31 ecophysiological vegetation parameters that affect photosynthesis, respiration, carbon allocation, and other vegetation traits (Table 1.1). To generate parameter sets for Sobol, values for each parameter were randomly sampled from a uniform distribution across a range of values. The minimum and maximum range of values were set based on RHESSys parameter libraries and defaults, plant functional types, and values found in the literature (Table 1.1). A unique set of random permutations of the selected parameters was then input for each RHESSys model run.

RHESSys simulates phenology differently for evergreen and deciduous, where deciduous trees have complete leaf loss annually; for this reason the sensitivity was done for both functional types. For both evergreen and deciduous functional types, the model was run separately for 10,500 parameter sets. For each parameter set, the model was simulated through a 'spin-up' with climate data from 1940-2020 to establish mature trees and stabilize soil carbon and nitrogen pools. The final 10 years of the simulation were output with daily values of LAI and carbon fluxes. The model outputs were then aggregated to annual values for pre-drought LAI, LAI resilience, pre-drought NPP, and NPP resilience, to apply with Sobol and generate indices (Figure 1.1).

Table 1.1: Vegetation and Soil parameters used in sensitivity analysis. Most values are taken from RHESSys definition files, full descriptions and a list of sources are shown in Appendix A 1.7. The range over which parameters were sampled is given here for deciduous and evergreen.

	parameter	**evergreen**	**deciduous**	**units**
Soils	pore size index	0.16-0.24	0.16-0.24	–
	psi air entry	0.17-0.26	0.17-0.26	mH_2O
Allometry	height to stem coef	0.25-0.75	0.25-0.75	–
	root distribution	3.8-6.9	3.8-6	–
Carbon allocation	fine root C:coarse root C	0.2-0.8	0.2-1.5	ratio
	fine root C:leaf C	0.6-1.0	0.6-1.2	ratio
	daily photosynthate used for growth	0.44-0.56	0.44-0.69	fraction
	stem C:leaf C	1.3-1.9	1.3-1.9	ratio
	C transfer to storage proportion	0.56-0.84	0.56-0.84	percent
	waring A	0.3-0.45	0.2-0.45	–
	waring B	0.05-1	0.05-1	–
LAI	leaf C:N	27-60	40-60	kgC/kgN
	projected SLA	6-27	22-35	m^2/kgC
	light ext. coef	0.54-0.81	0.54-0.81	–
Mortality	branch turnover	0.0082-0.012	0.0082-0.012	/day
	NSC pool mortality	0.0018-0.7	0.0001-0.1	percent
	fine root turnover	0.2-0.75	0.6-1.2	/year
	leaf turnover	0.3-0.8	0.6-1.2	/year
	livewood turnover	0.56-0.84	0.56-0.84	/year
	min leaf carbon for resprouting	0.001-0.02	0.001-0.02	kgC
	resprout leaf carbon	0.005-0.01	kgC	
Carbon fluxes	fraction leaf N in rubisco age multipier	0.035-0.53	0.035-0.53	percent
	net fPAR age multiplier	0.23-0.35	0.23-0.35	percent
	mrc Q10	2.0-2.3	1.8-2.5	–
Stomatal conductance	max leaf scale stomatal conductance	0.0048-0.0072	0.0048-0.0072	meters
	psi at stomatal close	-7.5- -3	-6- -3	MPa
	VPD at stomatal close	2500-6000	2500-6000	Pa
Leaf phenology	day leaf on	284-300	255-283	day of year
	day leaf off	56-70	114-140	day of year
	number of days expand	50-54	55-90	days
	number of days litfall	49-52	50-80	days
Water Storage	litter moist coef	0.00047-0.0007	0.00047-0.0007	$m/kg/m^2$
	specific rain capacity	0.00019-0.00029	0.00019-0.00029	mH_2O/LAI

Model parameterization and outcomes

To obtain vegetation parameter sets specific to the selected tree species, model outputs of LAI from the sensitivity analysis were compared to remote-sensing observations and this comparison was used to narrow down to the parameter sets that resulted in acceptable modeled LAI values by tree species. Spatial variation from the Alonzo data (32) created a range of LAI estimates. This data was only available for pre-drought LAI, and was used to set up the model parameters within an acceptable range of modelled pre-drought LAI. Modeled estimates within two standard deviations of the mean LAI estimates from the data were selected for each tree species.

To account for the changes in LAI during the drought, we used temporal data of NDVI from (30) that captured pre-drought, July 2011, post-drought, June 2017, and 1 year in the middle of the drought, in June of 2014. NDVI has been found to be related to LAI in natural forested areas (51), and acts as an approximation for leaf phenology in response to climate variation (52). We used the changes to remote sensing derived changes in NDVI as a proxy for changes in LAI from the model. Rather than compare direct values, we used the percent differences between 2011-2014 and 2011-2017 for NDVI and model estimated LAI. The parameter sets that resulted in percent differences in modeled LAI within the interquartile range of percent differences in NDVI were filtered to be used in the final parameter sets for each tree species.

For each tree species, the parameter sets that met the filters of pre-drought LAI and changes to LAI during drought were used in all subsequent model scenarios (Table 1.3). Multiple parameter sets meet these criteria for each tree species due to the interactions between different parameters, and this parameter uncertainty is maintained to represent the range of possible outcomes. A full description of parameters along with the range of parameter values for each tree species is available in A.

Once parameters sets were selected, we used the metrics of resistance (Eq. 1.1) and resilience (Eq. 1.2) to compare across tree species and temperature scenarios. With the average annual LAI and NPP for each tree species parameter ensemble and each year in the 2011-2017 sequence we calculated the resistance to drought as the ratio of the state of the variable during drought to the pre-drought state. We calculated resilience as the ratio of post-drought values in 2017 to pre-drought values. For example:

$$resistance = \frac{LAI_{during-disturbance}}{LAI_{pre-disturbance}} = \frac{LAI_{droughtyear}}{LAI_{2011}} \tag{1.1}$$

$$resilience = \frac{LAI_{post-disturbance}}{LAI_{pre-disturbance}} = \frac{LAI_{2017}}{LAI_{2011}} \tag{1.2}$$

1.2.4 Temperature Scenarios

To simulate future drought periods, we identified potential temperature changes in future drought years from statistically downscaled climate projections for Santa Barbara (53). We analyzed precipitation, minimum temperature, and maximum temperature

Table 1.2: Temperature differences were added to historic temperature data. Precipitation anomaly of the year where temperatures occurred are shown.

Scenario name	Temperature Difference	Precip. anomaly
Historic	0	-0.55 to -0.35
Warm	+1.8°C	-0.53
Hot	+4.6°C	-0.48
Cool	-4°C	-0.48

for four general circulation models (GCMs). These 4 GCMs were selected based on recommendation from Pierce et al. 2018 (53) who identified the four as spanning a range of temperature and precipitation, with RCP4.5 and RCP8.5 emissions scenarios. To classify drought years, annual anomalies for observed precipitation data were calculated as the percent difference from the mean of data used for the spin-up period from 1940-2020. This was compared to precipitation anomalies of the GCMs by each of their historic rainfall simulations. Within the GCM simulations, we identified the largest positive, average positive, and largest negative temperature differences that occur with a year that has a precipitation anomaly similar to those observed during the 2012-2016 drought (Table 1.2).

Minimum and maximum daily temperature inputs to the model were altered by the difference in temperature shown in Table 1.2. By uniformly changing daily values, the seasonal fluctuation in temperature is maintained and seasonal patterns replicate the observed data. We acknowledge that in a future climate, more extreme temperature changes may be occurring seasonally with hot, drier summers (54; 55). However, in order to isolate the effect of different temperatures on tree resilience to a multi-year drought, we maintain the uniform changes made to temperature. To simplify the naming convention, we refer to the scenarios based on their differences relative to the actual historic period: hot(+4,6), warm(+1.8), and cool(-4.0).

1.3 Results

1.3.1 Vegetation parameter calibration and sensitivity analysis

We ran a Sobol sensitivity analysis to determine which vegetation parameters affect the model outcomes of LAI, NPP, and LAI and NPP resilience. By identifying the parameters that model outputs were more sensitive to, we were able to narrow down parameter uncertainty for the selected tree species and provide insights into how ecophysiology influences tree responses. The modeled LAI and changes to LAI during drought were within the ranges constrained by the remote sensing data although modelled and remote sensing LAI have different averages (Table 1.3). Given the uncertainty in remote sensing estimates and likely spatial and within-species variation in tree conditions (32), these parameter sets are reasonably consistent with observations. The mean and stan-

dard deviation of modeled LAI, and the LAI and NPP resistance and resilience across the accepted parameter sets for each tree species are shown in Table 1.3.

Parameters with the highest Sobol total order index for each of the four model outcomes are shown in Figure 1.1; these include parameters that control soil field capacity, carbon turnover rates, carbon allocation, and leaf traits. Evergreen LAI and NPP were particularly sensitive to specific leaf area (SLA) (Figure 1.1 panels (b) and (f)), while deciduous LAI and NPP were more sensitive to leaf turnover rates. Some of the parameters, including the leaf turnover rate for the deciduous resilience (Figure 1.1 panels (c) and (g)), have large confidence interval ranges, which suggests the effect of the parameter on the outcome has substantial uncertainty. For pre-drought deciduous, the confidence interval of leaf turnover rates is relatively small and has a more stable first and total order effect on LAI and NPP. With both tree types, LAI and NPP resilience was highly sensitive to leaf turnover rates, but only evergreen was sensitive to fine root turnover rates. Sensitivity to soil pore size index was high across all outcomes and tree types. Pre-drought NPP differed from pre-drought LAI in that it was more sensitive to the leaf water potential at stomatal closure ('psi at complete stomatal reduction'). Many of the parameters resulted large confidence intervals that include zero, which indicates either substantial uncertainty in the effect of these parameters, or for the smaller ranges, little to no influence on the outcome. See the full results of the Sobol indices in the Appendix (A.1).

1.3.2 Changes to water and carbon fluxes during drought

For all drought years, temperature scenarios, and tree parameters, annual transpiration is lower in the summer compared to a wet year (Figure 1.2 panels (d) and (h)). In comparing mean annual transpiration during drought years to an average wet year we found less variation across temperature scenarios and tree species (Figure 1.2 panels (a-b) and (e-f)). This is likely due to transpiration demands exceeding water availability, so at an annual timescale, all plant-available water is used no matter the temperature or ecophysiological parameter values. When there is enough water available, there are greater transpiration response to warmer temperatures and more sensitivity to vegetation parameters, as shown in panels (a) and (e) of Figure 1.2.

During drought years, there was a decline in annual NPP for all tree species parameters and temperature scenarios, driven largely by drought effects on gross primary productivity (GPP). In the warm and hot droughts, net GPP during all drought years was on average lower than the historic drought, with minor differences in plant respiration (R_p), leading to lower or negative NPP. (Figure 1.3).

For all tree species, extreme heat exacerbates the decline in NPP during a drought by altering the seasonal magnitude and timing of both GPP and R_p (Figure 1.4). Temperature is linearly related to R_p, while GPP and temperature have a nonlinear relationship: during the growing season, which takes place in late winter and spring in Santa Barbara, daily GPP increases with temperature until there is not enough water available, which

Table 1.3: Tree species parameterization results and historic drought resistance and resilience with values shown as the mean±s.d.. The variation in LAI from Alonzo et al. 2016 is due to spatial variability, while the variation from RHESSys values are from parameter uncertainty. For the average resistance, the year shown is the lowest resistance reached during the drought period.

Tree code		QUAG	EUGL	PICA	PIUN	PLRA
Tree species		*Quercus agrifolia*	*Eucalyptus globulus*	*Pinus canariensis*	*Pittosporum undulatum*	*Platanus racemosa*
Common name		Coast live oak	Blue gum eucalyptus	Canary island pine	Victorian box	California sycamore
number of parameter sets		206	254	117	481	283
LAI (Alonzo et al. 2016)		4.27 ± 0.47	5.25 ± 0.52	6.42 ± 1.30	4.16 ± 0.67	4.95 ± 0.59
LAI (RHESSys)		4.52 ± 0.19	4.82 ± 0.50	5.17 ± 0.55	4.85 ± 0.37	4.75 ± 0.67
Resistance	LAI (2014)	0.72 ± 0.06	0.8 ± 0.12	0.8 ± 0.12	0.7 ± 0.14	0.77 ± 0.08
	NPP (2013)	0 ± 0.08	0.2 ± 0.09	0.01 ± 0.16	0 ± 0.06	0.49 ± 0.17
Resilience	LAI (2017)	1 ± 0.05	1.19 ± 0.09	1 ± 0.04	0.99 ± 0.06	1.14 ± 0.2
	NPP (2017)	1.08 ± 0.04	1.88 ± 0.3	0.97 ± 0.05	1.09 ± 0.05	1.66 ± 0.35

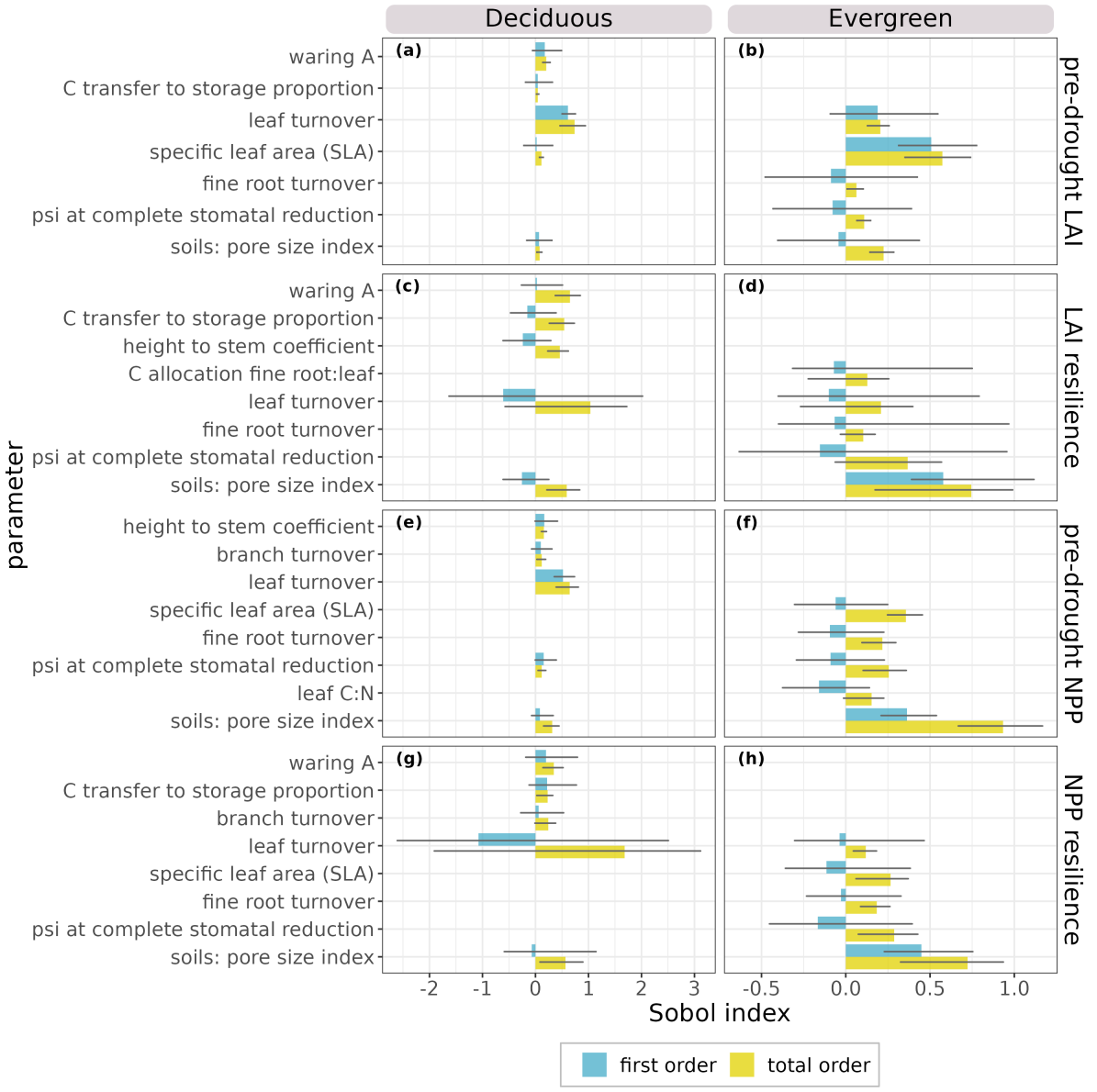

Figure 1.1: Sobol sensitivity results for 5 highest ranking parameters of each of the four outcomes: pre-drought LAI and NPP, and resilience of LAI and NPP. Confidence intervals are shown as grey errorbars, which correspond to each output estimation of Sobol index.

occurs in the mid to late summer (Figure 1.4). In the hot temperature scenario, higher summer temperatures also increase vapor pressure deficit (VPD) and water demand, causing peak GPP to decrease and occur earlier in the year.

For all temperature scenarios, the magnitude of annual GPP during drought years is lower compared to the pre- and post-drought years, and the timing of peak GPP is earlier

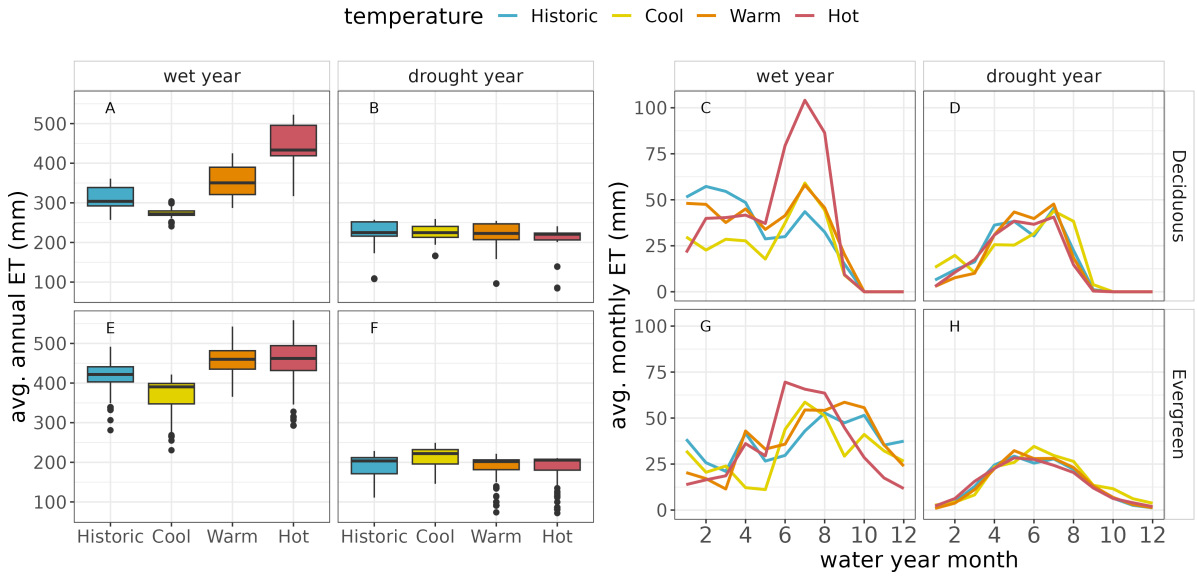

Figure 1.2: Average annual and monthly transpiration for each temperature scenario, with wet year showing years before and after drought (2011 and 2017) and drought years as 2012-2016. Monthly panels are shown as water year months.

in the year for all temperature scenarios except the cool drought (Figure 1.4). While summer GPP decreases due to the lack of water available, R_p is maintained throughout the year, causing NPP to fall below zero for drought years in the historic, warm, and hot droughts. In RHESSys, negative NPP reduces non-structural carbohydrate stores. In this case, declines in these stores reduces carbon availability for growth but were not sufficient to cause mortality.

When there is water available, winter GPP can be limited by lower temperatures in Santa Barbara, where winter and early spring temperatures have an average of 13.8° C. In the warm scenario, the year following the drought had increased rainfall with higher winter temperatures, leading to increased magnitude of GPP compared to the drought years and aiding in post-drought growth and tree NPP resilience.

1.3.3 Drought resistance and resilience

We define resistance and resilience in equations 1.1 and 1.2, and use average annual LAI and total annual NPP to show drought resilience of each tree species. Table 1.3 summarizes estimates of resistance and resilience across tree species for the historic drought, with the year of drought with lowest resistance reported. For all tree species, the first two years of the historic drought show a decline in NPP, with the lowest average resistance occurring in 2013 at 0.14, followed by a gradual increase in resistance and an average NPP resilience of 1.34 in 2017 – meaning that on average the post-drought NPP was greater than the pre-drought NPP (Figure 1.5). For LAI during the historic drought,

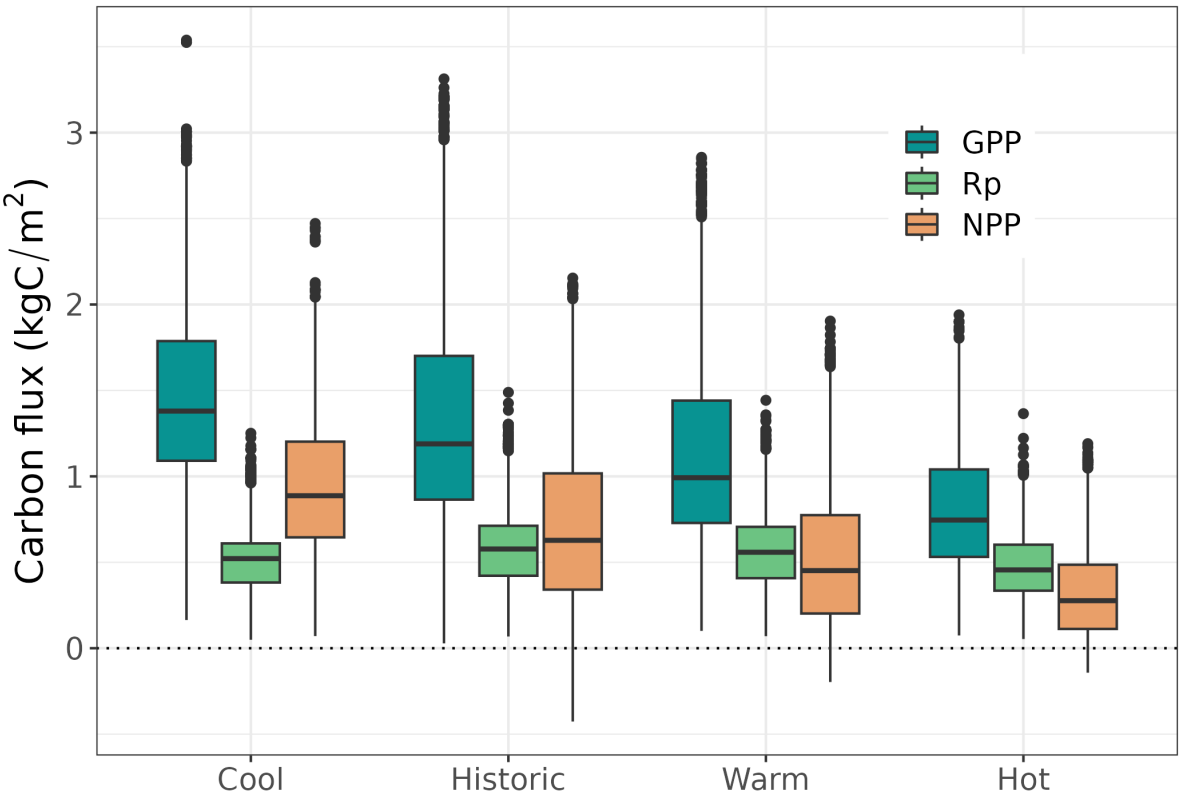

Figure 1.3: Average annual carbon fluxes from 2012-2016, across all tree species parameter uncertainty.

LAI declined the most by 2014 to an average resistance of 0.76. Following the lowest resistance in 2014, LAI begins to recover. The average LAI resilience across all trees was 1.07 for the historic drought (Figure 1.6). A full time series of LAI and NPP resistance and resilience is included in Appendix A.

Compared to the historic drought, the temperature scenarios maintained a similar temporal pattern of NPP and LAI resistance and resilience but altered the magnitudes. In the cool drought, the average NPP resistance was higher than in the historic drought, but the resilience was lower. NPP resilience was sensitive to the temperature increase: the warm drought was similar to the historic drought, with an average resilience of 1.33, however, the hot drought average NPP resilience was the lowest of all the drought scenarios at 0.94 (Figure 1.5).

LAI resistance and resilience had greater variation across temperature scenarios than NPP. The cool drought had a higher average LAI resistance than the historic drought at 0.94 and about the same resilience of 1.08. Both warm and hot temperature scenarios had less LAI resistance and resilience compared to the historic, with hot drought being the lowest with a resistance of 0.52 and resilience of 0.73 (Figure 1.6).

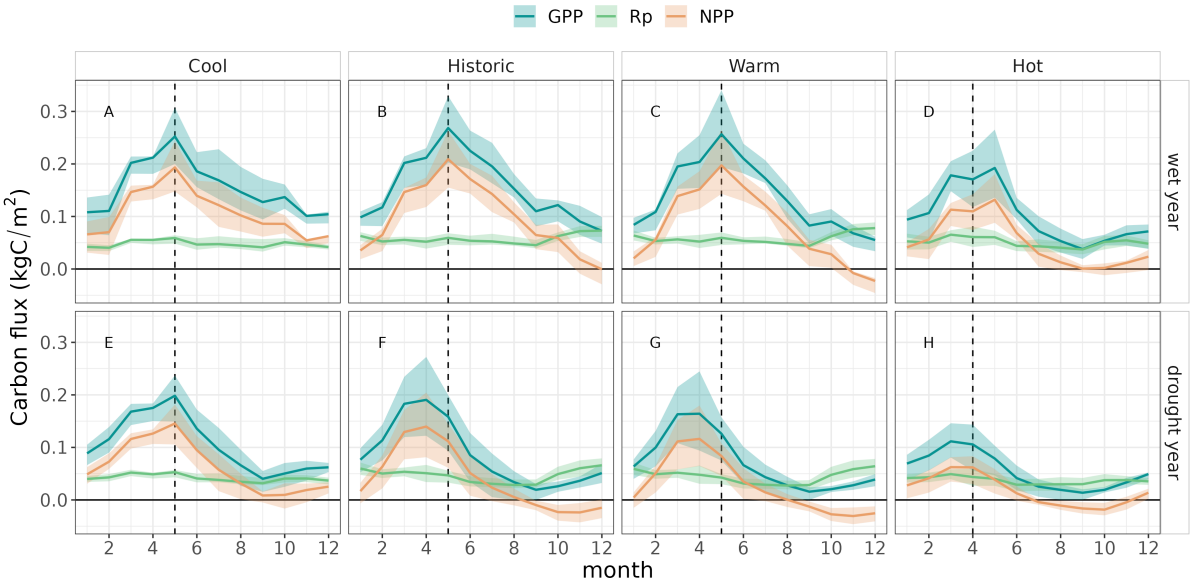

Figure 1.4: Monthly carbon fluxes for wet years (2011 and 2017) and drought year (2012-2016). Bold line is the mean, and shaded area is first and third quartiles, with parameter uncertainty across all tree species. Dashed vertical line represents month when 50% of annual GPP is reached, on average.

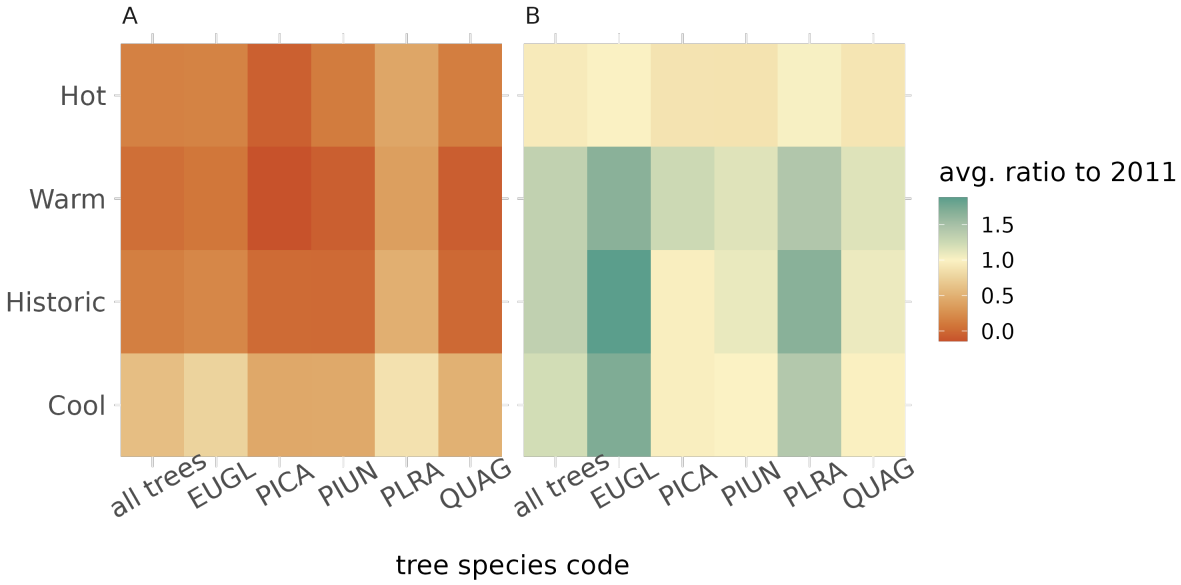

Figure 1.5: Aggregated by tree species and temperatures: (a) Lowest average NPP resistance during drought in 2013 and (b) average NPP resilience post-drought in 2017. In the historic scenario, all trees had an average resilience of 1.34. Tree species codes are shown in Table 1.3.

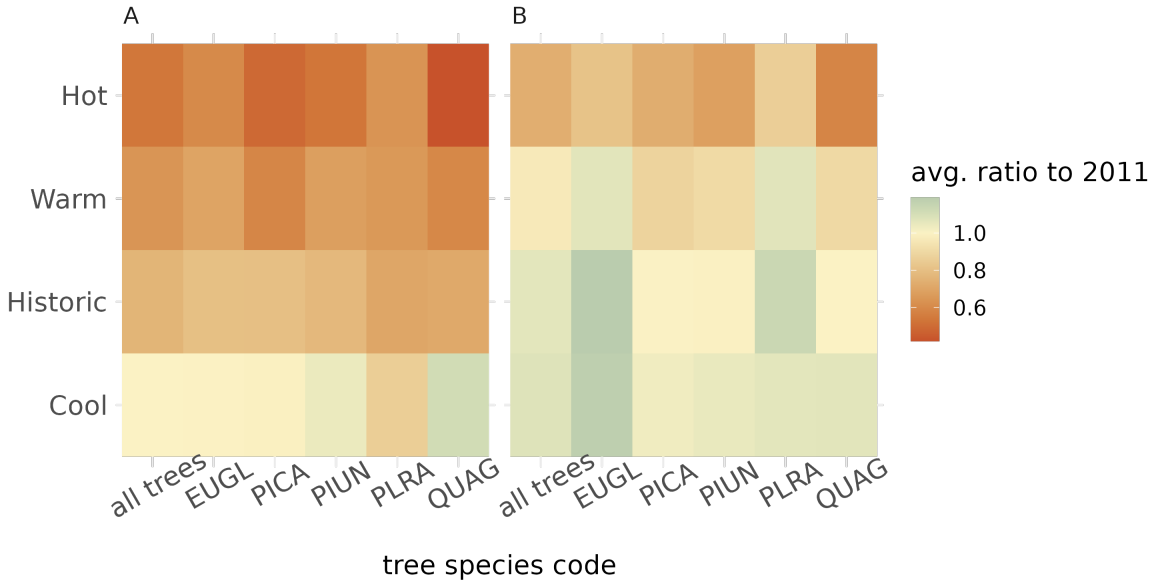

Figure 1.6: Across all tree species and temperatures: (a) Lowest average LAI resistance during drought in 2014 and (b) average LAI resilience post-drought in 2017. Tree species codes are shown in Table 1.3.

Resistance and resilience metrics were also compared across tree species parameter sets. Most tree species were sensitive to temperature differences, with the cool drought increasing resistance and the warm and hot droughts decreasing resistance and resilience, with the exception of EUGL and PLRA. These two species stand out due to their lack of temperature sensitivity and high resilience. In the historic drought, PLRA and EUGL had the highest average NPP resilience of 1.6 and 1.8 (Figure 1.5), and the highest average LAI resilience at 1.14 and 1.19 (Figure 1.6). Despite most of the trees having low resistance and a resilience less than 1 in the hot drought, PLRA, the only deciduous tree, maintains resistance and resilience values comparable to the other species cool and historic drought values. In comparison, QUAG and PIUN, both evergreen species, show the greatest variation in response to temperature changes. For example, QUAG has an average cool drought LAI resistance and resilience of 1.11 and 1.07, but these are lowered to 0.42 and 0.58 in the hot drought.

1.4 Discussion

1.4.1 Model validation and limitations

The results for average annual NPP during the period 2011-2017 for the historic temperature scenario had a mean and standard deviation of 0.67 ± 0.45 kgCm^{-2}yr^{-1} across tree species. These model outputs of annual carbon fluxes are comparable to results

from other RHESSys modeling studies done in the Santa Barbara region, where values of annual NPP ranged from -0.2 to 0.6 (56; 37). Field studies on urban carbon sequestration and fluxes are limited, however, RHESSys estimates are within range of field studies that estimated NPP with biometric equations for other California cities, including Los Angeles, where estimates of annual NPP were between 0.107-0.33 $kgCm^{-2}yr^{-1}$ (57). While the average of modeled values in this study is larger than these estimates, the lower end of model estimates are comparable, and larger values may be expected for Santa Barbara which is slightly cooler and wetter relative to Los Angeles.

Comparing drought resistance and resilience metrics to observational studies can be challenging due to differences in ecological variables used and definitions of pre-drought and post-drought periods. Along with post-drought timing, metrics of drought resistance and resilience are sensitive to the baseline used, and depend on the process or state being looked at (23; 22; 58; 59). These limitations should be considered when comparing the metrics across studies, however, we find the resistance and resilience metrics useful for comparing across the different temperature scenarios and tree species within this study.

We defined resilience using the year 2017 as post-drought conditions because it was a normal wet year that brought an end to the drought, and because we had vegetation data for this year. In reality, the resilience of vegetation to drought depends on which process or property is being looked at, and how post-drought is being defined. Subsequent droughts that occur during the recovery process can have increasingly severe impacts on already weakened trees, especially for conifers (60). Lloret et al. 2011 (24) used tree ring data from natural ponderosa pine forests to look at drought resilience, considering a post-drought performance of 5 years, while Yang et al. 2021(26) used the Enhanced Vegetation Index to show that natural forests in California had not fully recovered 24-36 months post-drought. For GPP, Schwalm et al. 2017 (61) found that, globally, recovery periods ranged from 6-24 months post-drought, which is comparable to our timing and results.

There are limitations to our study as models are imperfect representations of reality. Data limitations also preclude accounting for microclimate and subsurface storage and drainage distinctions across tree locations. Finally, our study did not account for irrigation, which may affect tree resilience in Santa Barbara. While most of the tree species are located in natural parks, there is a possibility that there are additional water sources to the trees from neighboring irrigated turfgrass lawn areas or from subsurface pipe leakage. During the drought, residents were encouraged to stop watering their lawns, however, some mature trees required irrigation to maintain (62), and this was not included in this study.

1.4.2 Tree species differences and ecophysiological parameters

The variation in drought resistance and resilience across tree species is due to differences in ecophysiological parameters, most of which represent species traits. While previous ecohydrologic modeling studies have used general vegetation parameters representa-

tive of tree plant functional types based on available data (42; 63; 64), this study went a step further to parameterize vegetation using a sensitivity analysis and tree species-level remote sensing data of LAI and NDVI.

The sensitivity analysis compared differences in evergreen and deciduous tree parameters that affect the uncertainty in model outcomes of LAI and NPP, and their resilience. For evergreen trees, SLA was among the most responsible for the uncertainty in the outcomes, while for the deciduous tree leaf turnover rate had the most influence for all outcomes (Figure 1.1). This result was expected, as both SLA and leaf turnover contribute to the allometric equations in RHESSys that estimate LAI (56; 35). Deciduous tree resilience results were slightly sensitive to parameters associated with the carbon allocation strategy used in this study, including the 'C transfer to storage proportion', which determines annual allocation to storage, and 'waring A', which affects how much leaf carbon allocation changes with water limitation (Table 1.1). This agrees with (41), who also found that parameter uncertainty within a selected carbon allocation strategy should be considered when modeling forest carbon cycling.

In comparing the drought response of different tree species, we found the California Sycamore (PLRA) maintained a higher resistance and resilience for all temperature scenarios due to greater leaf turnover rates than the other species as a deciduous tree. The Blue Gum Eucalyptus also had higher drought resilience, which could be due to a combination of different parameters including specific leaf area and soil pore size index.

Besides parameters relating to LAI and carbon allocation, parameters that relate to water potential contributed to model output. Both tree types' pre-drought NPP were sensitive to the parameter that determines the water potential when stomates close ('psi at complete stomatal closure' in Figure 1.1). However, the resilience of evergreen was sensitive to this parameter while deciduous was not, which could be due to evergreen trees using stomatal conductance as a water-saving measure in the dry season (65). Of the two soil parameters tested, the pore size index was important for all results, which is aligned with (42), who found that RHESSys soil parameter uncertainty influenced plant water use. Drought resilience sensitivity to soil pore size index suggests that a single tree species will have spatial variability in drought responses due to differences in site soil properties, especially for urban areas where the soil is often compacted or altered (66; 67; 68).

Although some of the parameters tested are specific to RHESSys and represent values that are not quantifiable through fieldwork, other parameters, such as stomatal closure, carbon turnover rates, and SLA, are measurable characteristics. Available data on these traits for this study site were limited, but there is a growing number of field studies collecting data on urban tree traits and phenology (69; 70; 71). The high sensitivity of modeled drought responses to these parameters suggests that field-based measurements under different climate conditions would be a valuable contribution to understanding urban tree drought responses.

1.4.3 Drought effects on NPP and LAI

We found that with increased temperature, drought resistance for both LAI and NPP decreases, suggesting there will be less carbon sequestration during future droughts with warming due to climate change. However, in the warm drought with temperatures increased by 1.8°C, a low resistance was followed by a high resilience for both NPP and LAI (Figures 1.5, 1.6). Changes to NPP during drought were driven by the changes to GPP, which was affected more by water limitation than R_p (72).

The pattern of low resistance and high resilience is a strategy for tree drought survival, where growth is restrained under water limitation but is followed by an increase in GPP after a rewatering event (73; 26). In Mediterranean climates, forest productivity depends on seasonal climate patterns for annual rainfall which occurs during the winter and early spring (74; 75; 76). The higher temperatures in the winter during the rewatering in 2017 caused the historic and warm drought scenarios to increase GPP during the winter when vegetation is normally energy limited.

In addition to a decline in annual GPP, our model simulations of NPP during drought were a result of reduced LAI. While RHESSys does not explicitly account for elevated leaf senescence as a strategic drought response within the phenology model, it does implicitly account for greater leaf senescence because of drought effects on carbon intake. In the carbon allocation submodule, during a normal hydrologic year, the leaf turnover gets replaced by new leaf growth to maintain a full canopy. Once water is limited, the lost leaf biomass is not replaced because there is less carbon available to allocate to leaves due to the decline in NPP. The carbon allocation strategy used in the model is based on resource limitation and is set up for carbon allocation to prioritize roots rather than leaves when water limited. This agrees with studies that found that under a moderate soil drought, plants will increase their root-to-shoot ratio to expand their access to available water, at the loss of leaf carbon (77; 78; 73). This shift in carbon allocation from new leaves to roots may help reduce drought stress but it may also reduce photosynthesis and carbon storage, which could lessen the ability to regrow LAI post-drought or in extreme conditions lead to mortality from carbon starvation (79; 80; 81).

This study focused on short-term recovery and found that most trees had fully recovered their LAI and returned to pre-drought NPP values within a year following the cool, historic, and warm droughts. As noted by Gessler et al. 2020 (22), it is possible that post-disturbance trees will not return to pre-drought states and instead acclimate to a new state. This could be the case for the hot drought scenario, where the average LAI resilience for all trees was below 1. In the future as extreme heat and repeated droughts intensify, trees may acclimate by reducing their LAI to less than the pre-drought state (60).

1.5 Conclusion

Trees planted in Southern California cities will need to survive more frequent extreme heat and drought in the future. To gain insight on how tree canopy drought resilience changes with temperature, this study used a novel method of parameterization for common urban trees in an ecohydrological model. We then simulated how tree LAI and NPP changed over the 2012-2016 California drought, which was compared with scenarios of cooler and warmer future drought. We did not include irrigation as a part of this study, but it should be noted that many cities in arid and semi-arid climates rely on irrigation to maintain their vegetation. In the following chapters, I consider the role of irrigation on urban tree resilience to drought and heatwaves.

Using the model, we found that the more temperature increases during drought the greater the decline in tree LAI and NPP resistance. However, in Mediterranean climates where energy and water availability are typically seasonal, moderate warming up to 1.8°C during a wet year can help stimulate post-drought LAI recovery and increase resilience to values above 1. With extreme warming of 4°C, average LAI resilience was reduced to below 1. This difference in post-drought LAI response indicates there is likely a temperature threshold above which warmer droughts will impact resilience and may lead to further decline or acclimation for subsequent drought events.

With remote sensing estimates of LAI and NDVI to constrain vegetation parameters, we assessed which ecophysiological characteristics were important for drought responses in a sensitivity analysis. We found that LAI and NPP response to drought are sensitive to carbon turnover rates, leaf carbon allocation, and specific leaf area. All outcomes were sensitive to soil pore size index.

Urban trees that support drought resilience should be prioritized for climate change adaptation and for maintaining ecosystem services during extreme events (82; 21). With the threat of increasing drought frequency in Mediterranean climates including the U.S. Southwest (83; 33; 55), we have shown that future urban trees may experience greater resilience due to warmer wet seasons post-drought, or decreased resilience if warming is extreme at 4°C. By incorporating field data and simulating species-level traits that contribute to drought resilience, modeling studies can help inform tree selection and management decisions for climate adaptation.

1.6 Permissions and Attributions

1. The content of Chapter 1 and information on RHESSys vegetation parameters in Appendix A is the result of the generous contribution of data and insight from Mike Alonzo and David Miller.

A Appendix

This appendix contains an additional Figure (1.7) that displays a time series of NPP and LAI changes during drought for each temperature scenario with tree parameter uncertainty across all species. It also includes 3 supporting tables that are linked as files on Box (section A.1). These tables include full lists of RHESSys parameters and sources (Table A1), filtered parameter sets by tree species (Table A2), and full Sobol sensitivity results (Table A3). This appendix also includes a data availability statement with links to data sources and references to R packages in section A.2.

A.1 Tables and Figures

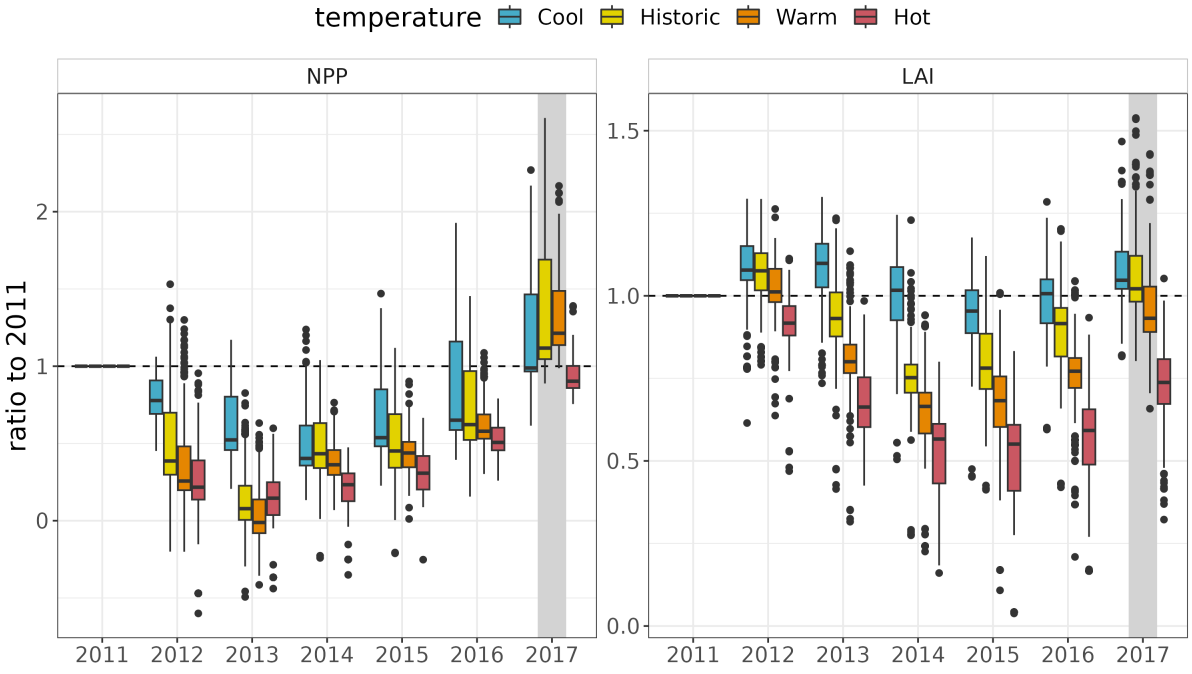

Figure 1.7: Drought resistance (years 2012-2016) and resilience (grey bar highlighting 2017) for NPP (left) and LAI (right). Boxplots include parameter uncertainty across all tree species.

Three excel files to support the set up and results of the Sobol sensitivity analysis done in this study are included here. This chapter has plans for a future publication where these tables will be available as Supplementary information.

Table A1. List of RHESSys vegetation and soil parameters used in Sobol sensitivity analysis, with parameter name used in model, a short description, units, and a list of sources for starting values of the parameter range input to sensitivity analysis. Sources

include field studies, other modeling studies, and information about specific parameters, and are listed in the references of main paper.

Link to Table A1

Table A2. For each tree species, list of parameter minimum, maximum, and mean from the ranges used in this study after filtering.

Link to Table A2

Table A3. Full results of Sobol sensitivity analysis for all parameters. The file includes 4 sheets for each model outcome: LAI, LAI resilience, NPP, and NPP resilience. Each table contains the parameters, in order of descending Sobol index values, with the first and total order indices, the bias, standard error (std. error), minimum confidence interval (min c.i.), and maximum confidence interval (max c.i.). The tables are repeated for evergreen and deciduous functional types.

Link to Table A3

A.2 Data Availability

The Regional Hydrio-Ecologic Simulation System (RHESSys), version 7.4 (36) was used, along with the R package RHESSysIOinR (84) for running model simulations and processing output. Both RHESSys and RHESSysIOinR can be accessed via github (`https://github.com/RHESSys`). R and RStudio was used to analyze model outputs and create all plots (85). Sobol analysis was done using the R package Sensitivity (86). The following data used to input to the model is publicly available: daily rainfall from Santa Barbara county (87), daily minimum and maximum temperature from NOAA (88), Cal-Adapt downscaled climate projections (89) , and tree characteristics from the Biomass And Allometry Database for woody plants (BAAD), which was accessed using the R package baad.data (found at `https://github.com/dfalster/baad` (90). RHESSys model outputs for this paper are available to download on Hydroshare (91).

The code used to run RHESSys and analyze output, and resulting tables, are available to view on GitHub at: `https://github.com/rachtorr/VegParamsSA`

Chapter 1 References

[1] P. Bolund and S. Hunhammar, *Ecosystem services in urban areas*, *Ecological Economics* **29** (1999), no. 2 293–301.

[2] S. J. Livesley, G. M. McPherson, and C. Calfapietra, *The Urban Forest and Ecosystem Services: Impacts on Urban Water, Heat, and Pollution Cycles at the Tree, Street, and City Scale*, *Journal of Environment Quality* **45** (2016), no. 1 119.

[3] G. Sun, D. Hallema, and H. Asbjornsen, *Ecohydrological processes and ecosystem services in the Anthropocene: a review*, *Ecological Processes* **6** (2017), no. 1 35.

[4] A. Paschalis, T. Chakraborty, S. Fatichi, N. Meili, and G. Manoli, *Urban Forests as Main Regulator of the Evaporative Cooling Effect in Cities*, *AGU Advances* **2** (2021), no. 2 e2020AV000303.

[5] J. B. Winbourne, T. S. Jones, S. M. Garvey, J. L. Harrison, L. Wang, D. Li, P. H. Templer, and L. R. Hutyra, *Tree Transpiration and Urban Temperatures: Current Understanding, Implications, and Future Research Directions*, *BioScience* **70** (2020), no. 7 576–588.

[6] A. AghaKouchak, L. Cheng, O. Mazdiyasni, and A. Farahmand, *Global warming and changes in risk of concurrent climate extremes: Insights from the 2014 California drought*, *Geophysical Research Letters* **41** (2014), no. 24 8847–8852.

[7] Lund Jay, Medellin-Azuara Josue, Durand John, and Stone Kathleen, *Lessons from California's 2012–2016 Drought*, *Journal of Water Resources Planning and Management* **144** (2018), no. 10 04018067.

[8] D. J. N. Young, J. T. Stevens, J. M. Earles, J. Moore, A. Ellis, A. L. Jirka, and A. M. Latimer, *Long-term climate and competition explain forest mortality patterns under extreme drought*, *Ecology Letters* **20** (2017), no. 1 78–86.

[9] N. S. Diffenbaugh, D. L. Swain, and D. Touma, *Anthropogenic warming has increased drought risk in California*, *Proc Natl Acad Sci USA* **112** (2015), no. 13.

[10] J. Zscheischler and S. I. Seneviratne, *Dependence of drivers affects risks associated with compound events*, *Science Advances* **3** (2017), no. 6 e1700263.

[11] N. S. Bijoor, H. R. McCarthy, D. Zhang, and D. E. Pataki, *Water sources of urban trees in the Los Angeles metropolitan area*, *Urban Ecosystems* **15** (2012), no. 1 195–214.

[12] C. Gómez-Navarro, D. E. Pataki, G. J. Bowen, and E. J. Oerter, *Spatiotemporal variability in water sources of urban soils and trees in the semiarid, irrigated Salt Lake Valley*, *Ecohydrology* **12** (2019), no. 8 e2154.

[13] E. Litvak, K. F. Manago, T. S. Hogue, and D. E. Pataki, *Evapotranspiration of urban landscapes in Los Angeles, California at the municipal scale*, *Water Resources Research* **53** (2017), no. 5 4236–4252.

[14] H. R. McCarthy and D. E. Pataki, *Drivers of variability in water use of native and non-native urban trees in the greater Los Angeles area*, *Urban Ecosyst* **13** (2010), no. 4 393–414.

[15] C. J. Fettig, L. A. Mortenson, B. M. Bulaon, and P. B. Foulk, *Tree mortality following drought in the central and southern Sierra Nevada, California, U.S.*, *Forest Ecology and Management* **432** (2019) 164–178.

[16] C. Calfapietra, J. Peñuelas, and Ü. Niinemets, *Urban plant physiology: adaptation-mitigation strategies under permanent stress*, *Trends in Plant Science* **20** (2015), no. 2 72–75.

[17] C. Ordóñez and P. Duinker, *Assessing the vulnerability of urban forests to climate change*, *Environ. Rev.* **22** (2014), no. 3 311–321.

[18] A. Roloff, S. Korn, and S. Gillner, *The Climate-Species-Matrix to select tree species for urban habitats considering climate change*, *Urban Forestry & Urban Greening* **8** (2009), no. 4 295–308.

[19] J. Yang, *Assessing the Impact of Climate Change on Urban Tree Species Selection: A Case Study in Philadelphia*, *Journal of Forestry* **107** (2009), no. 7 364–372.

[20] M. Avolio, D. E. Pataki, T. Gillespie, G. D. Jenerette, H. R. McCarthy, S. Pincetl, and L. Weller-Clarke, *Tree diversity in southern California's urban forest: the interacting roles of social and environmental variables*, *Front. Ecol. Evol.* **3** (2015).

[21] E. McPherson, A. M. Berry, and N. S. van Doorn, *Performance testing to identify climate-ready trees*, *Urban Forestry & Urban Greening* **29** (2018) 28–39.

[22] A. Gessler, A. Bottero, J. Marshall, and M. Arend, *The way back: recovery of trees from drought and its implication for acclimation*, *New Phytologist* **228** (2020), no. 6 1704–1709.

[23] D. Castagneri, G. Vacchiano, A. Hacket-Pain, R. J. DeRose, T. Klein, and A. Bottero, *Meta-analysis Reveals Different Competition Effects on Tree Growth Resistance and Resilience to Drought*, *Ecosystems* (2021).

[24] F. Lloret, E. G. Keeling, and A. Sala, *Components of tree resilience: effects of successive low-growth episodes in old ponderosa pine forests*, *Oikos* **120** (2011), no. 12 1909–1920.

[25] S. L. Malone, M. G. Tulbure, A. J. Pérez-Luque, T. J. Assal, L. L. Bremer, D. P. Drucker, V. Hillis, S. Varela, and M. L. Goulden, *Drought resistance across California ecosystems: evaluating changes in carbon dynamics using satellite imagery*, *Ecosphere* **7** (2016), no. 11 e01561.

[26] X. Yang, X. Xu, A. Stovall, M. Chen, and J.-E. Lee, *Recovery: Fast and Slow—Vegetation Response During the 2012–2016 California Drought*, *Journal of Geophysical Research: Biogeosciences* **126** (2021), no. 4 e2020JG005976.

[27] E. B. Wetherley, J. P. McFadden, and D. A. Roberts, *Megacity-scale analysis of urban vegetation temperatures*, *Remote Sensing of Environment* **213** (2018) 18–33.

[28] M. A. Allen, D. A. Roberts, and J. P. McFadden, *Reduced urban green cover and daytime cooling capacity during the 2012–2016 California drought*, *Urban Climate* **36** (2021) 100768.

[29] M. Alonzo, B. Bookhagen, and D. A. Roberts, *Urban tree species mapping using hyperspectral and lidar data fusion*, *Remote Sensing of Environment* **148** (2014) 70–83.

[30] D. L. Miller, M. Alonzo, D. A. Roberts, C. L. Tague, and J. P. McFadden, *Drought response of urban trees and turfgrass using airborne imaging spectroscopy*, *Remote Sensing of Environment* **240** (2020) 111646.

[31] K. J. Quesnel, N. Ajami, and A. Marx, *Shifting landscapes: decoupled urban irrigation and greenness patterns during severe drought*, *Environ. Res. Lett.* **14** (2019), no. 6 064012.

[32] M. Alonzo, J. P. McFadden, D. J. Nowak, and D. A. Roberts, *Mapping urban forest structure and function using hyperspectral imagery and lidar data*, *Urban Forestry & Urban Greening* **17** (2016) 135–147.

[33] B. I. Cook, T. R. Ault, and J. E. Smerdon, *Unprecedented 21st century drought risk in the American Southwest and Central Plains*, *Science Advances* **1** (2015), no. 1 e1400082.

[34] W. Rouse and R. H. Haas, *Monitoring vegetation systems in the great plains with erts*, *NASA special publications* (1974).

[35] C. L. Tague and L. Band, *RHESSys: Regional Hydro-Ecologic Simulation System—An Object-Oriented Approach to Spatially Distributed Modeling of Carbon, Water, and Nutrient Cycling*, *Earth Interactions* **8** (2004), no. 19 1–42.

[36] Tague and Band, *Regional hydor-ecological simulation system*, 2004.

[37] C. Shields and C. Tague, *Ecohydrology in semiarid urban ecosystems: Modeling the relationship between connected impervious area and ecosystem productivity*, *Water Resources Research* **51** (2015), no. 1 302–319.

[38] E. J. Hanan, C. N. Tague, and J. P. Schimel, *Nitrogen cycling and export in California chaparral: the role of climate in shaping ecosystem responses to fire*, *Ecological Monographs* **87** (2017), no. 1 76–90.

[39] C. D. Bell, C. L. Tague, and S. K. McMillan, *Modeling Runoff and Nitrogen Loads From a Watershed at Different Levels of Impervious Surface Coverage and Connectivity to Storm Water Control Measures*, *Water Resources Research* **55** (2019), no. 4 2690–2707.

[40] B. Miles and L. E. Band, *Green infrastructure stormwater management at the watershed scale: urban variable source area and watershed capacitance*, *Hydrological Processes* **29** (2015), no. 9 2268–2274.

[41] E. S. Garcia, C. L. Tague, and J. S. Choate, *Uncertainty in carbon allocation strategy and ecophysiological parameterization influences on carbon and streamflow estimates for two western US forested watersheds*, *Ecological Modelling* **342** (2016) 19–33.

[42] C. Shields and C. Tague, *Assessing the Role of Parameter and Input Uncertainty in Ecohydrologic Modeling: Implications for a Semi-arid and Urbanizing Coastal California Catchment*, *Ecosystems* **15** (2012), no. 5 775–791.

[43] G. D. Farquhar and S. von Caemmerer, *Modelling of Photosynthetic Response to Environmental Conditions*, in *Physiological Plant Ecology II: Water Relations and Carbon Assimilation* (O. L. Lange, P. S. Nobel, C. B. Osmond, and H. Ziegler, eds.), Encyclopedia of Plant Physiology, pp. 549–587. Springer, Berlin, Heidelberg, 1982.

[44] P. G. Jarvis, J. L. Monteith, and P. E. Weatherley, *The interpretation of the variations in leaf water potential and stomatal conductance found in canopies in the field*, *Philosophical Transactions of the Royal Society of London. B, Biological Sciences* **273** (1976), no. 927 593–610.

[45] J. J. Landsberg and R. H. Waring, *A generalised model of forest productivity using simplified concepts of radiation-use efficiency, carbon balance and partitioning*, *Forest Ecology and Management* **95** (1997), no. 3 209–228.

[46] D. W. Pierce, D. R. Cayan, and B. L. Thrasher, *Statistical Downscaling Using Localized Constructed Analogs (LOCA)*, *J. Hydrometeor.* **15** (2014), no. 6 2558–2585.

[47] I. M. Sobol', *Global sensitivity indices for nonlinear mathematical models and their Monte Carlo estimates*, *Mathematics and Computers in Simulation* **55** (2001), no. 1 271–280.

[48] J. Nossent, P. Elsen, and W. Bauwens, *Sobol' sensitivity analysis of a complex environmental model*, *Environmental Modelling & Software* **26** (2011), no. 12 1515–1525.

[49] F. Sarrazin, F. Pianosi, and T. Wagener, *Global Sensitivity Analysis of environmental models: Convergence and validation*, *Environmental Modelling & Software* **79** (2016) 135–152.

[50] F. Pianosi, K. Beven, J. Freer, J. W. Hall, J. Rougier, D. B. Stephenson, and T. Wagener, *Sensitivity analysis of environmental models: A systematic review with practical workflow*, *Environmental Modelling & Software* **79** (2016) 214–232.

[51] D. P. Turner, S. V. Ollinger, and J. S. Kimball, *Integrating Remote Sensing and Ecosystem Process Models for Landscape- to Regional-Scale Analysis of the Carbon Cycle*, *BioScience* **54** (2004), no. 6 573.

[52] Q. Wang, S. Adiku, J. Tenhunen, and A. Granier, *On the relationship of NDVI with leaf area index in a deciduous forest site*, *Remote Sensing of Environment* **94** (2005), no. 2 244–255.

[53] D. W. Pierce, J. F. Kalansky, and D. R. Cayan, *Climate, Drought, and Sea Level Rise Scenarios for California's Fourth Climate Change Assessment*, 2018.

[54] K. A. McKinnon, A. Poppick, and I. R. Simpson, *Hot extremes have become drier in the United States Southwest*, *Nature Climate Change* **11** (2021), no. 7 598–604. Number: 7 Publisher: Nature Publishing Group.

[55] P. A. Ullrich, Z. Xu, A. Rhoades, M. Dettinger, J. Mount, A. Jones, and P. Vahmani, *California's drought of the future: A midcentury recreation of the exceptional conditions of 2012–2017*, .

[56] E. J. Hanan, C. Tague, J. Choate, M. Liu, C. Kolden, and J. Adam, *Accounting for disturbance history in models: using remote sensing to constrain carbon and nitrogen pool spin-up*, *Ecol Appl* **28** (2018), no. 5 1197–1214.

[57] D. J. Nowak, E. J. Greenfield, R. E. Hoehn, and E. Lapoint, *Carbon storage and sequestration by trees in urban and community areas of the United States*, *Environmental Pollution* **178** (2013) 229–236.

[58] L. Nikinmaa, M. Lindner, E. Cantarello, A. S. Jump, R. Seidl, G. Winkel, and B. Muys, *Reviewing the Use of Resilience Concepts in Forest Sciences*, *Curr Forestry Rep* **6** (2020), no. 2 61–80.

[59] J. Schwarz, G. Skiadaresis, M. Kohler, J. Kunz, F. Schnabel, V. Vitali, and J. Bauhus, *Quantifying Growth Responses of Trees to Drought—a Critique of Commonly Used Resilience Indices and Recommendations for Future Studies*, *Curr Forestry Rep* **6** (2020), no. 3 185–200.

[60] W. R. L. Anderegg, A. T. Trugman, G. Badgley, A. G. Konings, and J. Shaw, *Divergent forest sensitivity to repeated extreme droughts*, *Nature Climate Change* (2020).

[61] C. R. Schwalm, W. R. L. Anderegg, A. M. Michalak, J. B. Fisher, F. Biondi, G. Koch, M. Litvak, K. Ogle, J. D. Shaw, A. Wolf, D. N. Huntzinger, K. Schaefer, R. Cook, Y. Wei, Y. Fang, D. Hayes, M. Huang, A. Jain, and H. Tian, *Global patterns of drought recovery*, *Nature* **548** (2017), no. 7666 202–205.

[62] A. McCumber, *Building "Natural" Beauty: Drought and the Shifting Aesthetics of Nature in Santa Barbara, California*, *Nature + Culture* **12** (2017), no. 3 246–262.

[63] M. A. White, P. E. Thornton, S. W. Running, and R. R. Nemani, *Parameterization and Sensitivity Analysis of the BIOME–BGC Terrestrial Ecosystem Model: Net Primary Production Controls*, *Earth Interactions* **4** (2000), no. 3 1–85.

[64] V. Marchionni, S. Fatichi, N. Tapper, J. P. Walker, G. Manoli, and E. Daly, *Assessing vegetation response to irrigation strategies and soil properties in an urban reserve in southeast Australia*, *Landscape and Urban Planning* **215** (2021) 104198.

[65] A. I. Chacon, A. Baer, J. K. Wheeler, and J. Pittermann, *Two coastal Pacific evergreens, Arbutus menziesii, Pursh. and Quercus agrifolia, Née show little water stress during California's exceptional drought*, *PLOS ONE* **15** (2020), no. 4 e0230868. Publisher: Public Library of Science.

[66] B. Scharenbroch and M. Catania, *Soil Quality Attributes as Indicators of Urban Tree Performance*, *Arboriculture & Urban Forestry* **38** (2012) 214–228.

[67] L. F. Ow and S. Ghosh, *Urban tree growth and their dependency on infiltration rates in structural soil and structural cells*, *Urban Forestry & Urban Greening* **26** (2017) 41–47.

[68] J. Zhu, Y. Cao, W. He, Q. Xu, C. Xu, and X. Zhang, *Leaf functional traits differentiation in relation to covering materials of urban tree pits*, *BMC Plant Biol* **21** (2021), no. 1 556.

[69] M. Esperon-Rodriguez, P. D. Rymer, S. A. Power, A. Challis, R. M. Marchin, and M. G. Tjoelker, *Functional adaptations and trait plasticity of urban trees along a climatic gradient*, *Urban Forestry & Urban Greening* **54** (2020) 126771.

[70] S. Gillner, S. Korn, M. Hofmann, and A. Roloff, *Contrasting strategies for tree species to cope with heat and dry conditions at urban sites*, *Urban Ecosystems* **20** (2017), no. 4 853–865.

[71] M. Sharmin, M. G. Tjoelker, S. Pfautsch, M. Esperón-Rodriguez, P. D. Rymer, and S. A. Power, *Tree Traits and Microclimatic Conditions Determine Cooling Benefits of Urban Trees*, *Atmosphere* **14** (2023), no. 3 606.

[72] J. von Buttlar, J. Zscheischler, A. Rammig, S. Sippel, M. Reichstein, A. Knohl, M. Jung, O. Menzer, M. A. Arain, N. Buchmann, A. Cescatti, D. Gianelle, G. Kiely, B. E. Law, V. Magliulo, H. Margolis, H. McCaughey, L. Merbold, M. Migliavacca, L. Montagnani, W. Oechel, M. Pavelka, M. Peichl, S. Rambal, A. Raschi, R. L. Scott, F. P. Vaccari, E. van Gorsel, A. Varlagin, G. Wohlfahrt, and M. D. Mahecha, *Impacts of droughts and extreme-temperature events on gross primary production and ecosystem respiration: a systematic assessment across ecosystems and climate zones*, *Biogeosciences* **15** (2018), no. 5 1293–1318.

[73] Z. Xu, G. Zhou, and H. Shimizu, *Plant responses to drought and rewatering*, *Plant Signaling & Behavior* **5** (2010), no. 6 649–654.

[74] C. Dong, G. MacDonald, G. S. Okin, and T. W. Gillespie, *Quantifying Drought Sensitivity of Mediterranean Climate Vegetation to Recent Warming: A Case Study in Southern California*, *Remote Sensing* **11** (2019), no. 24 2902.

[75] W. Nijland, E. Jansma, E. A. Addink, M. Domínguez Delmás, and S. M. De Jong, *Relating ring width of Mediterranean evergreen species to seasonal and annual variations of precipitation and temperature*, *Biogeosciences* **8** (2011), no. 5 1141–1152.

[76] C. Truettner, W. R. L. Anderegg, F. Biondi, G. W. Koch, K. Ogle, C. Schwalm, M. E. Litvak, J. D. Shaw, and E. Ziaco, *Conifer radial growth response to recent seasonal warming and drought from the southwestern USA*, *Forest Ecology and Management* **418** (2018) 55–62.

[77] R. P. Phillips, I. Ibáñez, L. D'Orangeville, P. J. Hanson, M. G. Ryan, and N. G. McDowell, *A belowground perspective on the drought sensitivity of forests: Towards improved understanding and simulation*, *Forest Ecology and Management* **380** (2016) 309–320.

[78] H. Poorter, K. J. Niklas, P. B. Reich, J. Oleksyn, P. Poot, and L. Mommer, *Biomass allocation to leaves, stems and roots: meta-analyses of interspecific variation and environmental control*, *New Phytol* **193** (2012), no. 1 30–50.

[79] L. Galiano, J. Martínez-Vilalta, and F. Lloret, *Carbon reserves and canopy defoliation determine the recovery of Scots pine 4 yr after a drought episode*, *New Phytologist* **190** (2011), no. 3 750–759.

[80] A. S. Jump, P. Ruiz-Benito, S. Greenwood, C. D. Allen, T. Kitzberger, R. Fensham, J. Martínez-Vilalta, and F. Lloret, *Structural overshoot of tree growth with climate variability and the global spectrum of drought-induced forest dieback*, *Global Change Biology* **23** (2017), no. 9 3742–3757.

[81] N. McDowell, W. T. Pockman, C. D. Allen, D. D. Breshears, N. Cobb, T. Kolb, J. Plaut, J. Sperry, A. West, D. G. Williams, and E. A. Yepez, *Mechanisms of plant survival and mortality during drought: why do some plants survive while others succumb to drought?*, *New Phytologist* **178** (2008), no. 4 719–739.

[82] K. Lanza and B. Stone, *Climate adaptation in cities: What trees are suitable for urban heat management?*, *Landscape and Urban Planning* **153** (2016) 74–82.

[83] C. D. Allen, A. K. Macalady, H. Chenchouni, D. Bachelet, N. McDowell, M. Vennetier, T. Kitzberger, A. Rigling, D. D. Breshears, E. H. T. Hogg, P. Gonzalez, R. Fensham, Z. Zhang, J. Castro, N. Demidova, J.-H. Lim, G. Allard, S. W. Running, A. Semerci, and N. Cobb, *A global overview of drought and heat-induced tree mortality reveals emerging climate change risks for forests*, *Forest Ecology and Management* **259** (2010), no. 4 660–684.

[84] R. Bart, W. Burke, and C. Tague, *Rhessysioinr*, 2021.

[85] R Core Team, *R: A Language and Environment for Statistical Computing*. R Foundation for Statistical Computing, Vienna, Austria, 2023.

[86] B. Iooss, S. D. Veiga, A. Janon, G. Pujol, with contributions from Baptiste Broto, K. Boumhaout, T. Delage, R. E. Amri, J. Fruth, L. Gilquin, J. Guillaume, M. Herin, M. I. Idrissi, L. Le Gratiet, P. Lemaitre, A. Marrel, A. Meynaoui, B. L. Nelson, F. Monari, R. Oomen, O. Rakovec, B. Ramos, O. Roustant, E. Song, J. Staum, R. Sueur, T. Touati, V. Verges, and F. Weber, *sensitivity: Global Sensitivity Analysis of Model Outputs*, 2021. R package version 1.27.0.

[87] "Daily rainfall data (xls), station 234."

[88] M. J. Menne, I. Durre, R. S. Vose, B. E. Gleason, and T. G. Houston, *Global historical climatology network - daily (ghcn-daily)*, 2012.

[89] N. Thomas, S. Mukhtyar, B. Galey, and M. Kelly, *Loca derived products*, 2018.

[90] D. Falster, R. FitzJohn, and B. Bond-Lamberty, *baad.data*, 2016.

[91] R. Torres, *Model output for urban trees in santa barbara (rhessys patch scale)*, 2023.

Chapter 2

Exploring potential trade-offs in outdoor water use reductions and urban tree growth during an extreme drought

2.1 Introduction

Cities in Southern California face the challenge of adapting to warmer temperatures and heat waves that exacerbate urban heat islands (UHI), and one strategy to combat heat is to increase and maintain urban tree cover. Climate change will cause not only rising temperatures but increased aridity and frequency of drought (1; 2; 3; 4). Because a large portion of urban water use goes towards outdoor use, the combination of drought and heat waves requires more efficient water use for Southern California to sustain urban water resources for landscape management (5; 6). Urban trees contribute to climate change adaptation by offering several ecosystem services including stormwater filtration, carbon sequestration, UHI mitigation, and psychological benefits for residents (7; 8; 9; 10). However, for trees to provide cooling they require adequate water, which becomes limited during drought because of scarcity and conservation mandates on outdoor water use (11; 12; 13).

Outdoor water use is a significant fraction of total water use in residential areas, estimated to be between 18-35% in Southern California (14), and up to 50% in some areas of Los Angeles (15). Because it takes up a substantial portion of the urban water balance, outdoor water use efficiency has been studied throughout Southern California. Irrigation has been shown to be a main driver of lawn transpiration (16; 17; 18), and has caused some urban trees in Los Angeles to acclimate and rely on irrigation along with natural water sources (19; 20). Vegetation outdoor water use has been quantified through estimating evapotranspiration of trees and turfgrass using portable chambers in the Los Angeles region (21; 22). Other tools for estimating outdoor water use include

using water billing data, remote sensing, or monitoring reference evapotranspiration with adjustments for plant types (15; 23).

While it is important to quantify vegetation water use to improve urban water efficiency, fully accounting for the value of outdoor water use should include the indirect effects of ecosystem services provided by trees. In semi-arid climates, outdoor water contributes to UHI mitigation through maintaining healthy tree canopy cover for shade provision and increasing latent heat from evapotranspiration (24; 25). Studies have used atmospheric coupled land surface models to demonstrate the effects of irrigation on cooling the microclimate in semi-arid cities (26; 11; 27; 28; 29). For urban parks in a variety of climates, it's been shown that intercepting solar radiation through shade and increasing leaf area index (LAI) is more effective for reducing heat load at the surface than reducing air temperatures (30; 31). Because of their ability to provide shaded areas and reduce heat stress on people, tree maintenance and health should be considered along with water use restrictions, especially when heat waves coincide with drought. However, balancing both maintaining tree health and conserving water may lead to trade-offs.

During drought, outdoor water conservation mandates have been set primarily to save water, and few studies have considered whether there are indirect effects on urban tree health. This study examines the role of irrigation in maintaining urban tree health during the 2012-2016 California drought that was classified as 'exceptional' by the U.S. Drought Monitor (3). In 2014, extreme warm temperatures coincided with low precipitation, further straining water resources (32; 33). In 2015, California set a mandatory 25% statewide water use reduction, with urban water districts assigned to different amounts ranging from 4-36% (**?**). We use an ecohydrologic model to explore how reductions to irrigation during drought affect the resilience of tree ecosystem services and whether there are trade-offs between outdoor water conservation and tree health. We also explore how these relationships differ under a warmer drought, as the frequency of higher temperatures during drought is expected to increase with climate change (3; 2).

2.2 Methods

Using an ecohydrologic model, we simulated tree response to historic drought conditions, and a warmer drought, under varied irrigation amounts for select urban tree species in a coastal semi-arid city. We analyzed the effects of reduced irrigation on model outputs of transpiration, net primary productivity (NPP), plant water use efficiency (WUE), and leaf area index (LAI).

2.2.1 Model description and set up

We used the Regional Hydro-Ecologic Simulation System, RHESSys (34), to simulate vegetation ecosystem services with varying scenarios of water input. RHESSys was previously used in semi-arid urban watersheds for analyzing hydrologic parameter uncertainty

on evapotranspiration (35), estimating the effects of urban development on runoff (36), and assessing parameter uncertainty in urban trees and their drought resilience (**?**).

RHESSys simulates carbon, water, energy, and nutrient cycling at several spatial scales. In RHESSys, a watershed is divided into patches, which vary by topography. For our study, we use a single patch to represent a localized area with a single tree species, at $10m^2$ resolution, with only vertical hydrologic flow. Vertical water inputs include precipitation, which can be intercepted by the canopy, infiltrate into the subsurface, or create overland flow. Irrigation is added to any precipitation that infiltrates into the top layer of soil. Soil subsurface layers include the rooting zone defined by the vegetation rooting depth, an unsaturated layer, and a saturated layer. Water flowing out of the saturated layer goes to deeper groundwater storage. Vegetation evapotranspiration is calculated daily using Penman-Monteith. Vapor pressure deficit for the Penman-Monteith is estimated based on minimum and maximum daily temperatures. Soil evaporation is based on energy, atmospheric conditions, and soil moisture.

Vegetation carbon cycling in the model is driven by daily estimates of photosynthesis through the Farquhar model, where the rate of carbon gain per unit LAI depends on available water, nutrients, and light (**?**). Vegetation maintenance and growth respiration depends on these environmental factors and temperature, and net primary productivity (NPP) is calculated from these two fluxes as the difference between gross photosynthesis and plant respiration. Assimilated carbon gets allocated to either the leaves, stems, coarse roots, or fine roots, based on vegetation parameters. The amount allocated uses a semi-mechanistic approach that accounts for resource limitations and LAI (37; 38).

Vegetation parameters play an important role in making the processes within the carbon cycling specific to different tree species. They are taken from a previous study that used RHESSys parameterized with remote sensing data of tree structure to investigate the impacts of drought on selected urban tree species in the same study area used for this current study (1.2.3). In chapter 1, I performed a sensitivity analysis on vegetation parameters that control carbon allocation, turnover rates, ecophysiological traits and mechanisms, as well as soil porosity and air entry pressure. Remote sensing studies' products of estimated LAI (39) and normalized differential vegetation index (NDVI)(40) were used to constrain and select parameters that affected RHESSys output of LAI and NPP at the tree species level. In Chapter 2, we used a sample of these parameters to set up tree species in Santa Barbara for RHESSys simulations under different irrigation scenarios.

2.2.2 Study site and data

The tree species that were parameterized are Coast Live Oak (*Quercus Agrifolia*), California Sycamore (*Platanus Racemos*), Blue Gum Eucalyptus (*Eucalyptus globulus*, Victorian Box (*Pittosporum Undulatum*), and Canary Island Pine (*Pinus canariensis*). These species are among the most common, non-palm trees, in the study area (41), and are representative of native (*Quercus Agrifolia, Platanus Racemos*), non-native (*Euca-*

lyptus globulus, Pittosporum Undulatum, Pinus canariensis), deciduous (*Platanus Racemos*), and evergreen (*Quercus Agrifolia, Eucalyptus globulus, Pittosporum Undulatum, Pinus canariensis*) trees. Most of the urban forest is located on residential property, as street trees, and in urban parks.

These species are a part of a diverse urban forest located in a coastal city with a Mediterranean climate comprised of hot, dry summers and wet winters. The average rainfall in the last 50 years is 482 mm. In 2012-2016 there was a multiyear drought that affected the state of CA, and became 'exceptional' in the U.S. Drought Monitor scale in Santa Barbara county in 2014 (3). The same year, the City of Santa Barbara declared a 'Stage One' drought and asked residents to reduce water consumption by 20%. In 2015 the state mandated that Santa Barbara cut 16% of water consumption (**?**) .

Climate data

The model study period includes water years 2011-2017, with 2011 and 2017 identified as non-drought years (annual average was 699mm) and 2012-2016 as drought years (annual average was 258mm). Several climate datasets were used as an input for the model. The first is a temperature dataset from NOAA (station USC00047902) that includes daily maximum and minimum temperatures. Daily precipitation is from a rain gauge located in downtown Santa Barbara (station ID 234), from Santa Barbara County Public Works Water Resources. The model goes through a 'spin up' period to establish soil and vegetation carbon and nitrogen stores, and this uses observed climate data from 1940-2010. Model outputs are then taken from 2011-2017.

Along with the observed drought, we simulated how this drought would affect urban trees if it were to occur in a future climate with potentially warmer temperatures. The climate change scenario inputs have the same precipitation data, with both minimum and maximum temperatures increased by 1.8°C. This increase is based on analyzing downscaled climate model projections for the city of Santa Barbara from the tool Cal-Adapt (42). The projections show an overall trend of warming, with increased precipitation variability in the Santa Barbara region. To determine potential temperature changes during future drought years, we looked at the temperature difference in years from the RCP8.5 projections with precipitation anomalies similar to the 2012-2016 drought. The mean annual positive temperature difference was about 1.8°C. This temperature increase is within range of temperature changes for this region reported in the California's Fourth Climate Change Assessment (**?**).

Water use data

Monthly irrigation data for the years 2010-2020 were obtained from the City of Santa Barbara Water Resources landscaping accounts, which include large landowners, private residences, and businesses (**?**). To protect the privacy of residents and account owners, the individual accounts were aggregated to a net monthly irrigation amount, which was then normalized by the aggregate area to get the average monthly amount per unit area.

Monthly irrigation was disaggregated to weekly values using the R package tempdisagg (43), which works similar to a linear regression model to transform a high frequency time series to a lower frequency. Weekly values were then split into two so that irrigation input occurred twice per week. It was input during the night, following previous modeling studies that included urban irrigation as an input (44; 29; 27). For this study, the focus is on effects due to reductions to total annual input. In the baseline scenario before the conservation mandates, the average input during summer months was 7mm per watering day. This resulted in annual inputs ranging from 331-566mm (Figure 2.1).

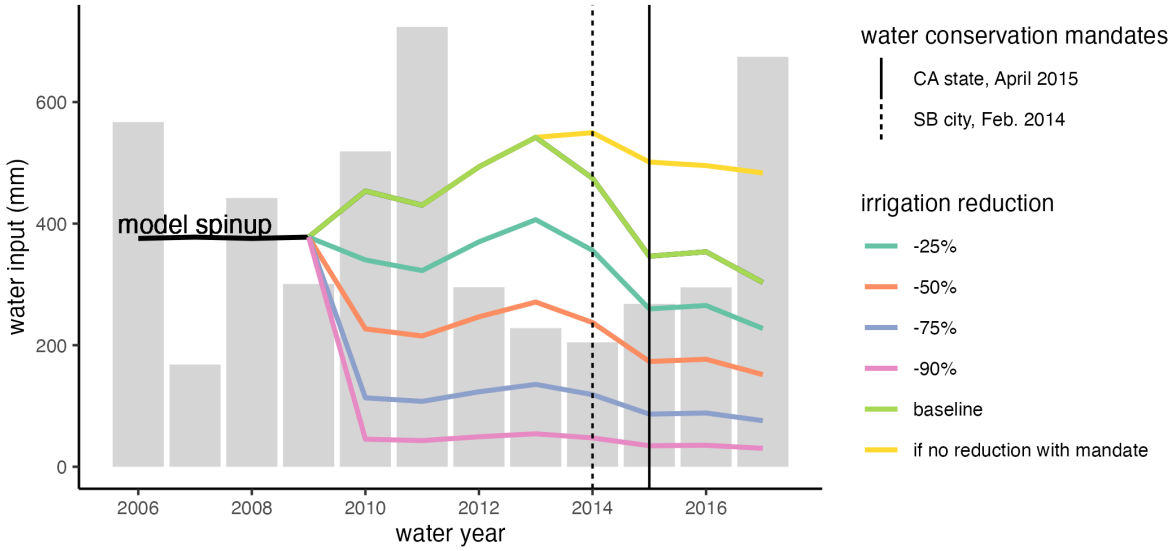

Figure 2.1: Water inputs to the model include rainfall, shown as grey columns, and irrigation, shown as colored lines. Years when water conservation mandates were set are marked with vertical lines, one for the city of Santa Barbara, and a second for the state of California. The yellow line displays the trend of baseline irrigation if it was not reduced with the conservation mandates.

With a baseline scenario from the monthly data from the city, we created 5 different scenarios of varying amounts of percent reduced. All scenarios went through the same model spinup period with an average irrigation input based on the average pre-drought water use data. Once the baseline data was in the biweekly format, each daily value was reduced by a percent (Figure 2.1). The baseline data does include a period of time with mandatory state water restrictions, beginning in 2014 with a proclamation of a state of emergency and advancing in April 2015 to a statewide 25% reduction in potable urban usage. It should be noted that for the irrigation scenarios input to the model, percent reductions were taken on top of this actual reduction (Figure 2.1).

2.2.3 Model output and analysis

Model simulations included the five tree species with 50 permutations of vegetation parameters , selected randomly from the parameter sets in Chapter 1 (1.2.3) to account for parameter uncertainty. Along with the 5 tree species there were two climate scenarios, and 5 irrigation scenarios 2.1, ran over the same time period, 2011-2017.

Table 2.1: Each column includes a model input that varied across simulations, in combination a total of 50 different scenarios.

Tree species	**Climate**	**Irrigation input**
Coast live oak, *Quercus agrifolia*, (QUAG)	Historic rainfall and temperatures	Baseline amount
California sycamore, *Platanus racemosa*, (PLRA)	Same rainfall, with 1.8° C warming	25% reduction
Blue gum eucalyptus, *Eucalyptus globulus*, (EUGL)		50% reduction
Victorian box, *Pittosporum undulatum*, (PIUN)		75% reduction
Canary Island pine, *Pinus canariensis*, (PICA)		90% reduction

We used RHESSys model outputs of transpiration, NPP, tree-level water use efficiency (WUE), and LAI to test for differences between irrigation scenarios over the course of the 2012-2016 drought. RHESSys runs at a daily time step, and outputs were aggregated to the total amount for transpiration, NPP, and WUE, and the average LAI over each water year. These model outputs are indicators of ecosystem processes driving the subsequent provisioning, regulating, and cultural ecosystem services (45). While we did not explicitly convert output of transpiration to latent energy or changes in temperature, we consider it as an important variable for estimating plant water use and as a proxy for potential evaporative cooling above the canopy. LAI resilience is the post-drought LAI compared to pre-drought LAI, following a the first chapter that looked at LAI resistance (Eq. 1.1) and resilience (Eq. 1.2). Lastly, annual transpiration and plant NPP were used to calculate annual plant water use efficiency (WUE) as the amount of kgC of NPP per mm of water transpired.

After aggregating RHESSys daily outputs to annual values for each irrigation reduction and temperature scenario, we statistically compared the rate of change in each outcome with irrigation reduction to compare across species and temperature. We also

compared across drought years (2012-2016) and non-drought years (2011, 2017). For transpiration, we ran a linear regression to compare the rate of increase in transpiration with irrigation input. A piece-wise linear regression was used to determine changes in annual NPP with irrigation input. We used the R package 'segmented' to test for the existence of breakpoints and to compare rates of change in NPP before and after the breakpoints. The linear regression was performed paired with a post-hoc Tukey's honest significance test in R to check for significance in difference in means of the outcome with reduced irrigation compared to the baseline irrigation.

2.3 Results

2.3.1 Transpiration

During the drought period with historic temperatures and baseline irrigation, average annual transpiration varied between 407-502mm across all tree species parameter sets, compared to 462-713mm in the non-drought years (Figure 2.2). Transpiration under a warmer climate had similar ranges (Figure 2.2), suggesting tree transpiration in Santa Barbara is more limited by water availability than temperature and vapor pressure deficit. Water limited transpiration is also apparent in comparing how mean annual transpiration varies with irrigation input during drought and non-drought years. Transpiration increased with more irrigation applied, but the rate of increase differed for drought and non-drought years (Figure 2.2). The less irrigation there is, the greater the difference in transpiration between a drought and non-drought year. For example, in comparing the means of the groups of irrigation amounts, under a non-drought year the difference between baseline irrigation and a 90% decrease was 130mm/yr, but during a drought year the average difference between these groups was 350mm/yr. The linear slopes for change in annual transpiration with irrigation input are shown in Table 2.2.

Table 2.2: Slopes of relationship between annual transpiration and irrigation input for each tree species and temperature scenario, also separated by drought and non-drought years.

Temperature	Drought year	QUAG	EUGL	PICA	PIUN	PLRA	All
Historic	non-drought	0.43	0.74	0.40	0.43	0.11	0.42
Historic	drought	1.01	1.09	0.91	1.03	0.85	0.98
Warmer	non-drought	0.48	0.74	0.48	0.50	0.16	0.47
Warmer	drought	0.99	1.08	0.87	1.01	0.83	0.96

The change in transpiration with irrigation reductions depends on not only the amount of total water input but also on the tree species. Tree species variation in transpiration depends on key parameters that control stomatal behavior and leaf lifespan.

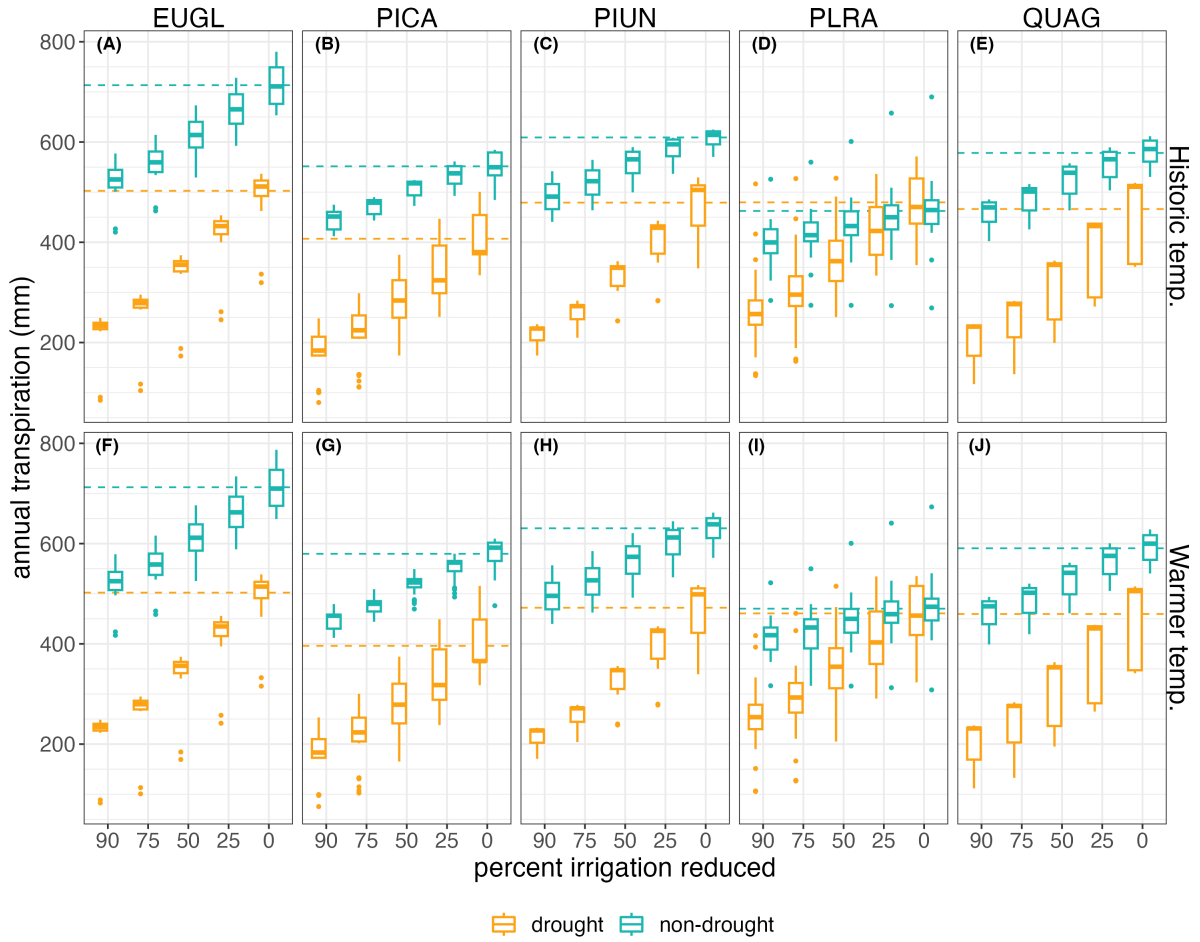

Figure 2.2: Annual transpiration for each irrigation scenario, with boxplots showing tree species parameter uncertainty. Drought years include 2012-2016, and non-drought are years before and after drought. Horizontal dashed lines show average annual transpiration for baseline irrigation of each tree and climate scenario.

During drought years there is less variation in slope between species relative to non-drought years. The tree species with the lowest slope is the only deciduous tree (PLRA), while the highest slope is the blue gum eucalyptus tree (EUGL) (Table 2.1). For most of the tree species, the rate of change in transpiration with irrigation reduction doubles during a drought year, with the exceptions of PLRA, which had a greater difference, and EUGL which had less of a difference. The variation in slopes between drought years and non-drought years is more substantial than the variation in slopes between the historic temperature and warmer temperature scenarios.

2.3.2 Carbon & WUE

Across tree parameter sets in the baseline irrigation scenario with the historic climate, average annual NPP during the drought ranged from 0.61-1.09kgCm^{-2}, compared to 0.56-1.21kgCm^{-2}in a non-drought year. These average values with baseline irrigation are shown in Figure 2.3 as dashed horizontal lines. This range is reduced to averages of 0.23-0.70kgCm^{-2} during drought and 0.48-1.31kgCm^{-2} in non-drought years with the maximum irrigation reductions of 90%.

While annual transpiration declines linearly with decreased irrigation, during drought years annual NPP declines at a non-linear rate. When it's not a drought year, there is less of a decline, and not a significant difference in mean NPP between baseline and irrigation reduction of -25%, and with smaller differences for larger irrigation reduction scenarios (Figure 2.3). Full comparisons of means between average annual NPP is shown in the Appendix (section 2.8).

Using a break point analysis in a piece-wise linear regression we identified the point in the relationship of average annual NPP to average irrigation input during a drought year. This point occurred between the 25% to 50% irrigation reduction scenarios. Fom 0-25% irrigation reduction during a drought year, the rate of decline in average annual NPP with irrigation has a gradual slope between 0.42 - 1.69kgCm^{-2}/mm depending on tree species. Beyond reductions of 25%, this rate can double or more to a range of 0.93-3.12kgCm^{-2}/mm (Figure 2.4). Species differences are greater for irrigation reductions above 25%, with PLRA showing relatively small declines in NPP. With warming, the slope of 0-25% irrigation reduction is similar to the slope for the historic temperature drought, with similar patterns across tree species and tree parameter uncertainty. However, when irrigation is further reduced, species respond differently to the warmer drought. The evergreen broadleaf trees QUAG and PIUN had higher slopes with warming, while the evergreen coniferous tree, PICA, slope decreased with warming. The deciduous tree, PLRA, had the lowest average slope for both temperature scenarios.

Water use efficiency (WUE), quantified here as the amount of NPP per amount of transpiration on average shows an increase during the drought (Figure 2.5). Across all tree parameter sets, average WUE ranged from 0.67 to 3.45 in the baseline drought years, and 0.73-2.85 during the non-drought years. There is steeper linear decline in transpiration (Figure 2.2) relative to a more gradual nonlinear decline in NPP (Figure 2.3), causing WUE to increase with decreasing irrigation. Decreasing irrigation input can cause WUE to increase, but this depends on tree species. For EUGL and PICA during drought years, average WUE increases under the scenarios of irrigation reduction from 25-50%, but then declines under higher reductions. For the other tree species parameter sets, WUE continues to increase under greater irrigation reductions. For two of the evergreen species, QUAG and PICA, irrigation reduction from 75-90% under warming has a greater average WUE during the non-drought years than the drought years. PICA however does have some large outliers with less irrigation input, due to some parameter sets having negative annual NPP, which means annual respiration was greater than photosynthesis in these scenarios and the tree was using carbon stores.

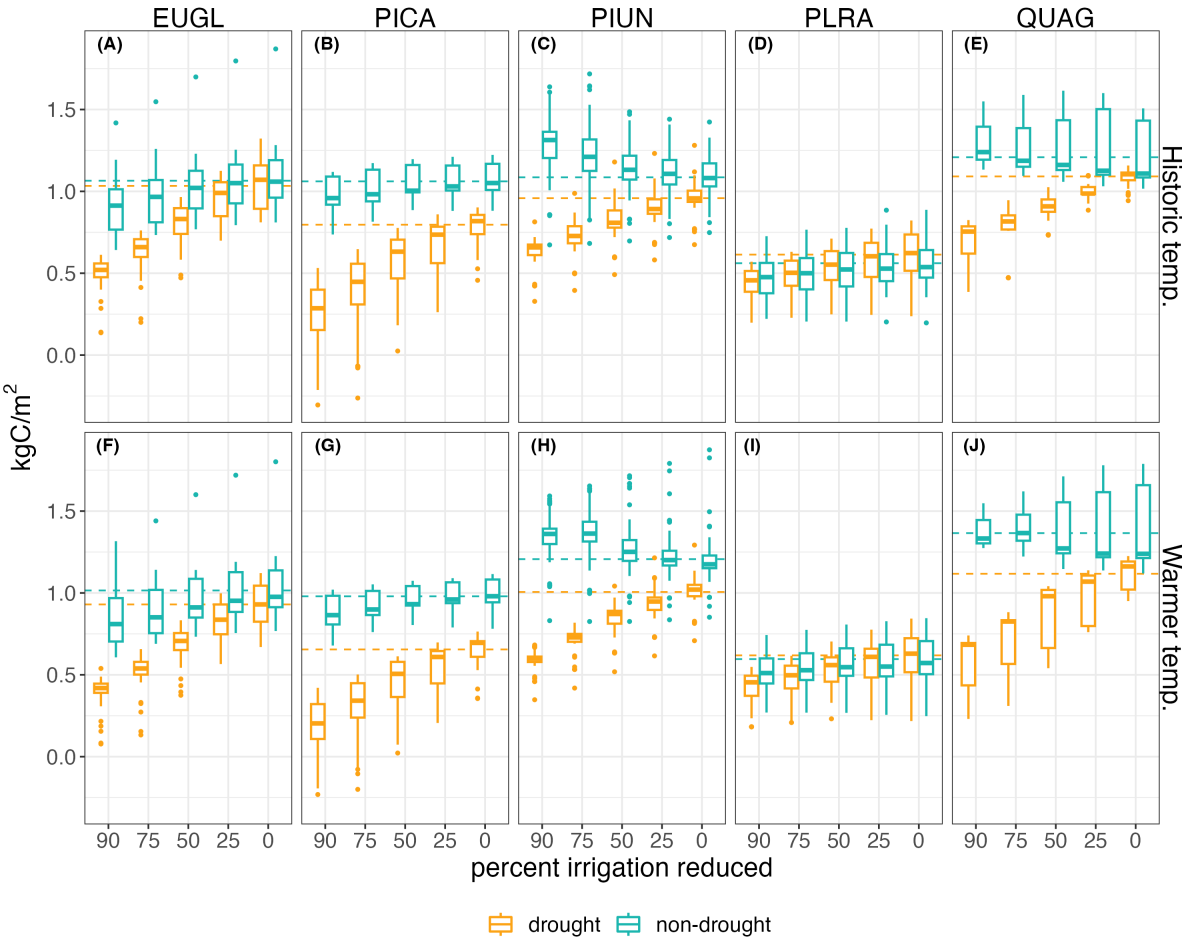

Figure 2.3: Annual net primary productivity (NPP) for each irrigation scenario, with boxplots showing tree species parameter uncertainty. Drought years include 2012-2016, and non-drought are years before and after drought. The horizontal dashed line shows the average annual amount for each tree species and climate with baseline irrigation.

2.3.3 LAI resilience

LAI resilience is calculated as the ratio of post-drought LAI to pre-drought LAI. Similar to patterns of NPP, LAI drought resilience declines at a greater rate with irrigation reductions above 25% - 50%. The average LAI resilience across tree species for the baseline scenario was 0.97 and 0.95 with warming, and this declines to 0.96 and 0.94 at 25% irrigation reduction - an insignificant difference for both current climate and warmer temperatures. Beyond 25%, the LAI resilience declines to as low as 0.46 with 90% reduced, and 0.37 with warming (Figure 2.6). Species showed substantial differences in the loss of resilience with irrigation reductions, although for historic drought, all show resilience

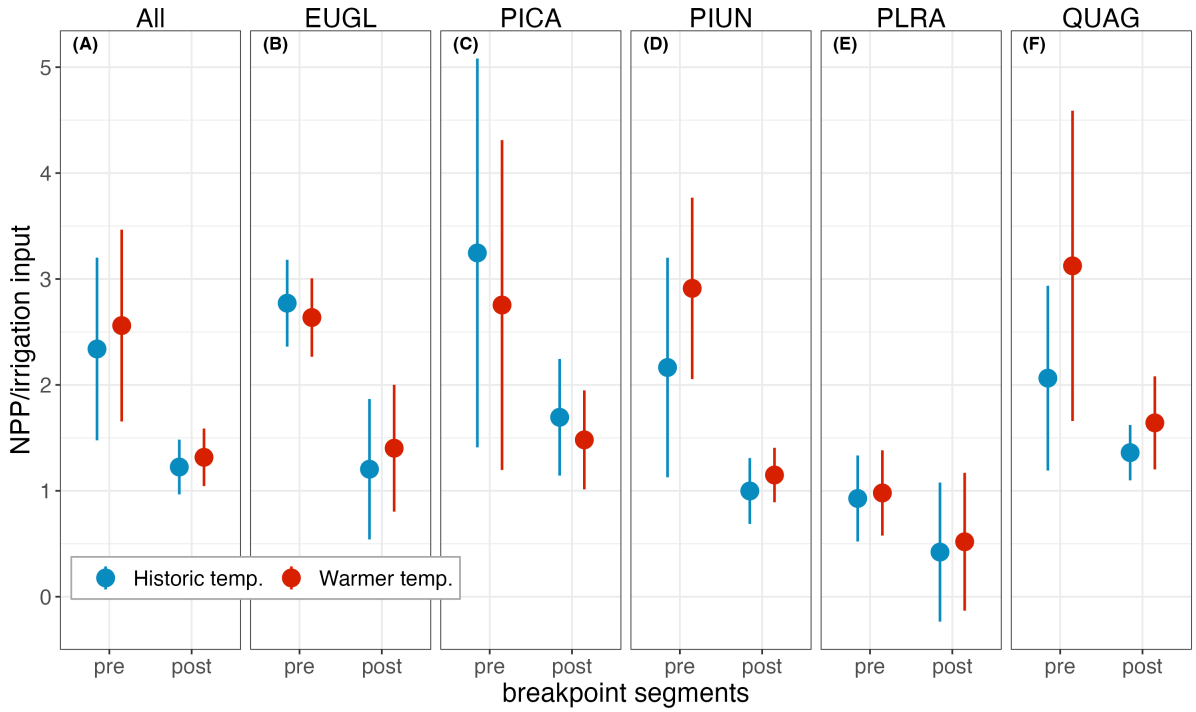

Figure 2.4: For a piece-wise linear relationship between annual net primary productivity (NPP) and irrigation reduction during drought years, two slopes were calculated for reductions up to 25% and beyond 25%. The y-axis shows the slope and 95% confidence intervals for both segments. Colors represent temperature, where blue is historic and red is warming. Box (A) shows the relationship for the average NPP across all tree types.

close to 1 for full irrigation, and most show only minor reductions in resilience for 25% reductions. EUGL shows greatest declines in resilience with irrigation reduction, while PIUN maintains resilience even with 90% reduction under the warmer drought. We also looked at the ratio to 2011 for the average LAI during the drought years to determine whether there was a significant loss of canopy during the drought. All tree species had a more significant loss of canopy mid-drought with irrigation reductions greater than 50%.

2.4 Discussion

2.4.1 Model outcomes

For the baseline irrigation scenario, model outputs of annual tree transpiration, annual NPP, WUE, and LAI are comparable with other studies. With observed historic temperatures, annual transpiration for all tree species averaged 450mm/year, which is comparable to in-situ studies that measured urban tree transpiration in coastal Southern

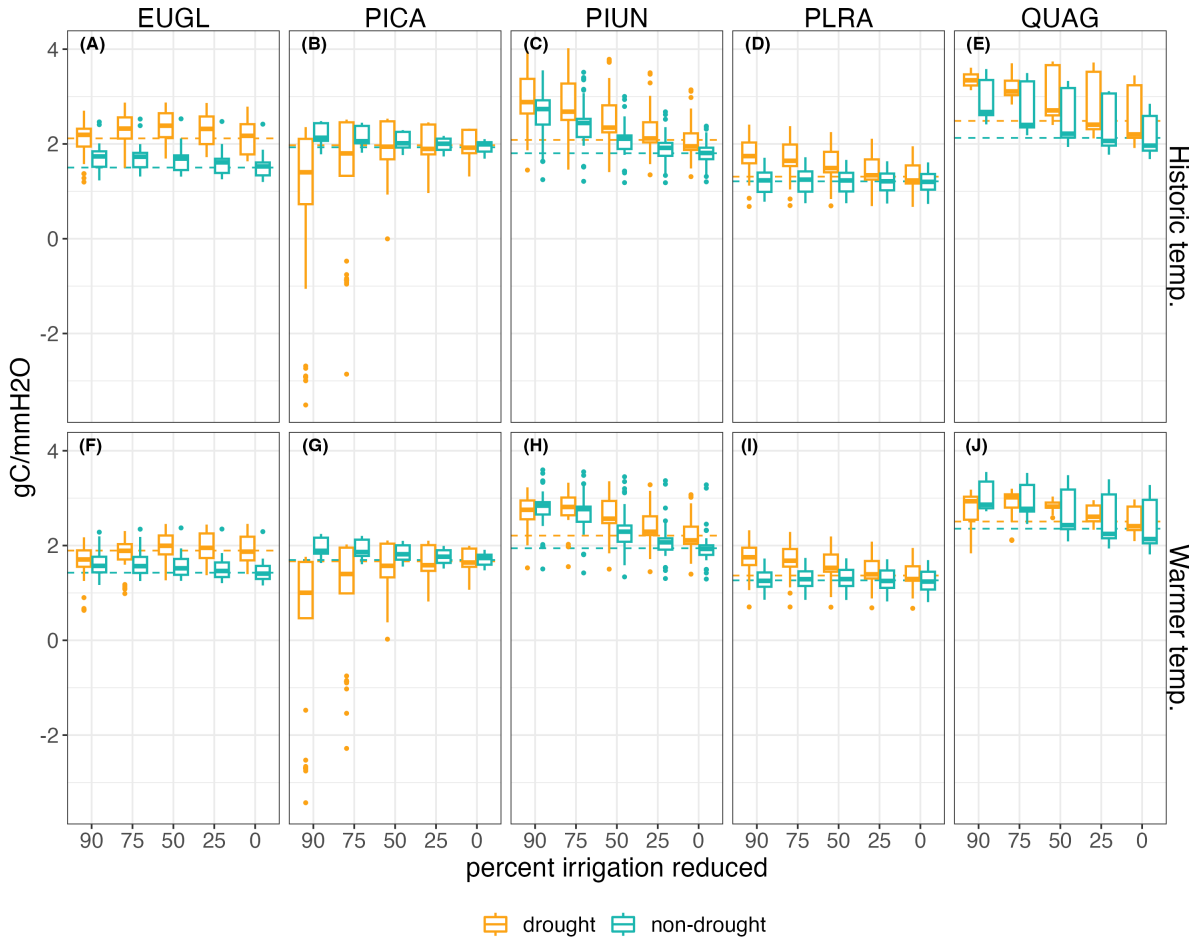

Figure 2.5: Water use efficiency (WUE) as tree species annaul NPP divided by tree transpiration, for each tree species, temperature scenario, and drought and non–drought year. Variation for each tree species shows parameter uncertainty. Horizontal dashed lines show average value for baseline irrigation.

California using sap-flux measurements and empirical models (21; 17; 22; 46). The tree species with the highest estimated annual transpiration rates were from the blue gum eucalyptus (EUGL), which could be due to higher modeled values of LAI from a high leaf turnover rate. The lowest annual transpiration rates during drought was the coniferous tree, the Canary Island Pine (PICA), which agrees with lower daily values observed in (17) .

Vegetation carbon fluxes and carbon storage in cities are challenging to quantify due to limited data and lack of transferability from natural vegetation models (47; 48). The average annual NPP across all species for the baseline irrigation was higher than field studies of natural forests (49; 50), which likely reflects irrigation inputs, differences in soils and species, and some model bias. The lower end of model estimates of annual NPP

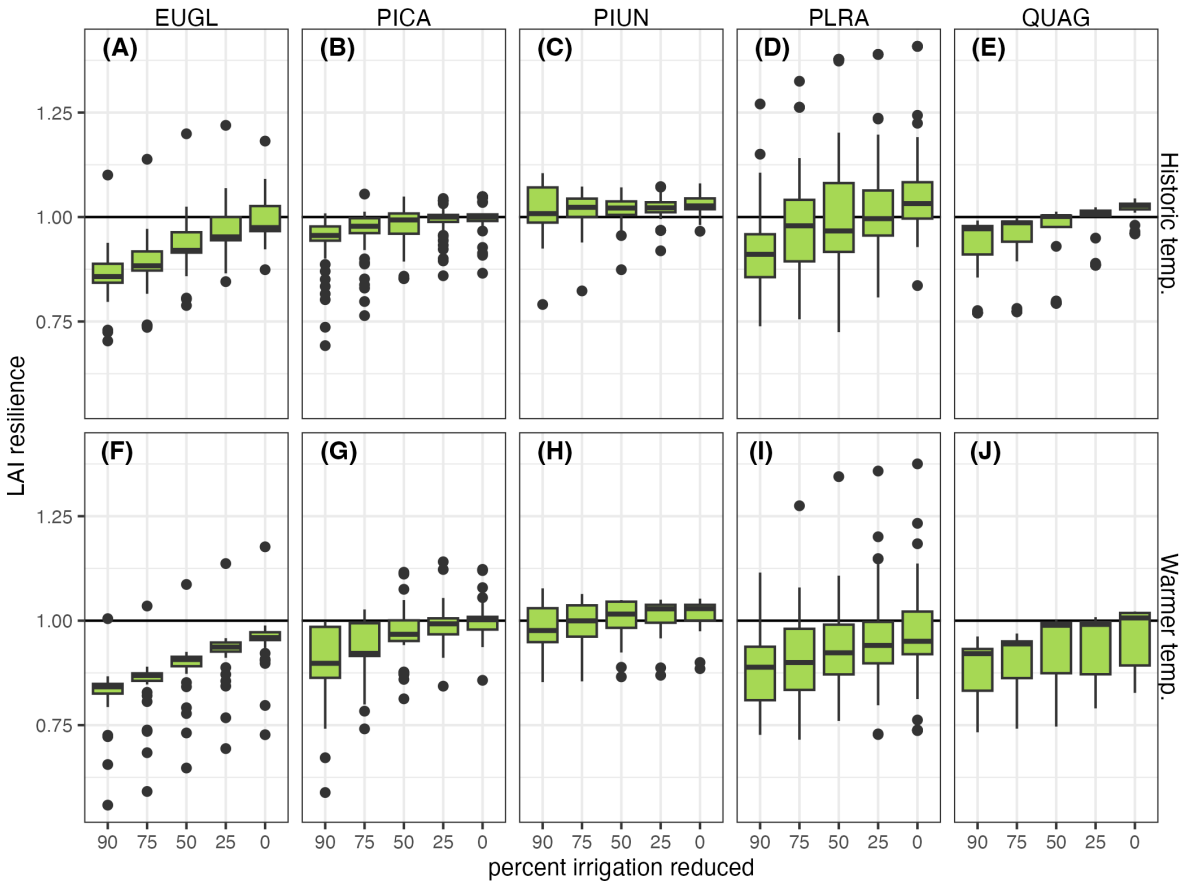

Figure 2.6: LAI resilience, the ratio of post-drought LAI to pre-drought LAI, for each tree species and irrigation scenario. Variation for each tree species shows parameter uncertainty. Horizontal line is shown at 1 for reference, where 1 is a return to pre-drought LAI.

were within range of comparable studies that estimated vegetation productivity in arid to semi-arid cities (51; 52; 53), as well as for a sub-humid city (**?**).

With baseline irrigation, for all tree species the average WUE increased during drought years. This is in agreement with (49), who found an increase in WUE of natural vegetation in arid to semi-arid regions of California during 2012-2016 drought. There are few studies of WUE in urban settings, but it was shown for an irrigated setting in Los Angeles, California, shrub species from arid regions had a smaller WUE compared to species from temperate regions due to the availability of excess water from irrigation (54). Increased WUE with low irrigation rates relative to higher irrigation rates was also found in an urban arid setting (55). In our study two of the tree species (QUAG, PIUN) experienced this pattern for both drought and non-drought years.

All tree types maintained average LAI throughout the drought period with baseline

irrigation. LAI can be compared to the remote sensing index equivalent water thickness (EWT) due to the relationship between canopy level water content and LAI (56). Model simulations of constant average annual LAI for the baseline temperature and irrigation scenario are in agreement with observed EWT for a similar time period in Santa Barbara done by Miller et al. 2022 (57), who found that tree canopy varied with seasonal summer drought, but the peak values in the spring were similar across years 2013-2015. In Chapter 1, these same tree species without any irrigation experienced more LAI loss, with some trees losing up to half of their LAI during drought (**?**).

2.4.2 Trade-offs in ecosystem services and water conservation

To determine whether trade-offs with irrigation reduction exist, we compared model outputs across scenarios of irrigation input for each tree species and temperature. For all tree species, annual transpiration was linearly related to water input. In drought years, the slope nearly doubles compared to non-drought years for most of the tree species (Table 2.2). The steeper slope shows a greater loss of transpiration with smaller amounts of irrigation reduction, which would result in short-term loss of evaporative cooling during drought. In other words, the importance of irrigation for maintaining evaporative cooling increases during drought. This is notable given that in semi-arid climates even non-drought years have long periods during the summer with little or no precipitation inputs. With warmer temperatures, the slopes increased in non-drought years relative to the historic temperatures for all tree species except EUGL, as shown in Table 2.2. These changes are small, but reflect the response of transpiration to not only water scarcity but indirectly to depletion in soil moisture and increased stomatal resistance with higher temperatures and vapor pressure deficit.

Despite reductions in transpiration with irrigation reduction, annual NPP had a non-linear response to the irrigation reduction scenarios. This is partially due to the effects of water limitations on the seasonal timing and amount of productivity. With 25% less irrigation than the baseline amount, there was not a significant difference in annual NPP or LAI resilience across all tree species, suggesting that over-watering was occurring before the drought. Maintaining adequate water supply during summer is costly even in non-drought years. Thus efforts towards general moderate (25%) reductions in irrigation during non-drought years may be worthwhile in the future (58). While there would be some reduction in evaporative cooling (e.g transpiration) these are small for non-drought years and changes in ecosystem services related to carbon cycling and shading would be minimal.

In comparing the rates of change between annual NPP and irrigation input during drought, the smaller slope from 0-25% suggests a gradual loss of NPP with small amounts of irrigation reduction could occur while still maintaining canopy structure and shade. If the goal is to maintain a resilient tree canopy post-drought, but prioritize water conservation during a drought, irrigation reductions up to 50% from the baseline will cause loss of NPP and LAI during the drought, but can maintain resilient LAI post-drought. For

reductions greater than 50%, we found there would be multi-year effects in NPP and LAI - trees would have less recovery post-drought and there may be structural loss and low to negative amounts of productivity during the drought. There are notable differences across species, and these are most apparent when irrigation reductions are greater than 50%. Species such as PLRA, the California Sycamore typically found in riparian areas, may tolerate more severe watering restrictions, although LAI resilience does declines with 75% or more irrigation reduction for warmer droughts. The relative small declines in resilience and NPP for irrigation reductions less than 50% for all species are useful for informing broad watering restrictions; while species differences can be used to guide longer term decisions about landscaping and tree selection for climate change (59).

The different responses in tree water use and NPP caused an increase in annual plant WUE during drought compared to non-drought years, across tree species and temperature scenarios (Figure 2.5). The increased WUE during drought happens for each irrigation scenario for all tree species except PICA, the coniferous tree. Across all tree species, compared to the baseline irrigation, average WUE also increases with 25% irrigation reduction, reflecting a greater loss of transpiration and little to no loss in NPP. WUE could be further monitored in urban systems as an indicator of efficient water use for tree planting in semi-arid to arid cities when prioritizing tree health and canopy.

It should be noted that the water use data used in this study was from a water resources account that represents large areas of private land. While it does reflect the seasonal changes to water use and the monthly amounts, it is specific to Santa Barbara, and the amounts may be above or below average for urban outdoor water use. Despite this potential bias, the annual irrigation rates used are comparable to the higher amounts estimated for outdoor water use rates in Los Angeles, California (15).

2.5 Conclusion

This study used an ecohydrologic model in a semi-arid city to show that urban tree health for select species can be maintained during a multiyear drought with moderate irrigation reductions of up to 25%. The drought period from 2012-2016 was an "exceptional" drought with both substantial precipitation declines and higher than normal temperatures. Similar and potential warmer droughts are expected to increase in Southern California in the future (32; 2). Irrigation in semi-arid cities is important for maintaining tree-related ecosystem services not only because of the direct potential for evaporative cooling, but because of its indirect importance for maintaining tree canopy for shade provision during warmer drought. When irrigation is reduced during drought years, both evapotranspiration and plant productivity become water limited. The amount of irrigation reduction, however, affects these two fluxes differently. Tree transpiration declined linearly with irrigation reduction, resulting in a short-term loss of evaporative cooling. NPP declined non-linearly with reduced irrigation and for moderate (less than 25%) reductions at a more gradual rate than transpiration loss. Tree resilience, as indicated by LAI, following the drought was also maintained for irrigation reductions of less than 50%

, even for warmer droughts. These results suggest that it is possible to maintain long term health of trees and tree cover for shade provision with partial irrigation reductions.

Our results also highlight both consistency across species and important differences. All species showed linear declines in transpiration (and consequently evaporative) cooling with irrigation reduction during droughts but much more stable transpiration for non-drought years - suggesting a general pattern of overwatering when not in drought. All species also show resilience to drought for irrigation reductions less than 50% and generally small declines in NPP, and finding that can guide general watering restrictions. Species differences however are notable, particularly for more substantial irrigation reductions. Species specific model results should be interpreted with caution, and we note that for some species, such as QUAG and PICA, uncertainty in model estimates are significant. Nonetheless, these estimates of species differences in transpiration, NPP, and LAI can motivate and guide additional species specific monitoring to guide landscape planning and tree selection.

Because outdoor water for landscaping is one of the highest sectors of urban water use in semi-arid climates (14), reducing outdoor water use and improving efficiency is essential to climate change adaptation for future drought and heatwaves. Decision makers might consider limiting outdoor water use during wet years when over-watering normally occurs to save water for dry years when vegetation needs it more (20). During drought, urban forestry management should be considered along with water conservation efforts, and allocating water use towards trees that provide shade and cooling. In addition, investing in rainwater catchment and recycled wastewater would be a more efficient way of allocating water towards urban trees and their ecosystem services (**?**).

B Appendix

This appendix contains a table of all results from the break point regression analysis (Table 2.3) with slopes from Figure 2.4 above, along with break point estimations and confidence intervals. All tree species had a p-value <0.05. This appendix also includes figures that display full results from the Tukey's honest significance test showing differences in means across irrigation scenarios for annual transpiration (Figure 2.7) and annual NPP (Figure 2.8). Finally, a short description of data and R packages is included in section B.2.

Species codes for the below table and figures are as follows:

EUGL Blue gum eucalyptus (*Eucalyptus globulus*)

PICA Canary Island Pine (*Pinus canariensis*)

PIUN Victorian Box (*Pittosporum unduluatum*)

PLRA California Sycamore (*Platanus racemosa*)

QUAG Coast live oak (*Quercus agrifolia*)

B.1 Tables and Figures

Table 2.3: For each tree species and all trees averaged together, results from segmented break point analysis are shown. First two columns are the estimates of slopes, as the rate of change in annual NPP per annual irrigation input, before and after the breakpoint, as shown in 2.4. Breakpoint estimate is shown under 'bp. est.' and break point confidence interval is shown in the following column 'bp. 95% C.I.'. Note that the breakpoint corresponds to the annual irrigation input during drought, which in the -50% scenario was between 0.113 and 0.174, and in the -25% scenario was between 0.169-0.261. Some trees have breakpoint confidence intervals that fall somewhere in between these two.

Tree sp.	**Historic temperature**				
	pre slope	post slope	bp. est.	bp. 95% C.I.	p-value
EUGL	2.77	1.20	0.169	[0.1224,0.214]	1.76×10^{-9}
PICA	3.24	1.69	0.120	[0.025, 0.216]	1.5×10^{-4}
PIUN	2.16	0.99	0.093	[0.038, 0.149]	7.13×10^{-11}
PLRA	0.93	0.42	0.166	[0.028, 0.304]	4.15×10^{-10}
QUAG	2.06	1.36	0.094	[0.015, 0.173]	1.86×10^{-14}
all trees	2.34	1.22	0.111	[0.0054, 0.168]	2.58×10^{-4}
Tree sp.	**Warmer temperature**				
	pre slope	post slope	bp. est.	bp. 95% C.I.	p-value
EUGL	2.63	1.40	0.172	[0.121, 0.222]	2.7×10^{-11}
PICA	2.75	1.48	0.121	[0.021, 0.220]	8.69×10^{-6}
PIUN	2.91	1.15	0.104	[0.070, 0.137]	6.20×10^{-14}
PLRA	0.98	0.52	0.166	[0.019, 0.317]	2.9×10^{-10}
QUAG	3.12	1.64	0.097	[0.033, 0.161]	2.39×10^{6}
all trees	2.56	1.31	0.111	[0.057, 0.164]	5.01×10^{-4}

Figure 2.7 displays differences in means for annual transpiration across scenarios and drought v. non-drought year. All differences were significant except: PLRA -25% for non-drought years and both climate scenarios, and PLRA -50% for non-drought historic temperatures.

Figure 2.8 shows the differences in means for annual NPP. For all trees, the difference between -25%-0 for non-drought years in both climate scenarios are insignificant. For all trees except PLRA, all scenarios under drought years are significantly different from the baseline.

B.2 Data Availability

Information on RHESSys download links and data used can be found in Appendix A (section A.2). Vegetation parameters used in this chapter were taken from parameters defined in the first chapter, also shown in Appendix A (section A.1).

This chapter used R for post-model processing and data analysis. Key packages used include:

`stats`: for running anova and TukeysHSD

`https://www.rdocumentation.org/packages/stats/versions/3.6.2`

`segmented`: for estimating break points

`https://cran.r-project.org/web/packages/segmented/index.html`

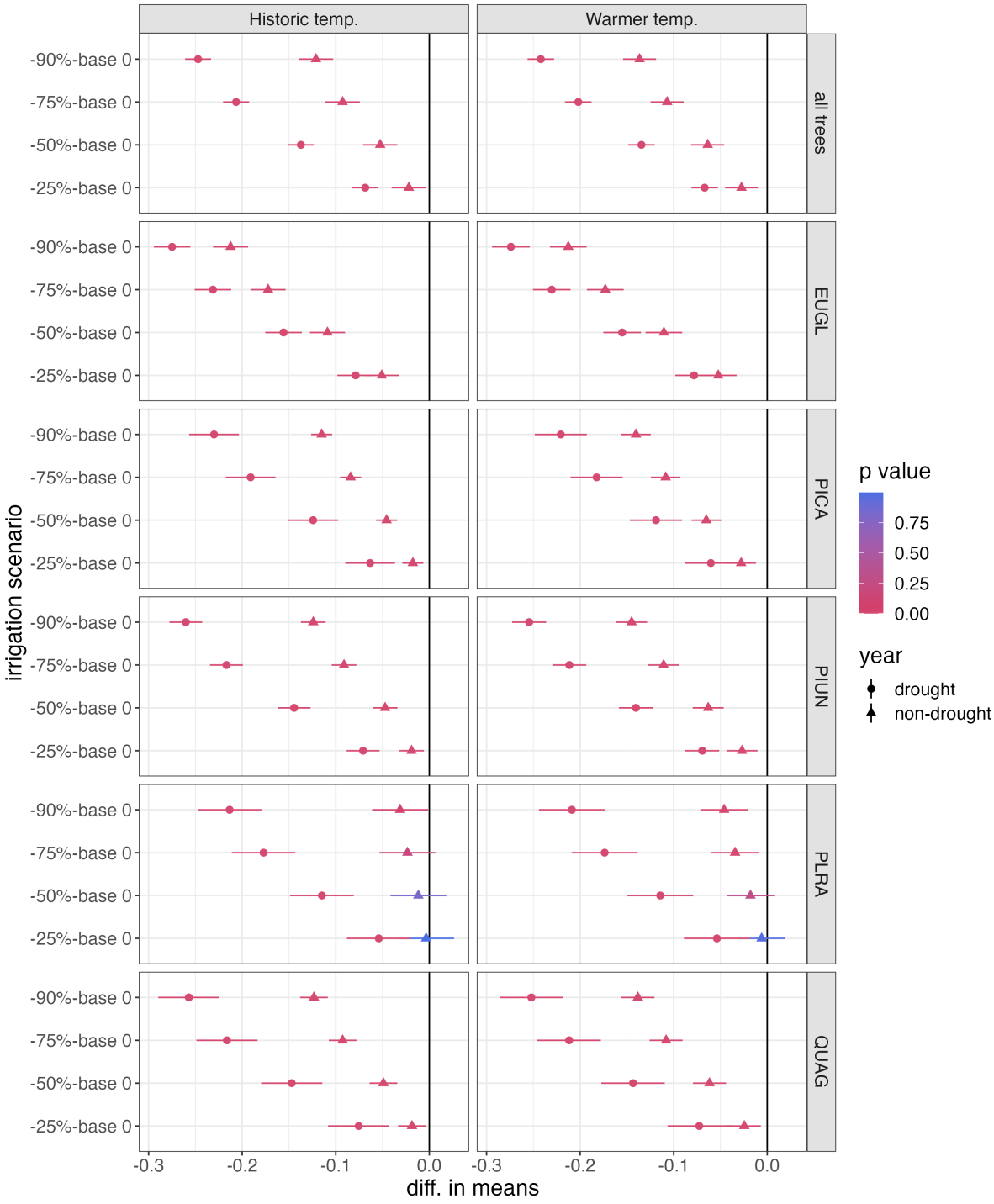

Figure 2.7: Annual transpiration results from Tukey's HSD comparing difference in means for irrigation scenarios, with the baseline labelled as 'base 0' and all reductions listed on the y-axis. X-axis shows the estimated difference in means. Red color signifies p-values at <0.05.

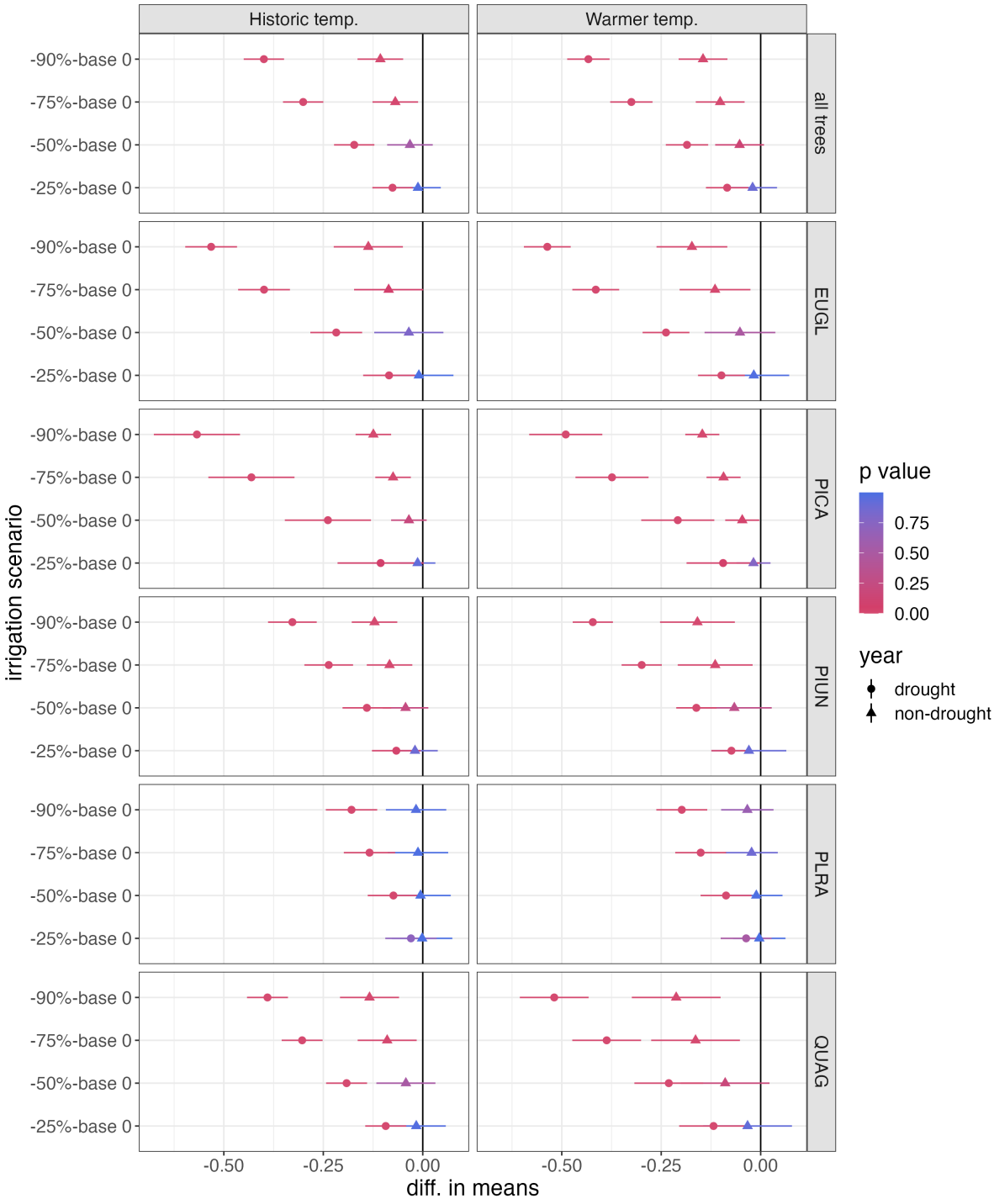

Figure 2.8: Annual transpiration results from Tukey's HSD comparing difference in means for irrigation scenarios, with the baseline labelled as 'base 0' and scenarios listed on the y-axis. X-axis shows the estimated difference in means. Red color signifies p-values at <0.05.

Chapter 2 References

[1] D. R. Cayan, T. Das, D. W. Pierce, T. P. Barnett, M. Tyree, and A. Gershunov, *Future dryness in the southwest US and the hydrology of the early 21st century drought*, *PNAS* **107** (Dec., 2010) 21271–21276.

[2] B. I. Cook, T. R. Ault, and J. E. Smerdon, *Unprecedented 21st century drought risk in the American Southwest and Central Plains*, *Science Advances* **1** (Feb., 2015) e1400082.

[3] N. S. Diffenbaugh, D. L. Swain, and D. Touma, *Anthropogenic warming has increased drought risk in California*, *Proc Natl Acad Sci USA* **112** (Mar., 2015) 3931–3936.

[4] K. A. McKinnon, A. Poppick, and I. R. Simpson, *Hot extremes have become drier in the United States Southwest*, *Nat. Clim. Chang.* **11** (July, 2021) 598–604. Number: 7 Publisher: Nature Publishing Group.

[5] Luthy Richard G., Wolfand Jordyn M., and Bradshaw Jonathan L., *Urban Water Revolution: Sustainable Water Futures for California Cities*, *Journal of Environmental Engineering* **146** (July, 2020) 04020065. Publisher: American Society of Civil Engineers.

[6] S. Pincetl, E. Porse, K. B. Mika, E. Litvak, K. F. Manago, T. S. Hogue, T. Gillespie, D. E. Pataki, and M. Gold, *Adapting Urban Water Systems to Manage Scarcity in the 21st Century: The Case of Los Angeles*, *Environmental Management* (Nov., 2018).

[7] S. J. Livesley, G. M. McPherson, and C. Calfapietra, *The Urban Forest and Ecosystem Services: Impacts on Urban Water, Heat, and Pollution Cycles at the Tree, Street, and City Scale*, *Journal of Environment Quality* **45** (2016), no. 1 119.

[8] S. Sudimac, V. Sale, and S. Kühn, *How nature nurtures: Amygdala activity decreases as the result of a one-hour walk in nature*, *Mol Psychiatry* (Sept., 2022) 1–7. Publisher: Nature Publishing Group.

[9] E. G. McPherson, Q. Xiao, N. S. van Doorn, J. de Goede, J. Bjorkman, A. Hollander, R. M. Boynton, J. F. Quinn, and J. H. Thorne, *The structure,*

function and value of urban forests in California communities, *Urban Forestry & Urban Greening* **28** (Dec., 2017) 43–53.

[10] P. Bolund and S. Hunhammar, *Ecosystem services in urban areas*, *Ecological Economics* **29** (May, 1999) 293–301.

[11] K. Gao, M. Santamouris, and J. Feng, *On the cooling potential of irrigation to mitigate urban heat island*, *Science of The Total Environment* **740** (Oct., 2020) 139754.

[12] P. Gober, A. Middel, A. Brazel, S. Myint, H. Chang, J.-D. Duh, and L. House-Peters, *Tradeoffs Between Water Conservation and Temperature Amelioration In Phoenix and Portland: Implications For Urban Sustainability*, *Urban Geography* **33** (Oct., 2012) 1030–1054.

[13] J. Yang and Z.-H. Wang, *Planning for a sustainable desert city: The potential water buffering capacity of urban green infrastructure*, *Landscape and Urban Planning* **167** (Nov., 2017) 339–347.

[14] P. H. Gleick, G. H. Wolff, and K. K. Cushing, *Waste not, want not: The potential for urban water conservation in California*. Pacific Institute for Studies in Development, Environment, and Security Oakland, CA, 2003.

[15] C. Mini, T. S. Hogue, and S. Pincetl, *Estimation of residential outdoor water use in Los Angeles, California*, *Landscape and Urban Planning* **127** (July, 2014) 124–135.

[16] N. S. Bijoor, D. E. Pataki, D. Haver, and J. S. Famiglietti, *A comparative study of the water budgets of lawns under three management scenarios*, *Urban Ecosyst* (2014) 23.

[17] E. Litvak, K. F. Manago, T. S. Hogue, and D. E. Pataki, *Evapotranspiration of urban landscapes in Los Angeles, California at the municipal scale: EVAPOTRANSPIRATION OF URBAN LANDSCAPES*, *Water Resources Research* **53** (May, 2017) 4236–4252.

[18] E. Litvak and D. E. Pataki, *Evapotranspiration of urban lawns in a semi-arid environment: An in situ evaluation of microclimatic conditions and watering recommendations*, *Journal of Arid Environments* **134** (Nov., 2016) 87–96.

[19] N. S. Bijoor, H. R. McCarthy, D. Zhang, and D. E. Pataki, *Water sources of urban trees in the Los Angeles metropolitan area*, *Urban Ecosyst* **15** (Mar., 2012) 195–214.

[20] Y.-J. Chen, J. P. McFadden, K. C. Clarke, and D. A. Roberts, *Measuring Spatio-temporal Trends in Residential Landscape Irrigation Extent and Rate in Los Angeles, California Using SPOT-5 Satellite Imagery*, *Water Resources Management* **29** (Dec., 2015) 5749–5763.

[21] E. Litvak, H. R. McCarthy, and D. E. Pataki, *A method for estimating transpiration of irrigated urban trees in California*, *Landscape and Urban Planning* **158** (Feb., 2017) 48–61.

[22] D. E. Pataki, H. R. McCarthy, E. Litvak, and S. Pincetl, *Transpiration of urban forests in the Los Angeles metropolitan area*, *Ecological Applications* **21** (2011), no. 3 661–677.

[23] H. Nouri, S. Beecham, A. M. Hassanli, and F. Kazemi, *Water requirements of urban landscape plants: A comparison of three factor-based approaches*, *Ecological Engineering* **57** (Aug., 2013) 276–284.

[24] S. Gillner, J. Vogt, A. Tharang, S. Dettmann, and A. Roloff, *Role of street trees in mitigating effects of heat and drought at highly sealed urban sites*, *Landscape and Urban Planning* **143** (Nov., 2015) 33–42.

[25] J. B. Winbourne, T. S. Jones, S. M. Garvey, J. L. Harrison, L. Wang, D. Li, P. H. Templer, and L. R. Hutyra, *Tree Transpiration and Urban Temperatures: Current Understanding, Implications, and Future Research Directions*, *BioScience* **70** (July, 2020) 576–588.

[26] A. M. Broadbent, A. M. Coutts, N. J. Tapper, and M. Demuzere, *The cooling effect of irrigation on urban microclimate during heatwave conditions*, *Urban Climate* **23** (Mar., 2018) 309–329.

[27] B. Reyes, T. Hogue, and R. Maxwell, *Urban Irrigation Suppresses Land Surface Temperature and Changes the Hydrologic Regime in Semi-Arid Regions*, *Water* **10** (Nov., 2018) 1563. Number: 11 Publisher: Multidisciplinary Digital Publishing Institute.

[28] P. Vahmani and G. Ban-Weiss, *Climatic consequences of adopting drought-tolerant vegetation over Los Angeles as a response to California drought*, *Geophysical Research Letters* (Feb., 2017) 8240–8249.

[29] J. Yang, Z.-H. Wang, F. Chen, S. Miao, M. Tewari, J. A. Voogt, and S. Myint, *Enhancing Hydrologic Modelling in the Coupled Weather Research and Forecasting–Urban Modelling System*, *Boundary-Layer Meteorol* **155** (Apr., 2015) 87–109.

[30] R. D. Brown, J. Vanos, N. Kenny, and S. Lenzholzer, *Designing urban parks that ameliorate the effects of climate change*, *Landscape and Urban Planning* **138** (June, 2015) 118–131.

[31] M. A. Rahman, L. M. F. Stratopoulos, A. Moser-Reischl, T. Zölch, K.-H. Häberle, T. Rötzer, H. Pretzsch, and S. Pauleit, *Traits of trees for cooling urban heat islands: A meta-analysis*, *Building and Environment* **170** (Mar., 2020) 106606.

[32] A. AghaKouchak, L. Cheng, O. Mazdiyasni, and A. Farahmand, *Global warming and changes in risk of concurrent climate extremes: Insights from the 2014 California drought*, *Geophysical Research Letters* **41** (2014), no. 24 8847–8852.

[33] Lund Jay, Medellin-Azuara Josue, Durand John, and Stone Kathleen, *Lessons from California's 2012–2016 Drought*, *Journal of Water Resources Planning and Management* **144** (Oct., 2018) 04018067.

[34] C. L. Tague and L. E. Band, *RHESSys: Regional Hydro-Ecologic Simulation System—An Object-Oriented Approach to Spatially Distributed Modeling of Carbon, Water, and Nutrient Cycling*, *Earth Interactions* **8** (Dec., 2004) 1–42.

[35] C. A. Shields and C. L. Tague, *Assessing the Role of Parameter and Input Uncertainty in Ecohydrologic Modeling: Implications for a Semi-arid and Urbanizing Coastal California Catchment*, *Ecosystems* **15** (Aug., 2012) 775–791.

[36] C. Tague and M. Pohl-Costello, *The Potential Utility of Physically Based Hydrologic Modeling in Ungauged Urban Streams*, *Annals of the Association of American Geographers* **98** (Sept., 2008) 818–833.

[37] J. J. Landsberg and R. H. Waring, *A generalised model of forest productivity using simplified concepts of radiation-use efficiency, carbon balance and partitioning*, *Forest Ecology and Management* **95** (Aug., 1997) 209–228.

[38] R. E. Dickinson, M. Shaikh, R. Bryant, and L. Graumlich, *Interactive Canopies for a Climate Model*, *Journal of Climate* **11** (Nov., 1998) 2823–2836. Publisher: American Meteorological Society Section: Journal of Climate.

[39] M. Alonzo, J. P. McFadden, D. J. Nowak, and D. A. Roberts, *Mapping urban forest structure and function using hyperspectral imagery and lidar data*, *Urban Forestry & Urban Greening* **17** (June, 2016) 135–147.

[40] D. L. Miller, M. Alonzo, D. A. Roberts, C. L. Tague, and J. P. McFadden, *Drought response of urban trees and turfgrass using airborne imaging spectroscopy*, .

[41] M. Alonzo, B. Bookhagen, and D. A. Roberts, *Urban tree species mapping using hyperspectral and lidar data fusion*, *Remote Sensing of Environment* **148** (May, 2014) 70–83.

[42] D. W. Pierce, D. R. Cayan, and B. L. Thrasher, *Statistical Downscaling Using Localized Constructed Analogs (LOCA)*, *J. Hydrometeor.* **15** (Sept., 2014) 2558–2585.

[43] C. Sax and P. Steiner, *Temporal Disaggregation of Time Series*, *The R Journal* **5** (2013), no. 2 80.

[44] P. Vahmani and T. S. Hogue, *Incorporating an Urban Irrigation Module into the Noah Land Surface Model Coupled with an Urban Canopy Model*, *Journal of Hydrometeorology* **15** (Aug., 2014) 1440–1456.

[45] G. Sun, D. Hallema, and H. Asbjornsen, *Ecohydrological processes and ecosystem services in the Anthropocene: a review*, *Ecological Processes* **6** (Oct., 2017) 35.

[46] H. R. McCarthy and D. E. Pataki, *Drivers of variability in water use of native and non-native urban trees in the greater Los Angeles area*, *Urban Ecosyst* **13** (Dec., 2010) 393–414.

[47] Q. Zhuang, Z. Shao, J. Gong, D. Li, X. Huang, Y. Zhang, X. Xu, C. Dang, J. Chen, O. Altan, and S. Wu, *Modeling carbon storage in urban vegetation: Progress, challenges, and opportunities*, *International Journal of Applied Earth Observation and Geoinformation* **114** (Nov., 2022) 103058.

[48] M. R. McHale, I. C. Burke, M. A. Lefsky, P. J. Peper, and E. G. McPherson, *Urban forest biomass estimates: is it important to use allometric relationships developed specifically for urban trees?*, *Urban Ecosystems* **12** (Mar., 2009) 95–113.

[49] S. L. Malone, M. G. Tulbure, A. J. Pérez-Luque, T. J. Assal, L. L. Bremer, D. P. Drucker, V. Hillis, S. Varela, and M. L. Goulden, *Drought resistance across California ecosystems: evaluating changes in carbon dynamics using satellite imagery*, *Ecosphere* **7** (2016), no. 11 e01561.

[50] J. D. Alexander, M. K. McCafferty, G. A. Fricker, and J. J. James, *Climate seasonality and extremes influence net primary productivity across California's grasslands, shrublands, and woodlands*, *Environ. Res. Lett.* **18** (May, 2023) 064021. Publisher: IOP Publishing.

[51] M. R. McHale, S. J. Hall, A. Majumdar, and N. B. Grimm, *Carbon lost and carbon gained: a study of vegetation and carbon trade-offs among diverse land uses in Phoenix, Arizona*, *Ecological Applications* **27** (2017), no. 2 644–661.

[52] D. J. Nowak, E. J. Greenfield, R. E. Hoehn, and E. Lapoint, *Carbon storage and sequestration by trees in urban and community areas of the United States*, *Environmental Pollution* **178** (July, 2013) 229–236.

[53] C. Shields and C. Tague, *Ecohydrology in semiarid urban ecosystems: Modeling the relationship between connected impervious area and ecosystem productivity*, *Water Resources Research* **51** (Jan., 2015) 302–319.

[54] C. M. Goedhart and D. E. Pataki, *Do arid species use less water than mesic species in an irrigated common garden?*, *Urban Ecosyst* **15** (Mar., 2012) 215–232.

[55] L. B. Stabler, *Management regimes affect woody plant productivity and water use efficiency in an urban desert ecosystem*, *Urban Ecosyst* **11** (June, 2008) 197–211.

[56] D. A. Roberts, S. L. Ustin, S. Ogunjemiyo, J. Greenberg, S. Z. Dobrowski, J. Chen, and T. M. Hinckley, *Spectral and Structural Measures of Northwest Forest Vegetation at Leaf to Landscape Scales*, *Ecosystems* **7** (Aug., 2004) 545–562.

[57] D. L. Miller, M. Alonzo, S. K. Meerdink, M. A. Allen, C. L. Tague, D. A. Roberts, and J. P. McFadden, *Seasonal and interannual drought responses of vegetation in a California urbanized area measured using complementary remote sensing indices*, *ISPRS Journal of Photogrammetry and Remote Sensing* **183** (Jan., 2022) 178–195.

[58] T. S. Wilson, B. M. Sleeter, and D. R. Cameron, *Future land-use related water demand in California*, *Environ. Res. Lett.* **11** (May, 2016) 054018.

[59] M. Esperon-Rodriguez, M. G. Tjoelker, J. Lenoir, J. B. Baumgartner, L. J. Beaumont, D. A. Nipperess, S. A. Power, B. Richard, P. D. Rymer, and R. V. Gallagher, *Climate change increases global risk to urban forests*, *Nat. Clim. Chang.* **12** (Oct., 2022) 950–955. Number: 10 Publisher: Nature Publishing Group.

Chapter 3

Does turfgrass water conservation during drought affect neighboring trees?

3.1 Introduction

Urban trees provide expansive ecosystem services (1; 2), and cities are working to expand and maintain their urban forest cover (3). In Southern California and other semi-arid climate regions, decision making around urban trees and outdoor landscaping is important for climate change adaptation both because of the ecosystem services provided by vegetation (4; 5; 6) and due to the need for urban areas to use water resources efficiently (7; 8). One land cover type in urban landscapes that is receiving particular attention for excessive water use is the turfgrass lawn (9; 10), which is often located interspersed with trees and built surfaces. During extreme drought, the first step to conserve water can be to reduce irrigation of turfgrass lawns, which alters the local water balance. This study aims to quantify the side effects of turfgrass irrigation and subsequent irrigation reductions on urban tree health under drought conditions.

The state of California experienced a widespread extreme drought from 2012-2016 which resulted in a statewide mandate for water conservation in 2015, with the goal of conserving water by 25% across the state. In order to reach this goal, there were specific orders to limit turf watering areas. Potable water was restricted for use on turf in public medians, and initiatives to replace lawns and ornamental turf with drought tolerant landscaping began (**?**). Despite initiatives taken, outdoor water use amount and location is often not well monitored (11; 12), which creates uncertainty for the effectiveness of water conservation programs and any effects on vegetation.

In semi-arid climates, water demand for trees is slightly lower than water demand for turfgrass (13), which may make trees more resilient to drought and loss of irrigation. When water-stressed, turfgrass senescence occurs, while trees may experience a loss of leaf area index (LAI) and photosynthesis (14). Outdoor water use is a significant component

of the water balance in Southern California (11; 15). As efforts targeting turfgrass for water conservation continue, we may begin to see indirect effects on urban trees. The extent of the indirect effects has not fully been explored and may take more time to be observed. While there is uncertainty in how much irrigation water is used by trees, it could become a critical water source during drought. For trees unable to access irrigation during drought due to water conservation, the degree of drought recovery may be reduced or take longer. LAI, which is important for ecosystem services of evaporative cooling and shade provision, may be impacted by irrigation reduction, causing a trade-off between cooling ecosystem services and water conservation (see Chapter 2). Water conservation efforts that target turfgrass may be expected to cause turfgrass senescence, however, less is known about whether it would also have indirect effects on neighboring tree growth. This indirect effect will depend on not only the amount of irrigation being reduced, but the area of the turfgrass that is irrigated and the additional presence of neighboring impervious surfaces.

Despite its high water use, turfgrass provides ecosystem services including erosion control and infiltration, along with recreational and social benefits for community spaces (16; 17). Along with increased infiltration, turfgrass has been shown to have lower runoff compared to xeriscaping or artificial turf (18), and a higher rate of nitrogen uptake in rain gardens (19). In arid to semi-arid climates, turfgrass alters hydrology because of the high irrigation requirements and decoupling from seasonal precipitation patterns (9). Excessive irrigation increases streamflow and summer baseflow (20); in one Southern California urban watershed streamflow dropped by 70% compared to non-urban watersheds when outdoor water use was restricted (21). The increased water input to the system through irrigation has a visible effect on streamflow and baseflow, and there is evidence that trees also use shallow soil water or baseflow originating from irrigation (22; 23). However, excess irrigation may not be accessible to trees if it drains below the rooting zone (24), and trees also rely on deeper stores of groundwater or precipitation so may be more resilient to reduced irrigation (22).

Green spaces featuring a mix of turfgrass and trees may receive or exchange water from the same irrigation system, and also interact in microclimate regulation through evaporative cooling and shade provision. Urban trees create shade and thereby reduce evapotranspiration of adjacent turfgrass compared to full sun exposure, lowering overall water demand (13; 25; 26). Urban trees alter the energy balance for below canopy ground cover and in return are also impacted by energy exchanges from the surface; higher temperatures from below canopy pavement have shown to decrease tree growth (27; 28). In an arid climate, trees with turfgrass understory experienced a higher growth rate in the summer due to the cooling effects from the turfgrass transpiration below the canopy that lowered tree temperatures (29). Decreased evaporative cooling from turfgrass is another side-effect on tree drought resilience that may arise with turfgrass water conservation. The first part of this study aims to simulate how urban trees may be affected by irrigation reductions to turfgrass areas using a small-scale hydrologic modeling method.

Along with irrigated turfgrass areas, trees are often located adjacent to impervious

surfaces such as asphalt, pavement, and buildings. These surfaces alter hydrologic processes due to reduced infiltration and increased surface runoff peaks and volume (30). Impervious area that is directly connected to the stormwater drainage system, known as effective impervious area (EIA), has a greater effect on runoff than hydrologically disconnected impervious area (HDIA), which instead routes stormwater towards vegetated spaces and green infrastructure. When hydrologically connected to neighboring trees, HDIA has the potential to increase tree productivity due to the additional direct water input from surface stormwater runoff (31). To reduce the impacts of impervious surface on hydrology and ecology, green infrastructure, including green spaces and urban trees (32), aims to restore natural processes and decrease runoff using vegetation (33). To continue developing efficient and resilient green infrastructure strategies, there is a need to better understand the small-scale hydrologic interactions between different vegetation types and between impervious surfaces and vegetation.

While green infrastructure has received much attention for the benefits of stormwater management (34; 33; 35), it has the potential to be multifunctional and provide other ecosystem services such as microclimate regulation, carbon sequestration, and biodiversity (2; 36; 37). To gain a better understanding of both ecologic and hydrologic ecosystem services, land surface models are useful for deconstructing how processes are connected and coupled to influence vegetation water use. Several hydrologic models include green infrastructure components to estimate how vegetation impacts runoff or infiltration (38; 39; 40), but fewer include how stormwater affects vegetation growth and resulting ecological processes (37). An additional challenge with land surface modeling is the heterogeneity of surfaces at small scales, especially in urban areas with mixed vegetation and impervious areas that can be differentiated to EIA or HDIA (41; 42).

As well as simulate small-scale hydrologic interactions between trees and irrigated turfgrass, the second goal of this study is to evaluate how neighboring HDIA affects the turfgrass interaction and tree carbon and water fluxes. We developed and tested a new modeling method, multiscale routing (MSR) for surface routing in an urban environment to assess the effects of different land covers on urban tree ecosystem services. We ask the following:

1. How does turfgrass water conservation during drought affect the health of neighboring urban trees?

2. How do hydrologically disconnected impervious areas affect the outcomes?

Landscape heterogeneity in land surface models is an ongoing challenge for modeling coupled eco-hydrologic processes at fine scales (43). Typically, hydrologic models are spatially divided into watersheds based on topography, which are further divided into a grid of smaller units, which can be known as a patch. The size of the patch depends on available elevation and land cover data, which can be between 10-30m^2, and there is often further heterogeneity occurring within a patch. Within a patch, land characteristics and processes are represented as single or aggregated values. There are several methods to

represent subgrid processes that involve aggregating from discrete homogenous areas or statistical dynamical approaches (44). This presents a challenge when subgrid traits are important for hydrologic processes of the entire system, such as in urban areas where hard surfaces route water into stormwater drainage systems. For vegetation within a patch, water accessibility depends on the vertical subsurface stores, with lateral flow from neighboring and upslope patches. In urban areas that have mixed land use at fine scales, additional exchanges of water within a patch are not fully represented. Additionally, land use data that is available at fine scales for urban surfaces can be computationally intensive to model and scale up to watershed level effects.

To account for the effects of small-scale water routing in an urban environment, this paper builds on a new methodology called multi-scale routing (MSR)(45). MSR was developed for the Regional Hydro-Ecological Simulation System (RHESSys), and addresses the challenge of sub-grid scale hydrologic processes through non-spatial specific water gradients between different land covers. With MSR, both hillslope topographical water routing as well as sub-grid water movement is simulated without the requirement of high resolution spatial data or higher computational loads. It addresses subsurface water routing as in the case of mixed vegetation with different rooting depths and distribution that may share water, and was first developed and used for the purpose of simulating the effects of forest thinning (46). Here we use it for an urban environment to assess the effects of subsurface routing between irrigated turfgrass and trees, and for surface routing between impervious land cover and vegetation.

3.2 Methods

3.2.1 RHESSys-MSR

We use the Regional Hydro-Ecological Simulation System (RHESSys)(47) to simulate the effects of small-scale water routing for different scenarios of irrigation and land cover during a drought period. RHESSys mechanistically simulates energy, water, and carbon cycling on the landscape, driven by climate input, land use parameters, and vegetation and soil parameters. In urban landscapes, RHESSys has been used to show how different amounts of connected impervious areas affect plant productivity (31), estimate the effects of urban development on runoff (48), and assess the effects of stormwater control measures on nitrogen loads (49).

Carbon and water cycling in RHESSys is linked through vegetation processes of photosynthesis and evapotranspiration. Gross photosynthesis is estimated by the Farquhar model, where the rate of carbon gain per unit LAI depends on available water, nutrients, and light. Net primary productivity (NPP) is calculated from RHESSys output as the difference between gross photosynthesis and plant respiration from growth and maintenance, which depend on temperature. Water fluxes are driven by precipitation, with vertical fluxes of canopy interception, infiltration, soil evaporation, and plant transpiration. Vegetation evapotranspiration depends on available water in the rooting zone

and is estimated using Penman-Monteith, where vapor pressure deficit depends on daily temperature minimum and maximums. Infiltration enters the rooting zone, and water drains below plant roots into an unsaturated layer, followed by a saturated layer below that drains to groundwater.

Within RHESSys, watersheds are spatially divided into a grid-like array of patches where processes for vegetation growth and vertical water fluxes occur. Typically, the patch level represents a single land use or vegetation type, and when modeling at the watershed scale the patch resolution depends on available elevation and land cover data. At the patch scale, vertical water inputs can include precipitation and irrigation, and if there are multiple patches as in the case of a watershed, lateral routing from upslope patches can bring in surface water from overland flow or lateral subsurface flow between patches in the subsurface. However, within a patch that contains land cover variability, water accessibility may not be driven by large-scale topography, but rather by local soil moisture gradients. Water sharing may occur as roots access soil water stores of neighboring plants, and on the surface due to small-scale variations in land type or soil.

RHESSys-MSR was developed for multiple aspatial patches to exist simultaneously within the same patch unit, which is described as a 'patch family' (Figure 3.1) with water exchanged between them (46). A 'patch family' is composed of multiple aspatial patches that are each assigned an area that is a sub-grid fractional cover, and are considered to be spatially inter-mixed. Each aspatial patch within a family is defined by different land use and vegetation parameters, which affect water fluxes and how much water is available for transferring between patches. Subsurface water transfers between vegetated aspatial patches is driven by their subsurface water content relative to the mean patch family subsurface water content. Differences could be due to infiltration rates, rooting depth, and how much soil water vegetation is using. Aspatial patches containing water above the average lose content, while patches below average gain water. Losses of water occur only for water above the wilting point and gains only occur up to the field capacity. Transfers between patches can be moderated by two sharing coefficients: $sh_L$for losing water and sh_G for gaining water. These coefficients are set to a value between 0-1, with 1 allowing all possible water to be transferred in a single model time step, and 0 turning off the MSR functioning and not allowing water transfer. Any value in between represents a rate, with lower values being a slower transfer and higher values being a quicker transfer. Although the values for sharing coefficients are not an observable physical trait, they represent differences in vegetation species root spread and distribution and soil properties for rate of water movement.

In addition to within patch water routing, patch families create fine-scale shading effects. With standard RHESSys functionality, vertical shade on tree understory is accounted for using Beer's Law and diffuse and direct radiation is estimated with a gap fraction. With MSR, within patch family shading occurs for not only direct vertical understory. Taller trees reduce radiation for shorter neighboring trees, or in our case, turfgrass. Shading is implemented based on the relative height of each vegetation within the patch family, and alters the incoming daily shortwave radiation. For a more detailed

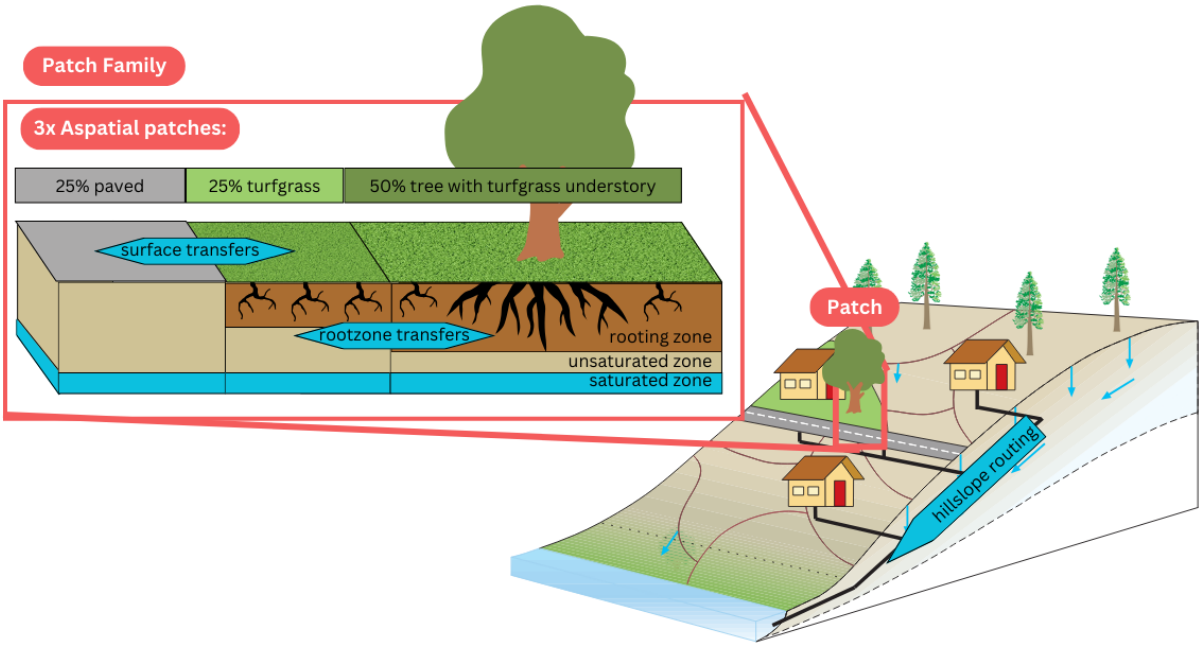

Figure 3.1: Diagram of RHESSys-MSR with a path family made up of 3 apsatial patches.

description on subsurface multiscale routing and shading, see Burke 2021 (46).

3.2.2 New functionality: Surface MSR

This study builds on RHESSys-MSR by developing a surface routing component that accounts for surface routing within a patch family. Within a single patch, water storage on the surface is due to infiltration excess or saturation excess. In the case of impervious surface area, there is no infiltration and any direct rainfall is added to the surface storage. Similar to the subsurface routing, surface water exchanges are driven by individual patch differences in water content on the surface. Surface transfers are all assumed to occur on a daily time step, and are not regulated by a sharing coefficient like the case of the subsurface transfers. To account for connectivity of the impervious surface, a surface parameter is set to 1 to allow impervious surface to gain water, or 0 to turn off gaining. The amount of surface water available to move between aspatial patches within a family is calculated as the area weighted mean of the sum of the total water on all aspatial patches divided by the sum of total area available to receive water (Eq. 3.1).

$$MSW = \frac{\sum_{n=1}^{N} SW * A}{\sum_{n=1}^{G} A} \tag{3.1}$$

MSW = Mean Surface Water

SW = surface water storage

A = area

N = total number of aspatial patches in patch family

G = number of aspatial patches in patch family able to gain water

Aspatial patches with surface water above the mean lose surface water (Eq. 3.2), and aspatial patches with surface water below the mean gain surface water (Eq. 3.3), which is then transferred to infiltration.

$$Loss_i = (SW_i - MSW) * A_i \tag{3.2}$$

$$Gain_i = (MSW - SW_i) * A_i \tag{3.3}$$

i is each aspatial patch

Any leftover water that is not able to infiltrate stays on the surface. Following the surface routing routine, the subsurface sharing module is run, taking into account the updated rooting zone storage and field capacity given the infiltration from the surface exchanges.

This study uses surface MSR with the goal of exploring the potential benefits of routing stormflow from impervious area to vegetated area, but surface MSR was developed for a broader range of application in urban environments. With RHESSys-MSR, impervious areas take up a user-specified fraction of the total patch family area. For routing between patches within a family, surface water from impervious areas can be set up to be transferred to the other patches or to be rerouted directly to stormwater drainage. In our study, the impervious patch has a surface gaining parameter of 0, so it can only lose surface water, and not gain from the other patches. Any precipitation that falls on the impervious area is routed directly to the next vegetation patch where it can infiltrate, evaporate, or be taken up by plants. Thus for the case of this study, all impervious areas are assumed to be HDIA from a watershed scale stormwater drainage perspective.This is set up with the assumption that the impervious area is directly connected to the vegetated area, such as in a residential neighborhood or other parts of a city where vegetation and impervious surfaces are intermixed at small spatial scales. This does not account for parking lots or streets with curbs, where surface runoff from excess stormflow is routed to stormwater drainage systems, as in EIA. This could be an area for future applications that explore EIA effects on runoff.

3.2.3 Model setup: parameters and scenario design

To investigate at the local scale how neighboring irrigated turfgrass affects urban tree health during drought, and how impervious surfaces alter the relationship, we ran simulations at the patch scale and set up two different scenarios of patch family. The

patch family, consisting of 2 to 3 patches that are either: turfgrass only, a tree with turf grass understory, or pavement. The baseline scenario is a 2 patch family, meant to represent a typical planted and managed green space, with irrigated turf grass in one patch and non-irrigated tree with turf grass understory in the other, as shown in Figure 3.2. Setting up both vegetation types required selecting relevant parameters (3.2.3), calibrating for turf grass traits(3.2.3), and doing a sensitivity analysis for the sharing coefficients (3.2.3).

Urban tree parameters

Vegetation parameter uncertainty for tree health during drought has been explored for the same study region in Chapters 1 and 2. These parameters were selected based on a Sobol sensitivity analysis that was performed, along with comparing model output values to high-resolution species level remote sensing data of LAI and NDVI. The model was successfully able to capture patterns in tree response to drought based on changes to NDVI during the drought period. For the parameter calibration, five species were used in that study, selected based on their abundance in the location area and their variety in plant functional types and origin. All five species calibration resulted in a range of parameter sets which were used for this current study.

The tree species used include: coast live oak (*Quercus agrifolia*), blue gum eucalyptus (*Eucalyptus globulus*), California sycamore (*Platanus racemosa*), Canary Island pine (*Pinus canariensis*), and victorian box (*pittosporum undulatum*). To reduce computation time while maintaining parameter uncertainty, for each tree species 50 parameter sets from the acceptable sets were randomly selected and used in this study.

Turfgrass parameters

RHESSys has previously been used to simulate natural grasslands and assess parameter uncertainty for the 'grass' type in the model (50; 51). The parameters used here were based on parameter values defined in these studies, however, turfgrasses are considerably different from native grasses in that they are highly managed and can tolerate defoliation (52), and so a sensitivity analysis for select turfgrass parameters was performed. There are a variety of turfgrass species used for landscaping, recreational, and residential purposes. Commonly used turfgrass species differ in the photosynthetic pathways, with cool-season, or C3, used in more humid climates, and warm-season, or C4, used in arid climates (52). We parameterized to a general perennial C3 grass type, a more traditional landscaping grass. Common C3 species include tall fescue (*Festuca arundinacea*), Kentucky bluegrass (*Poa pratensis L.*), and perennial ryegrass (*Lolium perenne L.*). To account for their variation in rooting depths and leaf area index, parameter uncertainty is included in the model scenarios.

C3 grasses are more productive in spring to early summer but productivity declines with warmer, drier seasons. To simulate these differences, the turfgrass vegetation type was classified as drought-evergreen in the model, following the approach used in a previous

modeling study of natural grasses in Santa Barbara county, where grass growth responded to annual water availability in the winter and amount of daylight (50).

RHESSys parameter values were selected and sampled from a range of values based on previous RHESSys studies as well as field studies of turfgrass lawns and available databases (24; 53; 10; 51). Key parameters that were tested to model traits of grass included specific leaf area (SLA), max rooting depth, and a parameter that transforms leaf carbon to height. Parameters were run with a baseline scenario which consisted of: a two-patch family, with one patch containing an oak tree overstory and turfgrass understory, irrigation in the turfgrass only patch, and MSR sharing coefficients set to 0, so there was no subsurface transfer. Parameter sets were selected based on the output phenology, rooting depth, height, and transpiration, and filtering model output resulted in 23 parameter sets that were used for turfgrass parameter uncertainty in this study. A full list of RHESSys turfgrass parameters varied for this study is provided in the appendix (section C.1).

MSR sharing parameter uncertainty

Gaining and losing subsurface sharing coefficients (sh_L and sh_G) for both vegetation patches were set to the same value, referred to as a single 'sharing coefficient' in the results text. Because there are no observations to suggest differences in these coefficients, we maintained these constant values to represent the aggregate effect of soil properties and root distributions on rates of transfer. Sharing coefficients were varied from 0 to 1 by 0.1 to test for sensitivity in the rate of subsurface water transferred, vegetation water use, and vegetation growth in the baseline scenario of two vegetation patches.

Model scenarios

California experienced an extreme drought from 2012-2016, in this study we focus on this time period as well as the years following the drought. Daily temperature and precipitation data from NOAA (station GHCND:USC00047902) are used as input. Model scenarios were varied by irrigation input and sharing coefficient, with parameter uncertainty for both turfgrass and tree species vegetation parameters, and with and without connected impervious surfaces present (Table 3.1). Each simulation went through a 20 year spin-up period to stabilize soil carbon pools and for tree growth to reach maturity, before values were output from 2010-2020. The spin up period included an average amount of irrigation applied to the grass patch.

The baseline irrigation scenario (on in Table 3.1) is the same input used in Chapter 2 (2.1), based on monthly outdoor water use data from Santa Barbara Water Resources from 2010-2020. A water conservation mandate for Santa Barbara county was set in 2014 which is reflected in the data; for our simulations to replicate the case of no mandates or conservation, we used the average weekly amount from previous years. For the other two scenarios we first used 25% as the reduction amount based on the California statewide water conservation goal during drought in 2015. Secondly, for the complete irrigation

reductions, the baseline irrigation rate was used until 2015, at which time it was reduced to zero.

Table 3.1: Summary of all model parameters and scenarios. Bolded names are used in text and figures as abbreviations.

Scenarios	Description	Count
Tree Species	number of species parameter uncertainty	5 50
Turfgrass	parameter uncertainty	24
Turfgrass irrigation	**on:** Cool-season turfgrass, pre-drought typical lawn, irrigated **off:** Irrigation turned off **-25%:**irrigation reduced by 25%	3
Patch families	**Turf-PF:** 50% turfgrass and 50% tree with turfgrass understory **Impervious-PF:** 25% impervious area, 25% turfgrass, and 50% tree with	2
Sharing coefficient	0 to 1 by 0.1 increments	11

We compare two patch family scenarios: the first is vegetation only, which contains two 50% patches with one turfgrass and one with a tree. The second patch family contains a 50% tree with turfgrass understory patch, a 25% impervious surface patch, and 25% of irrigated turfgrass (Figure 3.2). The 3 patch family mix with 25% impervious surface is representative of an area with neighboring sidewalk or pavement. The amount of pavement selected was based on a remote sensing study using 7.5m^2 imagery to extract subpixel fractional cover in the study area. Pavement was up to 31.8% for the entire study area, and pavement and roof combined made up around 20% for tree polygons ¡1000m^2 (14). The names of patch families will be referred to here as 'Turf-PF' and 'Impervious-PF'.

3.2.4 Post-model run analysis

Post-model run analysis was done using R version 3.6.3. Model output was aggregated to annual values and average daily values during and after the drought period to compare across tree species, sharing coefficients, patch families, and irrigation. Model output variables include tree net primary productivity (NPP), evapotranspiration (ET), and drought resilience of LAI. We defined drought resilience as the ability of the tree to return to a pre-drought level of canopy cover in the year following the drought. In this

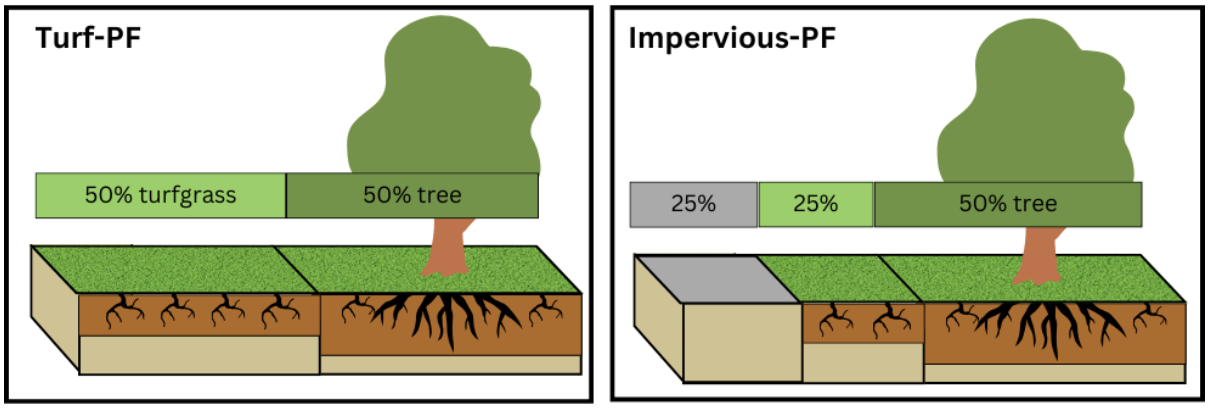

Figure 3.2: Patch family scenarios: Turf-PF is vegetation only with 50% turfgrass. Impervious-PF is 25% impervious area, with 25% turfgrass.

case, we use the ratio of the average LAI for 2017 to average LAI in 2011. A value of 1 or greater indicates the tree is resilient, whereas values ¡1 indicate that it was affected by drought. To compare across the different scenarios, results were aggregated to the mean of each combination of sharing coefficient, irrigation scenario, tree species, and patch family and ran with analysis of variance (anova). When significant differences were present, post-hoc tukey's test was performed to test for differences in means and check sensitivity of the output.

3.3 Results

3.3.1 Sensitivity to subsurface sharing coefficient

We varied sharing coefficients, which control the rate of water transfer between the vegetation rooting zones, from 0 to 1. When set to 0, transfer is turned off. For values greater than 0, the sharing coefficient controls the rate of transfer with smaller values being a slower rate. With the sharing coefficient set to 0, mean tree ET and NPP were lower than all other sharing coefficient scenarios (Figure 3.3). All sharing coefficients greater than 0 resulted in average tree NPP, ET, and transfers that were significantly different from the average when sharing coefficient was set to 0, indicating that within patch water routing plays an important role for estimating small scale vegetation water balance.

Sharing coefficients from 0.1 to 0.3 caused more variation in ET, while sharing coefficients 0.4 to 1 had similar values. Average annual subsurface transfers and NPP were highest with sharing coefficients of 0.2 and 0.3. Average annual tree ET was highest with a sharing coefficient of 0.2 (Figure 3.3). Full results showing differences in sharing coefficient scenarios are shown in Appendix C(Figure 3.8).

For the vegetated patch family, subsurface transfers occurred in both directions (e.g from tree to turfgrass patch and vice versa) but on average went from the turfgrass patch

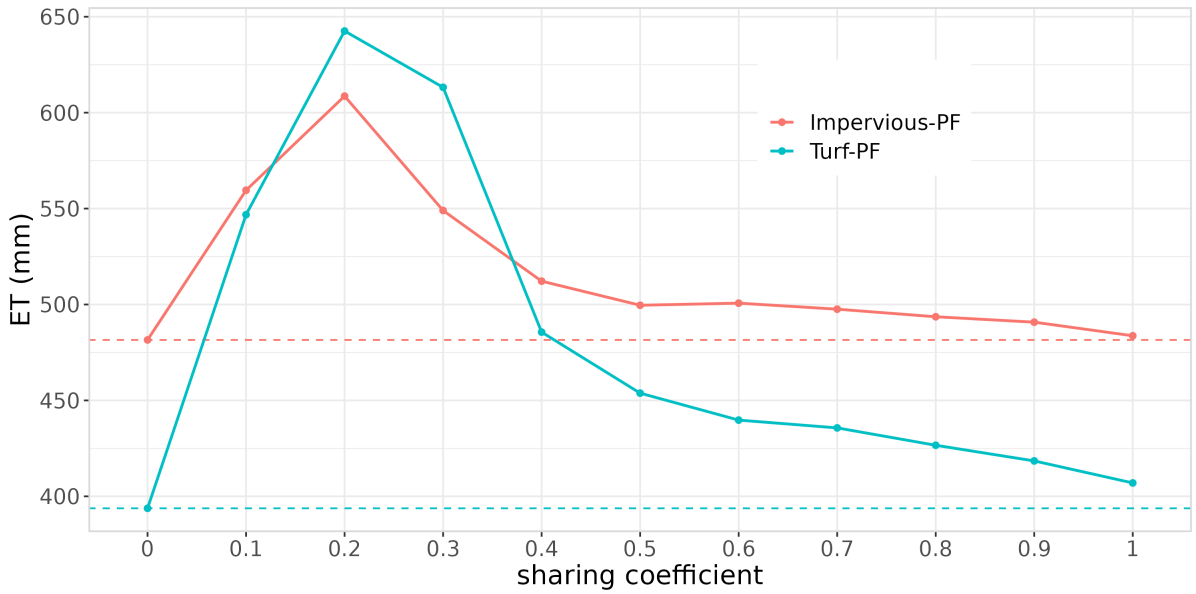

Figure 3.3: Average drought year ET for each sharing coefficient grouped by patch families. Dashed lines show value when the sharing coefficient is set to 0 and there are no subsurface transfers occurring.

to the tree patch (Figure 3.4, panel F). Subsurface transfers decreased during the drought years. Sharing coefficients had a greater effect on transfers and carbon and water fluxes when there was less water available, during the drought and in late summer (Figure 3.4).

3.3.2 Effects of irrigation reductions

For comparing irrigation scenarios, we are focusing on sharing coefficients that have the maximum effect on carbon and water fluxes, and show the average of sharing coefficients set to 0.2 to 0.3. Irrigation reduction effects resulted in less subsurface sharing and were most prominent under dry conditions (Figure 3.5). There were significant differences in mean LAI resilience for the different irrigation scenarios and tree species. Across all tree species the mean LAI resilience declined with less irrigation input, but the magnitude of reduction was dependent on tree species and, to a lesser extent, patch family configuration (Figure 3.6). Annual average tree ET and NPP in drought years declined with decreased irrigation input. However, in wet years following the drought, irrigation input had little effect on annual values of ET and NPP (Figure 3.7).

3.3.3 Comparing patch family impervious surface area

We compared the patch family with only vegetation (Turf-PF) to the patch family with 25% impervious surface (Impervious-PF). In both cases, trees comprised 50% of the patch family. Patch family configuration effects on LAI resilience, and tree carbon and

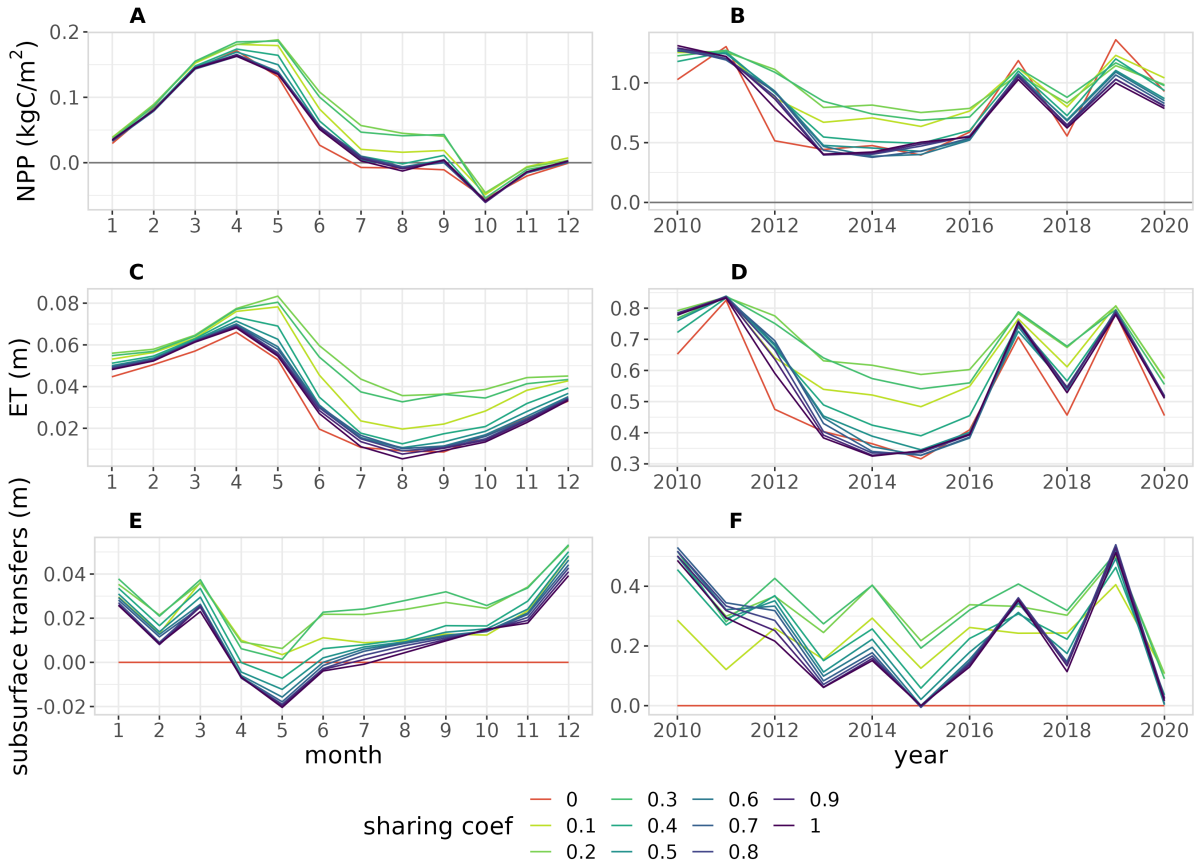

Figure 3.4: Model outputs for trees in the vegetated patch family, aggregated by sharing coefficient. Left panels show monthly averages for drought years 2012-2016. Right panels show annual averages.

water fluxes, were smaller relative to irrigation and tree species differences. Impervious areas increased the magnitude and peak of surface water transfers. Subsurface transfers were on average lower with Impervious-PF, and there were more occurrences of the tree patch losing water from the rooting zone compared to Turf-PF (Figure 3.7).

Because sharing coefficients had an effect on the differences between patch family water and carbon fluxes (Figure 3), we filtered the results to further analyze tree responses when sharing coefficients are set to 0.2-0.3. With sharing coefficients set to these values, the largest average subsurface sharing occurred, allowing us to explore the potential maximum benefits of turfgrass irrigation to tree water use. For example, Figure 4 shows the coefficients 0.2 and 0.3 have higher average ET and NPP during the drought. The effects of impervious areas interacted with irrigation scenarios for drought years. With irrigation on, and reduced by 25%, Turf-PF had greater average values for ET and NPP. However, with irrigation turned off, Impervious-PF had greater average ET and NPP. In the post-drought year with higher rainfall there were no significant differences between the patch families (Figure 3.7). When sharing coefficients were not equal to 0.2 or 0.3,

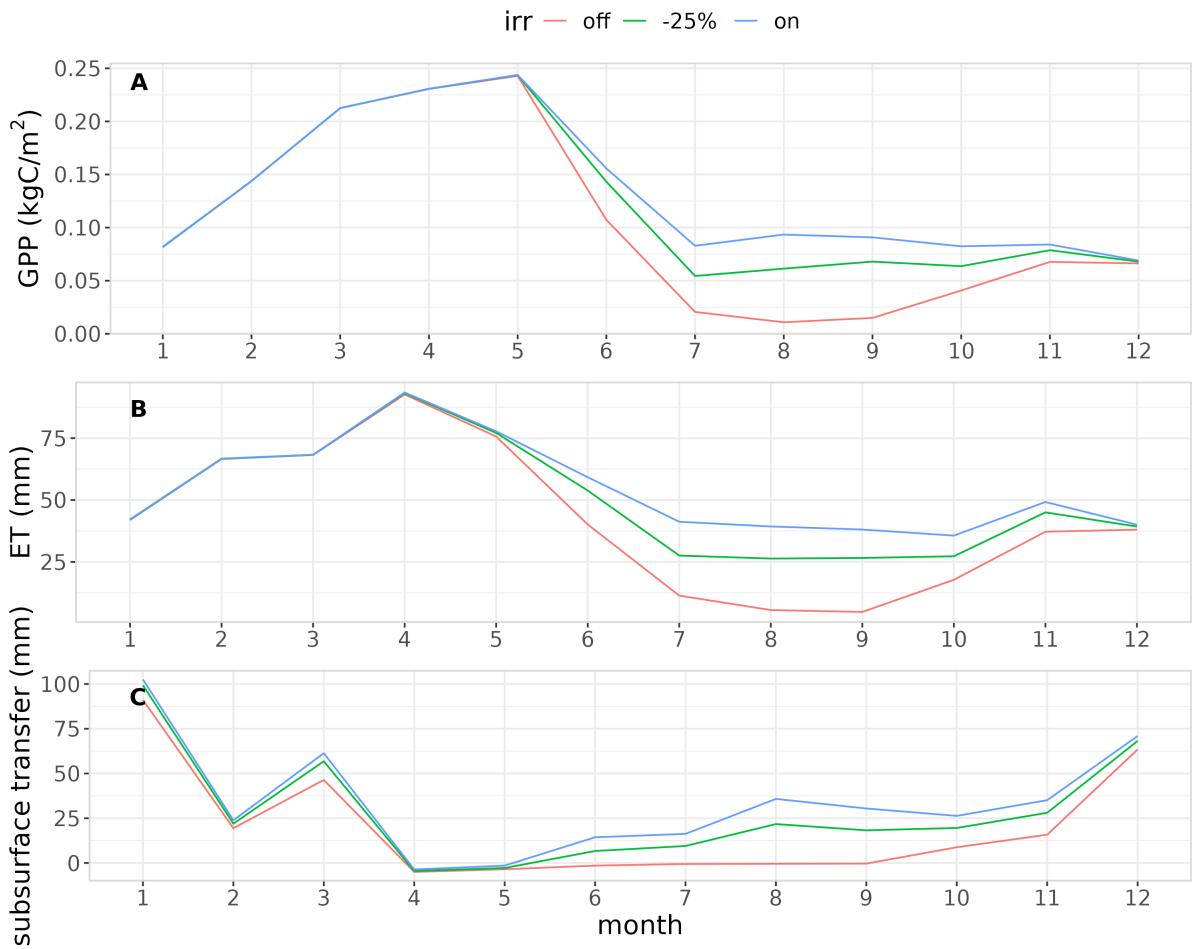

Figure 3.5: Average monthly values of A) GPP and B) ET, and C) subsurface transfers in drought year with irrigation reductions, averaged across all tree species with sharing coefficients set to 0.2 and 0.3

Impervious-PF had greater average ET, NPP, and LAI resilience compared to Turf-PF for all irrigation scenarios.

3.4 Discussion

3.4.1 Interacting effects among irrigation, tree species, and impervious area

Trees in arid to semi-arid cities receive several additional water inputs besides direct precipitation including irrigation, either directly or indirectly, and stormflow from increased impervious surfaces (22; 23; 54). We used a novel modeling approach to investigate how changes to different water sources affect tree health during a drought by

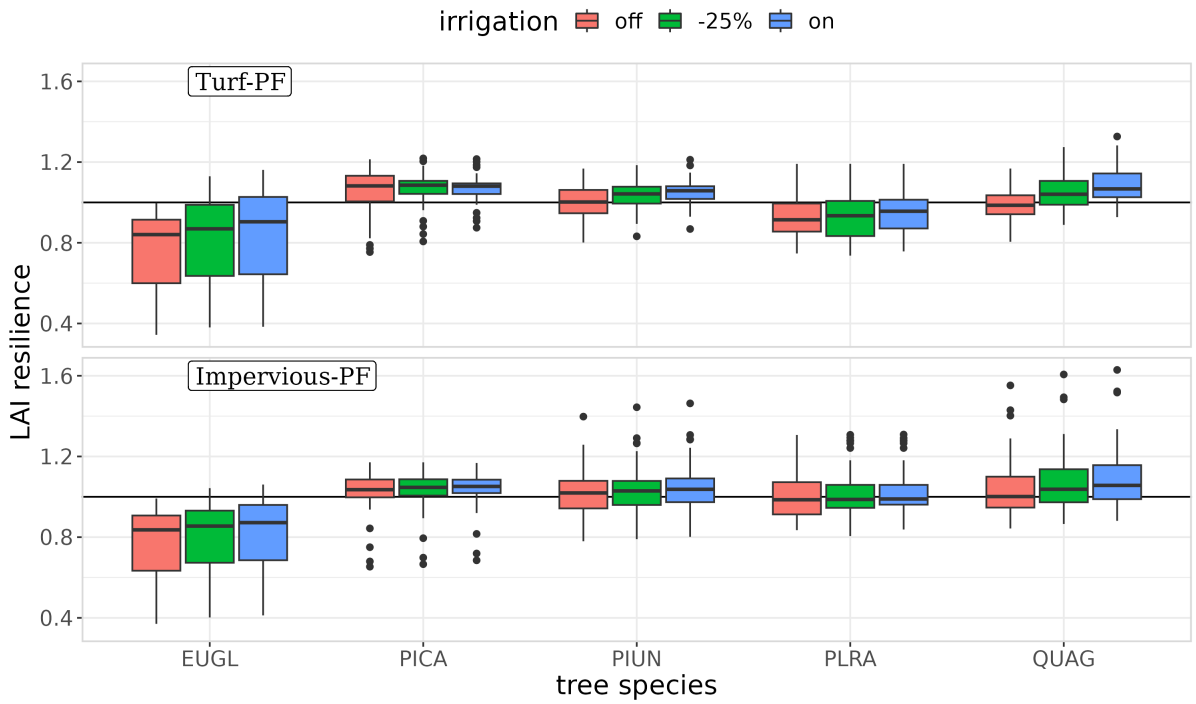

Figure 3.6: LAI resilience aggregated to sharing coefficients of 0.2 and 0.3, for each tree species and patch family. Variation in boxplots is from vegetation parameter uncertainty. LAI resilience is the ratio of post-drought LAI in 2017 to pre-drought LAI in 2011.

comparing model estimates of tree water use and productivity for scenarios of trees situated near irrigated turfgrass. We first compared a baseline of tree health with irrigated turfgrass against irrigation reductions, and secondly compared with a scenario of tree and irrigated turfgrass arranged with impervious surface areas. In our case of irrigation, trees received additional water that was not taken up by turfgrass for transpiration through lateral hydraulic transfers.

Our results show that irrigation input to turfgrass during a drought year can reduce vulnerability to drought of neighboring tree carbon and water fluxes. With full irrigation to turfgrass, average tree LAI drought resilience, drought year NPP, and ET were significantly greater than with irrigation turned off. In the case of irrigation reduced by 25%, LAI resilience slightly declined but it varied by tree species, suggesting turfgrass irrigation during drought can be conserved without having negative effects on neighboring trees.

These results vary slightly by tree species and patch family configuration. The California Sycamore (PLRA) and Canary Island Pine (PICA) had smaller differences in LAI drought resilience between irrigation scenarios, suggesting there is less reliance on irrigation as a water source. In field studies, the Canary Island Pine has been shown to maintain transpiration under low soil water availability (55; 56). Blue gum eucalyptus

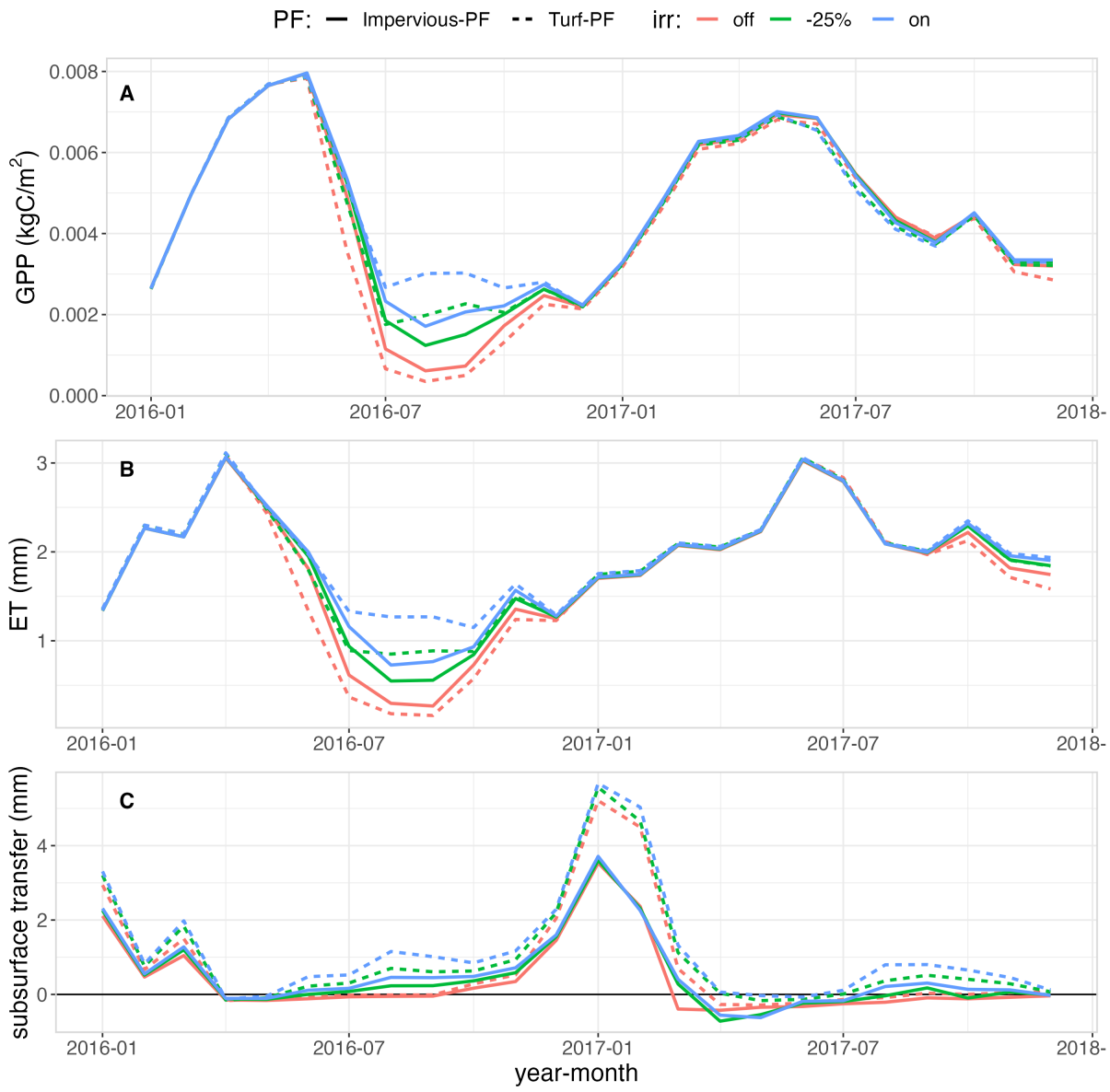

Figure 3.7: Monthly averages with sharing coefficients at 0.2 or 0.3 for A) GPP, B) ET and C) subsurface transfers. Changes to irrigation take effect in late 2015, and this plot shows irrigation effects for the last year of the drought in 2016, followed by 2017 which returned to normal rainfall levels.

(EUGL) LAI resilience varied more within irrigation scenarios due to vegetation parameter uncertainty, which could reflect more dependence on location than irrigation for drought resilience. The two broadleaf evergreens (PIUN and QUAG) had greater differences between the means (Figure 3.6); suggesting these tree species are more sensitive to the irrigation reduction, and may rely on soil water availability at shallow depths.

More data is needed to further explore which traits, such as rooting structure or response to drought stress, affect how much tree species benefit from excess irrigation input (57; 58; 59). Our results indicate that when planning for outdoor water conservation on turfgrass lawns and green spaces, not only proximity of trees, but the tree species should be considered.

We also considered the effects of irrigation reductions when there was an impervious area hydrologically disconnected from the stormwater drainage system. We compared tree carbon and water fluxes of two patch families with the varying irrigation scenarios. The differences between patch families during the post-drought wet year were minimal (Figure 3.7). In the drought year, the tree in the patch family that was half turfgrass (Turf-PF) had a greater average ET and NPP but only when irrigation was turned on. With irrigation turned off, the trees in Impervious-PF had greater mean ET and NPP (Figure 3.7). This suggests that trees in green spaces connected to impervious surfaces benefit from taking up stormwater, especially when water accessibility is limited during drought and irrigation is turned off for conservation. Shields and Tague, 2015 (31) also showed that stormwater runoff from impervious surfaces increased the primary productivity of vegetation receiving the runoff. Similarly, Voter and Loheide 2018 (60) demonstrated increased ET during dry years for a lawn with disconnected impervious surfaces. In water-limited places, there is potential for a multifunctional system, where trees both provide ecosystem services and directly benefit from being planted in locations designed to capture stormwater. The disadvantage of using stormwater runoff as a water source is its seasonality, especially in a Mediterranean climate, and more research is needed to quantify the effectiveness of trees in reducing stormwater runoff (32; 61). It was outside the scope of our study to consider the impacts on runoff, but there are a growing number of studies exploring vegetation that makes up the green infrastructure, including ET fluxes, for stormwater management (62; 63; 64; 65; 66).

3.4.2 Application of Multi-Scale Routing (MSR) and future directions

Modeling hydrologic processes in urban environments is complex due to the heterogeneity in land cover and vegetation and, when there is available data, computational cost of running process-based simulations at high spatial resolutions. To explore fine-scale hydrologic interactions, we used a novel methodology of small scale water routing, called multi-scale routing or MSR (45). One advantage of the MSR approach is that patches, or the smallest spatial unit in the model, are subdivided into different land cover types each with its own water balance, allowing for sub-grid variation in both surface and subsurface properties. Having explicit representation of land cover is helpful for improving surface routing estimates, but subtle differences in water availability, soil properties, and rooting depths can create subsurface hydrologic gradients that may be a more dominant pathway for vegetation water access, especially when stormwater is limiting such as during drought years. MSR allows us to implicitly account for these potential subsurface

variations through transfers mediated by the sharing coefficient. We tested the sensitivity to the subsurface sharing coefficient, and developed MSR on the surface to account for small-scale runoff from impervious areas disconnected from the stormwater drainage system.

For MSR in the subsurface, the sharing coefficient serves as an effective rate of water transfer across a soil moisture gradient. It is representative of the conductivity through the soil medium, and because the areas within the patch families are not spatially explicit, it also accounts for uncertainty in distance between the different patches. For example, with a lower sharing coefficient, transfers occur more slowly, which can be due to a larger distance between roots, more compacted soil, or a combination of these factors. Given the uncertainty in rooting lateral distribution and soil properties, we displayed a summary of results for all sharing coefficients (Figure 3.4), and focused on the outcomes with sharing coefficients set to 0.2 and 0.3 because of their increased effects on tree ET (Figure 3.2. When sharing coefficients were set to 0.2 or 0.3, there was an increase in annual subsurface transfers into the tree patch during drought years. Sharing coefficient values of 0.4 to 1 had lower amounts of transfer and similar daily and annual values, which is further shown in the Appendix (Figure 3.8). The larger amount of annual transfer with sharing coefficients set to 0.2 and 0.3 is partially due to the fact that most of the time the tree patch was gaining water, which is a positive transfer, while with the other coefficients the tree patch was losing water at times.

Multi-Scale Routing has potential to improve simulations of green infrastructure at small scales, and also scaling up to simulate the effects of widespread implementation at the catchment level. While plot-level studies are helpful to understand the local interactions occurring, there is a need for more catchment level studies on the benefits of comprehensive implementation of green infrastructure and how it affects runoff and water quality in streams (61; 67; 37). With the advancement of sub-pixel fractional urban land cover estimates from remote sensing data (68), more spatial data is becoming available that could be used to set up interconnected patch families in MSR. At larger scales, MSR can be used to account for both the implicit sub-grid local routing and the explicit topographical hillslope routing, and future work should explore how it would compare to standard hillslope routing without MSR for an urbanized watershed.

Finally, this study includes some limitations and potential for further research. While we accounted for uncertainty in vegetation parameters, there is more work to be done exploring the sensitivity to soil properties by including uncertainty in soil parameters and their interaction with sharing coefficients. It is known that soil in urban environments is highly heterogeneous and is often compacted beneath impervious surfaces (69; 70; 71). Variation in soil compaction and moisture affects infiltration, tree water accessibility, lateral transfer, and amount of runoff (72; 73; 74). We found that when sharing coefficients were not equal to 0.2 or 0.3, there were greater differences in results between land covers. The variation in our results due to different sharing coefficients affirms the importance of subsurface characteristics on vegetation water accessibility, and this could be an area for further research in urban hydrologic modeling. There are in-situ studies at the plot

level that measure both tree and turfgrass evapotranspiration (25; 26) and measurements of infiltration capacity of soil (74; 75) that could be used to validate MSR and reduce uncertainty in sharing coefficients. In addition, it's been shown that the slope of impervious surfaces affects how much runoff and infiltration occurs in neighboring turfgrass (60), but this is not yet accounted for in the surface MSR and could be an area of further development.

3.5 Conclusion

We applied a novel fine-scale hydrologic modeling approach to assess how selected urban trees responded to changes in indirect water sources during a drought in Southern California. We demonstrated that trees potentially receive water indirectly from turfgrass irrigation, consistent with field studies in semi-arid regions (22; 23). On average, irrigated turfgrass increased neighboring tree drought resilience, evapotranspiration, and productivity compared to turfgrass with irrigation cut off during drought. Trees responded to irrigation reduced by 25% with small declines in resilience, evapotranspiration, and productivity. Two of the tree species, California Sycamore and Canary Island Pine, were less affected by irrigation reductions, while the broadleaf evergreen species were more sensitive to it. When irrigation was fully turned off, trees benefited from stormwater runoff from neighboring impervious areas, which implies trees have potential to both provide ecosystem services in stormwater runoff reductions and benefit from it. Results varied by sharing coefficient, a key parameter in MSR modeling that represents heterogeneity in soil properties and distance between roots. Using multi-scale routing allowed us to capture fine-scale hydrologic interactions and highlight the uncertainty in soil moisture and subsurface characteristics in urban environments. Our findings are relevant for urban tree and turfgrass management during drought, future research in green infrastructure for stormwater management, and also for addressing spatial scale complexities in urban hydrologic modeling.

C Appendix

This appendix includes more information for the turfgrass parameterization done in this chapter, including Table 3.2 which shows the RHESSys parameters that were calibrated, values used, and sources. This also includes the resulting turfgrass output and measurement comparisons in Table 3.3. Figures showcase the differences in results due to different subsurface sharing coefficients. Figure 3.8 shows the difference in the mean for model outcomes: ET, LAI resilience, NPP, and subsurface transfers, displaying how sharing coefficients with values of 0, 0.2, or 0.3 vary the most from average. Figure 3.9 further explores the different outcomes when sharing coefficient is set to 0.2 or 0.3, by aggregating to those two scenarios compared to all the others. The sharing coefficients had an effect on how much impervious surface runoff altered tree carbon and water fluxes.

There is also a short description on data used and a link to the github for the RHESSys version with surface MSR in section C.2.

C.1 Tables and Figures

Table 3.2: Vegetation parameters varied for turfgrass sensitivity analysis. Other parameters that were changed to be C3-turfgrass specific included constraints on daylength response and height. The cool-season response to day length was set up with parameters that constrain maximum and minimum day length requirements in the dynamic phenology model, which created a peak in photosynthesis in the spring. To simulate a constant height, as the model does not account for mowing, the height exponential parameter is kept at a constant 1, so rather than height increasing exponentially it stays constant with the leaf carbon that gets replaced by new leaf turnover.

RHESSys turfgrass parameter	**Range [min, max]**	**Source**
epc.gl_smax	[0.004, 0.012]	Reyes al. 2017 (51)
epc.ndays_expand	[16, 30]	calibration
epc.ndays_litfall	[16, 30] 2	calibration
epc.leaf_turnover	[6, 12]	Christians et al. 2016 (52)
epc.waring_pa	[0.4, 1]	Reyes et al. 2017 (51)
epc.froot_cn	[28, 45]	TRY database (53)
epc.leaf_cn	[10, 50]	TRY database (53)
epc.height_to_stem_coef	[0.3, 1.5]	calibration
epc.proj_sla	[12, 27]	Bijoor et al. 2014 (24); TRY database (53)
epc.max_root_depth	[0.2, 0.5]	Christians et al. 2016 (52)

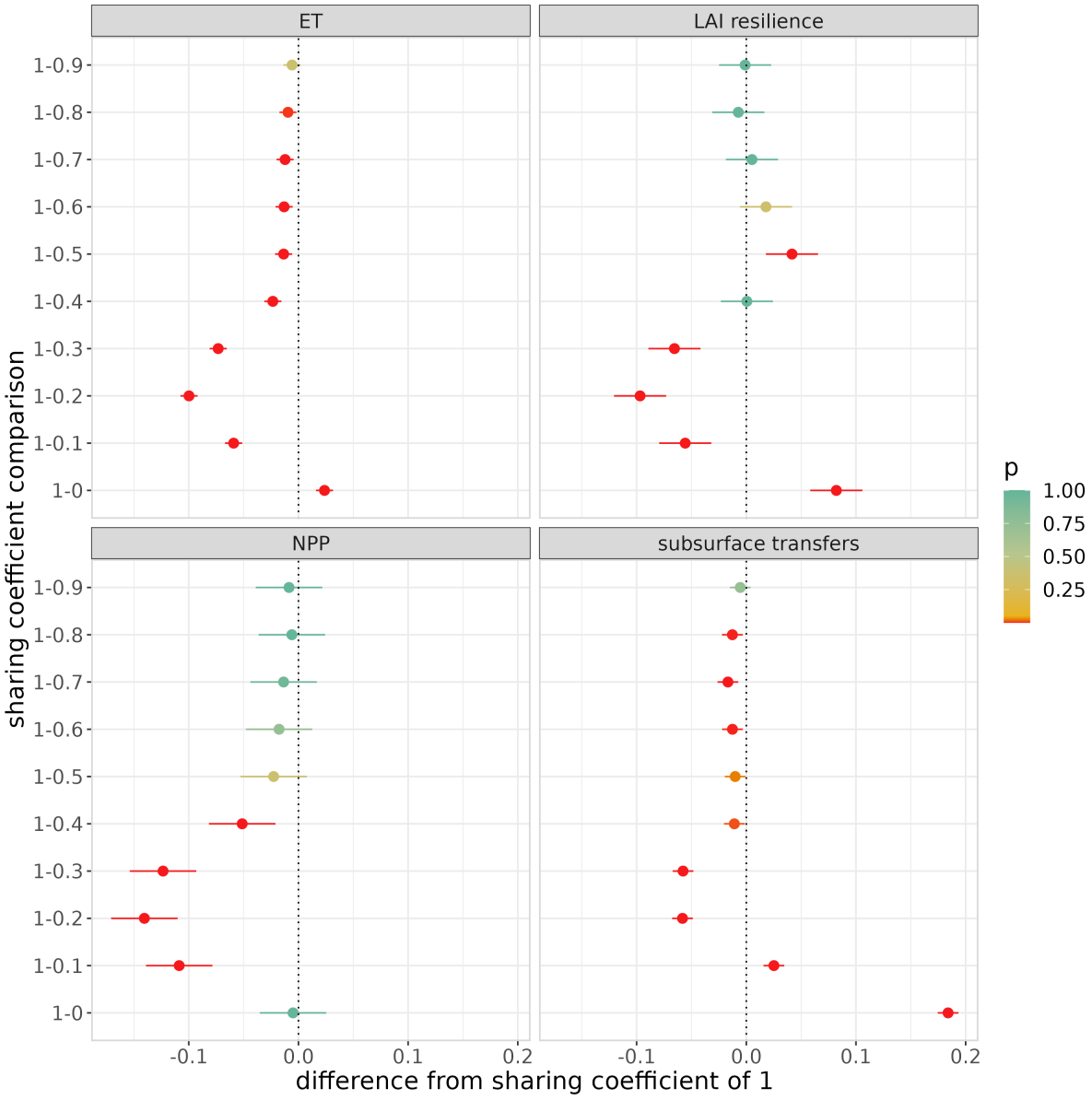

Figure 3.8: Sharing coefficients were statistically different for each tree outcome: annual ET, annual subsurface transfers (root zone and unsaturated), annual NPP, and LAI resilience. This figure shows results from post-hoc difference in means Tukey's test, with difference in means between sharing coefficient set to 1 and other sharing coefficient, and red representing p-values less than 0.05. All results except NPP had a significantly lower result when the sharing coefficient was set to 0. Sharing coefficients 0.1-0.3 stand out with statistically significant differences that are greater than the other means for subsurface transfers, NPP, and LAI resilience. Sharing coefficients from 0.4 to 1 had less variation for all outcomes except for LAI resilience.

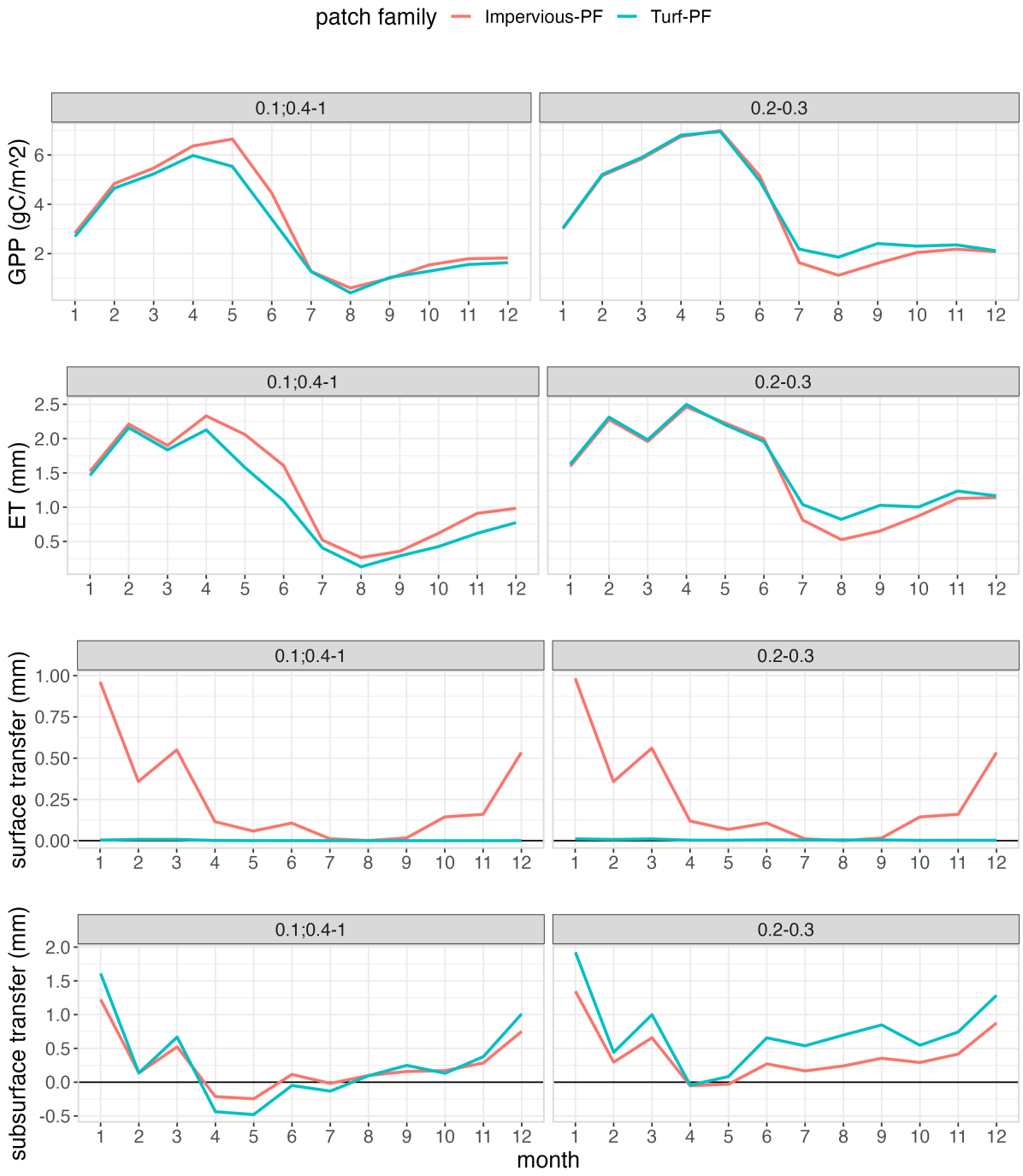

Figure 3.9: Average monthly tree fluxes for drought years 2012-2016, with left panels showing mean of sharing coefficients not equal to 0.2-0.3, and right panels showing mean of sharing coefficients set to 0.2-0.3. Pink line is a vegetated patch family with 50% turfgrass (Turf-PF) and the blue line is 25% turfgrass and 25% impervious area (Impervious-PF).

Table 3.3: Model output of turfgrass from filtered parameter sets, compared with variables from field studies and data provided by Joe Mcfadden (marked as JPM under source).

Variables	**Value Range**	**Source**	**Model Output Avg.**
Rooting Depth (cm)	20.3 - 45	Wu 1985 (**?**)	24
LAI (mm/mm)	0.7 - 2.7	JPM	1.6
Height (cm)	7.6 - 15.25	JPM	11
Evapotranspiration (mm/year)	834 ± 67; 722 ± 22	Bijoor et al. 2014, Litvak et al. 2017 (24; 10)	456

C.2 Data Availability

Information for data used here and tree vegetation parameters can be found in Appendix A (A.2). Post-model analysis was done in R using standard packages. The version of RHESSys used for Chapter 3 can be found in my Fork of RHESSys under the branch msr-lu (`https://github.com/rachtorr/RHESSys-rt/tree/msr-lu`).

Chapter 3 References

[1] S. J. Livesley, G. M. McPherson, and C. Calfapietra, *The Urban Forest and Ecosystem Services: Impacts on Urban Water, Heat, and Pollution Cycles at the Tree, Street, and City Scale*, *Journal of Environment Quality* **45** (2016), no. 1 119.

[2] S. T. Lovell and J. R. Taylor, *Supplying urban ecosystem services through multifunctional green infrastructure in the United States*, *Landscape Ecol* **28** (Oct., 2013) 1447–1463.

[3] E. G. McPherson, J. R. Simpson, Q. Xiao, and C. Wu, *Million trees Los Angeles canopy cover and benefit assessment*, *Landscape and Urban Planning* **99** (Jan., 2011) 40–50.

[4] M. Esperon-Rodriguez, P. D. Rymer, S. A. Power, A. Challis, R. M. Marchin, and M. G. Tjoelker, *Functional adaptations and trait plasticity of urban trees along a climatic gradient*, *Urban Forestry & Urban Greening* **54** (Oct., 2020) 126771.

[5] K. Lanza and B. Stone, *Climate adaptation in cities: What trees are suitable for urban heat management?*, *Landscape and Urban Planning* **153** (Sept., 2016) 74–82.

[6] E. McPherson, A. M. Berry, and N. S. van Doorn, *Performance testing to identify climate-ready trees*, *Urban Forestry & Urban Greening* **29** (Jan., 2018) 28–39.

[7] P. Gober, A. Middel, A. Brazel, S. Myint, H. Chang, J.-D. Duh, and L. House-Peters, *Tradeoffs Between Water Conservation and Temperature Amelioration In Phoenix and Portland: Implications For Urban Sustainability*, *Urban Geography* **33** (Oct., 2012) 1030–1054.

[8] S. J. Livesley, V. Marchionni, P. K. Cheung, E. Daly, and D. E. Pataki, *Water Smart Cities Increase Irrigation to Provide Cool Refuge in a Climate Crisis*, *Earth's Future* **9** (2021), no. 1 e2020EF001806.

[9] N. H. Grijseels, E. Litvak, M. L. Avolio, A. R. Bratt, J. Cavender-Bares, P. M. Groffman, S. J. Hall, S. E. Hobbie, S. B. Lerman, J. L. Morse, D. L. Narango, C. Neill, J. O'Neil-Dunne, J. Padullés Cubino, T. L. E. Trammell, and D. E. Pataki, *Evapotranspiration of Residential Lawns Across the United States*, *Water Resources Research* **59** (2023), no. 6 e2022WR032893.

[10] E. Litvak, K. Manago, T. S. Hogue, and D. E. Pataki, *Evapotranspiration of urban landscapes in Los Angeles, California at the municipal scale - Litvak - 2017 - Water Resources Research - Wiley Online Library*, 2017.

[11] C. Mini, T. S. Hogue, and S. Pincetl, *Estimation of residential outdoor water use in Los Angeles, California*, *Landscape and Urban Planning* **127** (July, 2014) 124–135.

[12] S. Pincetl, T. W. Gillespie, D. Pataki, E. Porse, S. Jia, E. Kidera, N. Nobles, J. Rodriguez, and D.-h. Choi, *Evaluating the Effect of Turf-Replacement Programs in Los Angeles County*, .

[13] J. H. Lowry, R. D. Ramsey, and R. K. Kjelgren, *Predicting urban forest growth and its impact on residential landscape water demand in a semiarid urban environment*, *Urban Forestry & Urban Greening* **10** (Jan., 2011) 193–204.

[14] D. L. Miller, M. Alonzo, D. A. Roberts, C. L. Tague, and J. P. McFadden, *Drought response of urban trees and turfgrass using airborne imaging spectroscopy*, *Remote Sensing of Environment* **240** (Apr., 2020) 111646.

[15] H. Cooley, *Urban and Agricultural Water Use in California, 1960–2015*, .

[16] J. B. Beard and R. L. Green, *The Role of Turfgrasses in Environmental Protection and Their Benefits to Humans*, *Journal of Environmental Quality* **23** (1994), no. 3 452–460.

[17] J. A. Monteiro, *Ecosystem services from turfgrass landscapes*, *Urban Forestry & Urban Greening* **26** (Aug., 2017) 151–157.

[18] B. Chang, B. Wherley, J. A. Aitkenhead-Peterson, and K. J. McInnes, *Effects of urban residential landscape composition on surface runoff generation*, *Science of The Total Environment* **783** (Aug., 2021) 146977.

[19] M. A. Nocco, S. E. Rouse, and N. J. Balster, *Vegetation type alters water and nitrogen budgets in a controlled, replicated experiment on residential-sized rain gardens planted with prairie, shrub, and turfgrass*, *Urban Ecosyst* **19** (Dec., 2016) 1665–1691.

[20] N. K. Fillo, A. S. Bhaskar, and A. J. Jefferson, *Lawn Irrigation Contributions to Semi-Arid Urban Baseflow Based on Water-Stable Isotopes*, *Water Resources Research* **57** (2021), no. 8 e2020WR028777.

[21] K. F. Manago and T. S. Hogue, *Urban Streamflow Response to Imported Water and Water Conservation Policies in Los Angeles, California*, *JAWRA Journal of the American Water Resources Association* **53** (2017), no. 3 626–640.

[22] N. S. Bijoor, H. R. McCarthy, D. Zhang, and D. E. Pataki, *Water sources of urban trees in the Los Angeles metropolitan area*, *Urban Ecosyst* **15** (Mar., 2012) 195–214.

[23] C. Gómez-Navarro, D. E. Pataki, G. J. Bowen, and E. J. Oerter, *Spatiotemporal variability in water sources of urban soils and trees in the semiarid, irrigated Salt Lake Valley*, *Ecohydrology* **12** (2019), no. 8 e2154.

[24] N. S. Bijoor, D. E. Pataki, D. Haver, and J. S. Famiglietti, *A comparative study of the water budgets of lawns under three management scenarios*, *Urban Ecosystems; Salzburg* **17** (Dec., 2014) 1095–1117.

[25] E. Litvak, N. S. Bijoor, and D. E. Pataki, *Adding trees to irrigated turfgrass lawns may be a water-saving measure in semi-arid environments*, *Ecohydrology* **7** (2014), no. 5 1314–1330.

[26] E. Litvak and D. E. Pataki, *Evapotranspiration of urban lawns in a semi-arid environment: An in situ evaluation of microclimatic conditions and watering recommendations*, *Journal of Arid Environments* **134** (Nov., 2016) 87–96.

[27] Y. Chen, X. Wang, B. Jiang, Z. Wen, N. Yang, and L. Li, *Tree survival and growth are impacted by increased surface temperature on paved land*, *Landscape and Urban Planning* **162** (June, 2017) 68–79.

[28] B. Cui, X. Wang, Y. Su, C. Gong, D. Zhang, Z. Ouyang, and X. Wang, *Responses of tree growth, leaf area and physiology to pavement in Ginkgo biloba and Platanus orientalis*, *Frontiers in Plant Science* **13** (2022).

[29] E. C. Mueller and T. A. Day, *The effect of urban ground cover on microclimate, growth and leaf gas exchange of oleander in Phoenix, Arizona*, *Int J Biometeorol* **49** (Mar., 2005) 244–255.

[30] L. B. Leopold, *Hydrology for urban land planning: A guidebook on the hydrologic effects of urban land use*, .

[31] C. Shields and C. Tague, *Ecohydrology in semiarid urban ecosystems: Modeling the relationship between connected impervious area and ecosystem productivity*, *Water Resources Research* **51** (Jan., 2015) 302–319.

[32] A. Berland, S. A. Shiflett, W. D. Shuster, A. S. Garmestani, H. C. Goddard, D. L. Herrmann, and M. E. Hopton, *The role of trees in urban stormwater management*, *Landsc. Urban Plan.* **162** (June, 2017) 167–177. WOS:000399627800016.

[33] L. Prudencio and S. E. Null, *Stormwater management and ecosystem services: a review*, *Environ. Res. Lett.* **13** (Feb., 2018) 033002.

[34] A. J. Jefferson, A. S. Bhaskar, K. G. Hopkins, R. Fanelli, P. M. Avellaneda, and S. K. McMillan, *Stormwater management network effectiveness and implications for urban watershed function: A critical review*, *Hydrological Processes* **31** (Nov., 2017) 4056–4080.

[35] C. J. Walsh, T. D. Fletcher, and A. R. Ladson, *Stream restoration in urban catchments through redesigning stormwater systems: looking to the catchment to save the stream*, *Journal of the North American Benthological Society* **24** (Sept., 2005) 690–705.

[36] D. E. Pataki, M. M. Carreiro, J. Cherrier, N. E. Grulke, V. Jennings, S. Pincetl, R. V. Pouyat, T. H. Whitlow, and W. C. Zipperer, *Coupling biogeochemical cycles in urban environments: ecosystem services, green solutions, and misconceptions*, *Frontiers in Ecology and the Environment* **9** (2011), no. 1 27–36.

[37] K. Zhang and T. F. M. Chui, *Linking hydrological and bioecological benefits of green infrastructures across spatial scales – A literature review*, *Science of The Total Environment* **646** (Jan., 2019) 1219–1231.

[38] A. Elliott and S. Trowsdale, *A review of models for low impact urban stormwater drainage*, *Environmental Modelling & Software* **22** (Mar., 2007) 394–405.

[39] C. R. Jacobson, *Identification and quantification of the hydrological impacts of imperviousness in urban catchments: A review*, *Journal of Environmental Management* **92** (June, 2011) 1438–1448.

[40] B. Miles and L. E. Band, *Green infrastructure stormwater management at the watershed scale: urban variable source area and watershed capacitance*, *Hydrological Processes* **29** (2015), no. 9 2268–2274.

[41] H. W. Suk and S. J. Burian, *Determining Effective Impervious Area for Urban Hydrologic Modeling*, *Journal of Hydrologic Engineering* **14** (Feb., 2009) 111–120.

[42] Q. Weng, *Remote sensing of impervious surfaces in the urban areas: Requirements, methods, and trends*, *Remote Sensing of Environment* **117** (Feb., 2012) 34–49.

[43] M. P. Clark, Y. Fan, D. M. Lawrence, J. C. Adam, D. Bolster, D. J. Gochis, R. P. Hooper, M. Kumar, L. R. Leung, D. S. Mackay, R. M. Maxwell, C. Shen, S. C. Swenson, and X. Zeng, *Improving the representation of hydrologic processes in Earth System Models*, *Water Resources Research* **51** (2015), no. 8 5929–5956.

[44] F. Giorgi and R. Avissar, *Representation of heterogeneity effects in Earth system modeling: Experience from land surface modeling*, *Reviews of Geophysics* **35** (1997), no. 4 413–437.

[45] W. Burke and C. N. Tague, *Multiscale Routing – Integrating the Tree-scale Effects of Disturbance into a Watershed Ecohydrologic Model*, AGU, Dec., 2019.

[46] W. D. Burke, C. Tague, M. C. Kennedy, and M. A. Moritz, *Understanding How Fuel Treatments Interact With Climate and Biophysical Setting to Affect Fire, Water, and Forest Health: A Process-Based Modeling Approach*, *Front. For. Glob. Change* **3** (2021). Publisher: Frontiers.

[47] C. L. Tague and L. E. Band, *RHESSys: Regional Hydro-Ecologic Simulation System—An Object-Oriented Approach to Spatially Distributed Modeling of Carbon, Water, and Nutrient Cycling*, *Earth Interactions* **8** (Dec., 2004) 1–42.

[48] C. Tague and M. Pohl-Costello, *The Potential Utility of Physically Based Hydrologic Modeling in Ungauged Urban Streams*, *Annals of the Association of American Geographers* **98** (Sept., 2008) 818–833.

[49] C. D. Bell, C. L. Tague, and S. K. McMillan, *Modeling Runoff and Nitrogen Loads From a Watershed at Different Levels of Impervious Surface Coverage and Connectivity to Storm Water Control Measures*, *Water Resources Research* **55** (2019), no. 4 2690–2707.

[50] R. R. Bart, C. L. Tague, and P. E. Dennison, *Modeling annual grassland phenology along the central coast of California*, *Ecosphere* **8** (2017), no. 7 e01875.

[51] J. J. Reyes, C. L. Tague, R. D. Evans, and J. C. Adam, *Assessing the Impact of Parameter Uncertainty on Modeling Grass Biomass Using a Hybrid Carbon Allocation Strategy*, *Journal of Advances in Modeling Earth Systems* **9** (2017), no. 8 2968–2992.

[52] N. E. Christians, A. J. Patton, and Q. D. Law, *Introduction to the Grasses*, in *Fundamentals of Turfgrass Management, Fifth Edition*, pp. 7–39. John Wiley & Sons, Ltd, 2016.

[53] J. Kattge, S. Díaz, S. Lavorel, I. C. Prentice, P. Leadley, G. Bönisch, E. Garnier, M. Westoby, P. B. Reich, I. J. Wright, J. H. C. Cornelissen, C. Violle, S. P. Harrison, P. M. V. Bodegom, M. Reichstein, B. J. Enquist, N. A. Soudzilovskaia, D. D. Ackerly, M. Anand, O. Atkin, M. Bahn, T. R. Baker, D. Baldocchi, R. Bekker, C. C. Blanco, B. Blonder, W. J. Bond, R. Bradstock, D. E. Bunker, F. Casanoves, J. Cavender-Bares, J. Q. Chambers, F. S. C. Iii, J. Chave, D. Coomes, W. K. Cornwell, J. M. Craine, B. H. Dobrin, L. Duarte, W. Durka, J. Elser, G. Esser, M. Estiarte, W. F. Fagan, J. Fang, F. Fernández-Méndez, A. Fidelis, B. Finegan, O. Flores, H. Ford, D. Frank, G. T. Freschet, N. M. Fyllas, R. V. Gallagher, W. A. Green, A. G. Gutierrez, T. Hickler, S. I. Higgins, J. G. Hodgson, A. Jalili, S. Jansen, C. A. Joly, A. J. Kerkhoff, D. Kirkup, K. Kitajima, M. Kleyer, S. Klotz, J. M. H. Knops, K. Kramer, I. Kühn, H. Kurokawa, D. Laughlin, T. D. Lee, M. Leishman, F. Lens, T. Lenz, S. L. Lewis, J. Lloyd, J. Llusià, F. Louault, S. Ma, M. D. Mahecha, P. Manning, T. Massad, B. E. Medlyn, J. Messier, A. T. Moles, S. C. Müller, K. Nadrowski, S. Naeem, Niinemets, S. Nöllert, A. Nüske, R. Ogaya, J. Oleksyn, V. G. Onipchenko, Y. Onoda, J. Ordoñez, G. Overbeck, W. A. Ozinga, S. Patiño, S. Paula, J. G. Pausas, J. Peñuelas, O. L. Phillips, V. Pillar, H. Poorter, L. Poorter, P. Poschlod, A. Prinzing, R. Proulx, A. Rammig, S. Reinsch, B. Reu, L. Sack,

B. Salgado-Negret, J. Sardans, S. Shiodera, B. Shipley, A. Siefert, E. Sosinski, J.-F. Soussana, E. Swaine, N. Swenson, K. Thompson, P. Thornton, M. Waldram, E. Weiher, M. White, S. White, S. J. Wright, B. Yguel, S. Zaehle, A. E. Zanne, and C. Wirth, *TRY – a global database of plant traits*, *Global Change Biology* **17** (2011), no. 9 2905–2935.

[54] I. A. Smith, P. H. Templer, and L. R. Hutyra, *Water sources for street trees in mesic urban environments*, *Science of The Total Environment* **908** (Jan., 2024) 168411.

[55] V. C. Luis, M. S. Jiménez, D. Morales, J. Kucera, and G. Wieser, *Canopy transpiration of a Canary Islands pine forest*, *Agricultural and Forest Meteorology* **135** (Dec., 2005) 117–123.

[56] H. R. McCarthy and D. E. Pataki, *Drivers of variability in water use of native and non-native urban trees in the greater Los Angeles area*, *Urban Ecosyst* **13** (Dec., 2010) 393–414.

[57] E. G. McPherson, Q. Xiao, N. S. van Doorn, J. de Goede, J. Bjorkman, A. Hollander, R. M. Boynton, J. F. Quinn, and J. H. Thorne, *The structure, function and value of urban forests in California communities*, *Urban Forestry & Urban Greening* **28** (Dec., 2017) 43–53.

[58] D. E. Pataki, H. R. McCarthy, E. Litvak, and S. Pincetl, *Transpiration of urban forests in the Los Angeles metropolitan area*, *Ecological Applications* **21** (2011), no. 3 661–677.

[59] G. Vico, R. Revelli, and A. Porporato, *Ecohydrology of street trees: design and irrigation requirements for sustainable water use: ECOHYDROLOGY OF STREET TREES*, *Ecohydrology* **7** (Apr., 2014) 508–523.

[60] C. B. Voter and S. P. Loheide, *Urban Residential Surface and Subsurface Hydrology: Synergistic Effects of Low-Impact Features at the Parcel Scale*, *Water Resources Research* **54** (Oct., 2018) 8216–8233.

[61] E. Kuehler, J. Hathaway, and A. Tirpak, *Quantifying the benefits of urban forest systems as a component of the green infrastructure stormwater treatment network*, *Ecohydrology* **10** (2017), no. 3 e1813.

[62] A. Ebrahimian, B. Wadzuk, and R. Traver, *Evapotranspiration in green stormwater infrastructure systems*, *Science of The Total Environment* **688** (Oct., 2019) 797–810.

[63] S. G. Gotsch, D. Draguljić, and C. J. Williams, *Evaluating the effectiveness of urban trees to mitigate storm water runoff via transpiration and stemflow*, *Urban Ecosyst* **21** (Feb., 2018) 183–195.

[64] V. Grey, S. J. Livesley, T. D. Fletcher, and C. Szota, *Establishing street trees in stormwater control measures can double tree growth when extended waterlogging is avoided*, *Landscape and Urban Planning* **178** (Oct., 2018) 122–129.

[65] C. Szota, M. J. McCarthy, G. J. Sanders, C. Farrell, T. D. Fletcher, S. K. Arndt, and S. J. Livesley, *Tree water-use strategies to improve stormwater retention performance of biofiltration systems*, *Water Research* **144** (Nov., 2018) 285–295.

[66] J. K. Thom, S. J. Livesley, T. D. Fletcher, C. Farrell, S. K. Arndt, J. Konarska, and C. Szota, *Selecting tree species with high transpiration and drought avoidance to optimise runoff reduction in passive irrigation systems*, *Science of The Total Environment* **812** (Mar., 2022) 151466.

[67] E. Salvadore, J. Bronders, and O. Batelaan, *Hydrological modelling of urbanized catchments: A review and future directions*, *Journal of Hydrology* **529** (Oct., 2015) 62–81.

[68] E. B. Wetherley, D. A. Roberts, and J. P. McFadden, *Mapping spectrally similar urban materials at sub-pixel scales*, *Remote Sensing of Environment* **195** (June, 2017) 170–183.

[69] C. R. De Kimpe and J.-L. Morel, *Urban soil management: a growing concern*, *Soil Science* **165** (Jan., 2000) 31.

[70] J. L. Edmondson, Z. G. Davies, S. A. McCormack, K. J. Gaston, and J. R. Leake, *Are soils in urban ecosystems compacted? A citywide analysis*, *Biology Letters* **7** (Apr., 2011) 771–774. Publisher: Royal Society.

[71] J. Morgenroth and G. Buchan, *Soil Moisture and Aeration Beneath Pervious and Impervious Pavements*, *Journal of Arboriculture* **35** (May, 2009) 135–141.

[72] J. Fidal and T. R. Kjeldsen, *Accounting for soil moisture in rainfall-runoff modelling of urban areas*, *Journal of Hydrology* **589** (Oct., 2020) 125122.

[73] J. H. Gregory, M. D. Dukes, P. H. Jones, and G. L. Miller, *Effect of urban soil compaction on infiltration rate*, *Journal of Soil and Water Conservation* **61** (May, 2006) 117–124. Publisher: Soil and Water Conservation Society Section: Research Section.

[74] T. H. Phillips, M. E. Baker, K. Lautar, I. Yesilonis, and M. A. Pavao-Zuckerman, *The capacity of urban forest patches to infiltrate stormwater is influenced by soil physical properties and soil moisture*, *Journal of Environmental Management* **246** (Sept., 2019) 11–18.

[75] A. Schaffitel, T. Schuetz, and M. Weiler, *A distributed soil moisture, temperature and infiltrometer dataset for permeable pavements and green spaces*, *Earth System Science Data* **12** (Mar., 2020) 501–517. Publisher: Copernicus GmbH.

Conclusion

Urban trees in semi-arid climates have the potential to provide a variety of ecosystem services through their role in water, energy, and carbon cycles. During drought, tree productivity may be reduced, affecting their other ecosystem services. Because drought in arid to semi-arid climates is expected to increase in frequency and intensity with climate change (Cook et al., 2014), urban areas will need to become more water efficient. To plan for the growth and maintenance of resilient urban forests, the effects of water limitations from both lack of precipitation and reduction in outdoor water use should be considered. This dissertation used an eco-hydrologic modeling approach to estimate the effects of drought on common urban tree species with varying temperature, irrigation input, and land cover.

The main methodology used for all three studies was experimental modeling with an eco-hydrologic process-based model, the Regional Hydro-Ecologic Simulation System (RHESSys). Using a process-based modeling approach enabled me to disentangle the complex interactions between climate, carbon cycling, and water use and simulate the physical mechanisms that drive tree carbon and water fluxes. By first parameterizing with vegetation observations from a historic drought, I then was able to simulate how different temperature and irrigation forcings may affect tree growth dynamically.

In the first chapter, I improved tree species level vegetation parameterisation with a Sobol sensitivity analysis and evaluated tree parameters under drought conditions with varying temperatures. Key vegetation parameters that influenced LAI and NPP varied based on phenology: for deciduous trees, leaf turnover rate had the most influence while for evergreen trees it was specific leaf area. For both phenology types, the soil pore size index was among the highest ranked parameters, which indicates the importance of soil properties in reducing uncertainty in vegetation growth outcomes. Temperature was an important factor for tree drought resilience and post drought growth. Warmer temperatures of 1.8C increased resilience due to longer growing seasons and higher post-drought productivity when there was enough rainfall. However, extreme warming of 4C caused lower post-drought productivity.

I used high-spatial resolution ($\tilde{4}$m) remote sensing derived data of tree species, leaf area index, and changes to normalized differential vegetation index (NDVI) during a drought to (1) constrain vegetation parameters to species level differences and (2) identify with a Sobol sensitivity analysis which vegetation parameters affect LAI, NPP, and their drought resilience. This parameterization method using remote sensing data at the tree

species level provides an example for future modeling studies to expand data sources for setting up vegetation. Although the data used here was specific to the study area of Santa Barbara, methods for high resolution LAI data in cities are advancing (1; 2) and have the potential to be paired with future modeling efforts that capture species level characteristics or scale up to larger areas. The Sobol sensitivity analysis revealed that key parameters for modeling LAI and NPP resilience depend on tree plant functional type, and include leaf turnover rates, specific leaf area, and soil porosity.

I maintained the same five tree species throughout the second two chapters to simulate drought responses to different levels of irrigation input. Urban tree water sources are uncertain, but in modeling different levels of irrigation input, I showed how irrigation can make a difference for tree drought resilience and water use efficiency (WUE). In the second chapter, I varied irrigation amounts during drought and found that the response of the average tree NPP to irrigation input was non-linear, with a break-point analysis displaying a steeper decline in NPP past irrigation reductions of 25%. Tree transpiration was linearly related to water input, causing an increase in WUE with less irrigation. In the third chapter, I considered the role of indirect irrigation from neighboring irrigated turfgrass and stormwater runoff from impervious surfaces. Using the novel hydrologic modeling approach of multi-scale routing, an extension of RHESSys that accounts for fine scale surface and subsurface routing, I found that it is likely trees are receiving water and benefiting from turfgrass irrigation. With irrigation turned off, I showed that impervious surface areas that route surface water into green spaces have the potential to help tree drought resilience.

In the third chapter, I further developed RHESSys multi-scale routing for use in an urban environment. With typical hydrologic and land surface models, land cover is defined as a single type, and water is routed topographically within a hillslope and vertically within the smallest spatial unit. This presents a challenge for highly heterogeneous areas such as cities because often the smallest spatial unit contains multiple land cover types that are represented through aggregation (3). With the multi-scale routing approach, sub-grid heterogeneity is accounted for and lateral, non-topographic water transfers are driven by water potential gradients (4). In the subsurface, this means that a tree and turfgrass can share water based on differences in soil moisture. On the surface, small scale transfers between impervious surfaces and other land types can be accounted for when there is stormwater runoff. My work developed the surface routing module, and tested it at the size of a single patch. This method has potential to scale up to catchment level and assess the impact of dispersed green infrastructure on stormwater management or cooling effects at the neighborhood scale.

Multi-scale surface routing (MSR) is a new development in RHESSys, and next steps for further developing it should include validation and reducing parameter uncertainty. This includes comparing standard RHESSys functioning with RHESSys-MSR at the watershed scale, and accounting for how impervious surfaces are connected to the stormwater drainage system, similar to methods in Shields and Tague, 2015 (5). Remote sensing data of sub-pixel fractional cover could be a valuable source of urban land cover input

to set up RHESSys-MSR for further testing. There are some limitations with using this method, as subsurface transfers are sensitive to a parameter that is not directly observable. However, having more data on soil type, soil porosity, or changes in soil moisture may aid in explaining some of the uncertainty. Urban soils are highly heterogeneous and play an important role for fine scale water routing, which could be an area for further exploration.

The results found in this dissertation are specific to Santa Barbara, a coastal Southern California town with a Mediterranean climate, and this has limitations for application of results. Tree species parameters are set up to trees located in Santa Barbara, but may be transferable for use of RHESSys in other locations with similar climates. However, model outcomes were sensitive to soil pore size index, which will vary across sites. In the first chapter, I showed that the seasonal timing of rainfall and temperature played an important role for drought resilience, and this is likely a pattern that could be similar in other Mediterranean climates that are energy limited in the winter and early spring. The water use data used in the second chapter is based off of monitored irrigation accounts in Santa Barbara, however, many places don't have data that tracks outdoor water use separately from indoor use, and this should be considered for other locations that may be different in their water management and conservation strategies.

Overall, this dissertation aimed to increase understanding of the complex dynamics between drought, urban trees, and water conservation. I also worked to enhance eco-hydrologic model capabilities at small scales to represent tree species characteristics and heterogeneous land cover water transfers. The results are specific to a Mediterranean climate and show that future water conservation will likely have effects on urban forests' ability to withstand extreme drought events. Response to future drought conditions will depend on tree species and water conservation strategies, which include amount and timing of outdoor water reductions and turfgrass water use.

Conclusion References

[1] K. A. García-Pardo, D. Moreno-Rangel, S. Domínguez-Amarillo, and J. R. García-Chávez, *Remote sensing for the assessment of ecosystem services provided by urban vegetation: A review of the methods applied*, .

[2] D. Richards and J. W. Wang, *Fusing street level photographs and satellite remote sensing to map leaf area index*, .

[3] G. Blöschl and M. Sivapalan, *Scale issues in hydrological modelling: A review*, .

[4] W. Burke and C. N. Tague, *Multiscale routing – integrating the tree-scale effects of disturbance into a watershed ecohydrologic model*, AGU, 2019.

[5] C. Shields and C. Tague, *Ecohydrology in semiarid urban ecosystems: Modeling the relationship between connected impervious area and ecosystem productivity*, *Water Resources Research* **51** (2015), no. 1 302–319.